



**Politecnico  
di Torino**

# **Politecnico di Torino**

**Master's Degree in Aerospace Engineering**

**Academic Year 2023/2024**

**“Development of ANSA meshing method”**

**Supervisors:**

**Prof. Andrea Tonoli**

**Ing. Luca Miretti**

**Candidate:**

**Luca Dell'Anna**



# Abstract

This thesis investigates the development and analysis of an alternative meshing methodology for Computational Fluid Dynamics (CFD) simulations, focusing on the comparison between meshes generated by ANSA and STAR-CCM+ software.

The study is applied to the single-seater car designed by “Squadra Corse PoliTo” for the Formula SAE international university competition.

The primary objective is to generate a high-quality mesh in ANSA and rigorously evaluate it against the STAR-CCM+ mesh using various quality criteria, such as element skewness, face validity, and overall mesh structure.

In addition, this new mesh is validated through a series of CFD simulations conducted using the ANSA mesh as a discretization of the computational domain.

In particular, the same rectilinear and symmetrical domain (half car) is used as simulations currently carried out during the design process and based on the STAR-CCM+ mesh.

These simulations aim to directly compare results from both meshing approaches, evaluating the ANSA mesh’s performance in terms of accuracy, computational efficiency, and robustness in capturing aerodynamic behavior.

Beyond technical validation, this project also explores the potential financial and strategic benefits of adopting ANSA for the meshing process, allowing the team to improve the relationship with our software providers (BETA CAE Systems and Siemens) and enabling more solver options for CFD simulations.

This expanded flexibility may reduce dependency on a single tool, improving adaptability to varying sponsorships and enhancing economic sustainability. By establishing ANSA as a viable alternative, the project contributes to Squadra Corse's long-term competitive strategy, providing a dual-meshing framework that supports ongoing design innovation and performance optimization in Formula SAE competitions.



# Table of Contents

|   |    |
|---|----|
| <b>1. Introduction</b>                    | 7  |
| 1.1. Formula SAE                          | 7  |
| 1.2. Aerodynamics & CFD Department        | 9  |
| 1.3. Research goals                       | 10 |
| <b>2. CFD Modeling</b>                    | 11 |
| 2.1. Governing Equations                  | 11 |
| 2.2. Discretization Methods               | 15 |
| 2.2.1. Finite Difference Method (FDM)     | 15 |
| 2.2.2. Finite Element Method (FEM)        | 17 |
| 2.2.3. Finite Volume Method (FVM)         | 19 |
| 2.3. Turbulence Models                    | 21 |
| 2.4. Types of Mesh                        | 25 |
| 2.4.1. Cell shapes                        | 25 |
| 2.4.2. Grids classification               | 26 |
| <b>3. StarCCM+ Meshing</b>                | 27 |
| 3.1. Method                               | 27 |
| 3.1.1. Trimmed cell mesher                | 27 |
| 3.1.2. Polyhedral Mesher                  | 29 |
| 3.1.3. Prism Layer Mesher                 | 31 |
| 3.2. Results                              | 35 |
| <b>4. ANSA Meshing</b>                    | 36 |
| 4.1. Tool and Method                      | 36 |
| 4.2. Results                              | 46 |
| <b>5. Comparisons</b>                     | 48 |
| 5.1. Meshes Comparison                    | 48 |
| 5.2. Simulations Comparison               | 63 |
| 5.2.1. Plots                              | 63 |
| 5.2.2. Skin Friction Coefficient          | 74 |
| 5.2.3. Pressure Coefficient               | 82 |
| <b>6. Conclusions and Recommendations</b> | 91 |



# 1. Introduction

## 1.1. Formula SAE

The Formula SAE is an international engineering design competition initially proposed by the Society of Automotive Engineers (SAE) which involves the design and production of a racing car, evaluated during a series of tests based on its design qualities and engineering efficiency.

Established in 1981, with the aim of giving university students the opportunity to challenge each other in a competition that gives them the opportunity to put into practice what they have learned during their studies and to help them to develop crucial skills like teamwork, communication, project management, and entrepreneurship, all of which are essential for their future careers in engineering and the automotive industries. {1}

The events take place across several regions worldwide and they cover a broad range of engineering disciplines, such as mechanical design, aerodynamics, electronics, and vehicle performance optimization.



Figure 1.1 Formula Student Austria 2024

The FSAE typically involves the following crucial factors:

- **Design and Production:**

Teams are required to design and build an open-wheel formula-style car.

This undertaking includes various aspects of the car, including the chassis, suspension, powertrain, aerodynamics, and other essential systems. The design must strike a balance between innovation and functionality, optimized to perform effectively across a series of dynamic performance events.

- **Static Events:**

These events evaluate the team's ability to present and justify their engineering decisions and business strategies.

- **Engineering Design Presentation** (engineering approach and design decisions are submitted to judges, providing detailed explanations for the choices the members made throughout the project).
- **Cost Analysis** (a comprehensive budget that outlines the costs involved in constructing and operating the vehicle, offering justifications for each expense, is sent before the competition and it is discussed with judges during the event).
- **Business Plan Presentation** (teams promote their car as a marketable product by highlighting their financial planning, sales tactics, and marketing strategies, demonstrating how the vehicle could be successful in a commercial setting).

- **Dynamic Events:**

These events evaluate the vehicle's performance on track.

- **Acceleration** (the car must accelerate for 75 meters along a straight course on flat surface, the test is divided into two batteries, the score is determined by the difference between the worst and the best time recorded).
- **Skid Pad** (the test assesses the cornering capability of the vehicle indeed the course consists of two pairs of concentric circles in a figure of eight pattern).
- **Autocross** (the handling of the car is tested by running two laps of a circuit, the track is designed to obtain average speeds between 30 and 40 km/ h and includes short straights, constant radius curves, hairpins, slaloms and chicanes).
- **Endurance** (this event aims to evaluate the overall performance of the prototype as speed, reliability, handling, efficiency, for this reason represents the main event of a Formula SAE competition, furthermore it takes place along a track very similar to the autocross test, for a total of 22 km).



## 1.2. Aerodynamics & CFD Department

The Aerodynamics & CFD Department develops the prototype's aerodynamic parts. These parts are designed using CAD software, rigorously analyzed through CFD and FEM simulations, and validated in a wind tunnel facility. Additionally, team members manufacture these components using composite materials and handle the assembly of the aerodynamic package.

The department is divided into three sub-groups:

“Designers” focus on shaping the car and performing CFD simulations to assess the aerodynamic performance of the components, “Structurists” manage material selection and conduct FEM analyses alongside experimental testing to ensure structural integrity, “CFD Engineers” develop advanced numerical models to maximize the efficiency of the available computational resources.



Figure 1.2 Aerodynamics and CFD department at rollout event of SC24

### 1.3. Research goals

This research aims to enhance the aerodynamic design workflow for the Formula SAE single-seater car developed by Squadra Corse for international university competitions:

- the main goal is to develop a high-quality computational mesh in ANSA and rigorously assess its performance against the STAR-CCM+ mesh currently utilized by the team. This comparison will focus on key mesh quality parameters, such as element skewness, face validity, and volume change.
- to validate the new ANSA mesh, a series of Computational Fluid Dynamics (CFD) simulations will be conducted, using it to discretize the computational domain. These simulations will employ the same rectilinear, symmetrical half-car domain as used in the STAR-CCM+ based simulations, allowing for a direct comparison between both meshing approaches. This will enable the evaluation of the ANSA mesh's effectiveness in terms of aerodynamic accuracy, computational efficiency, and resilience.
- this study also examines the strategic advantages of integrating ANSA into the meshing process. By diversifying meshing capabilities to include ANSA, the team can reduce reliance on a single tool, increase flexibility in solver options, and improve adaptability to potential changes in sponsorships or software partnerships. This dual-meshing strategy, facilitated by stronger collaboration with software providers like BETA CAE Systems and Siemens, is expected to strengthen the team's economic sustainability and competitive edge.
- in establishing ANSA as a feasible alternative to STAR-CCM+ for meshing and simulation tasks, this research aims to contribute to Squadra Corse's long-term vision. The findings will help the team build a more adaptable and innovative design process, supporting continuous performance advancements in future Formula SAE competitions.

# 2. CFD Modeling

## 2.1. Governing Equations

Computational Fluid Dynamics (CFD) is grounded in the core principles of fluid mechanics, specifically the Navier-Stokes equations for describing fluid motion and the heat conduction equation for thermal transfer. These equations govern the conservation of mass, momentum, and energy within a fluid.

This treatment can only be applied under the following assumptions:

- The flow is non-reactive and homogeneous.
- The flow has no electrical charges.
- The flow is continuous.

The assumption of continuous flow relates to the concept of the mean free path.

In the kinetic theory of gases, the mean free path is a term that describes the average distance over which a moving particle (such as an atom, a molecule, or a photon) travels before substantially changing its direction or energy (or, in a specific context, other properties), typically because of one or more successive collisions with other particles. {2} The expression for the mean free path is:

$$\lambda = \frac{1}{\sqrt{2} n \sigma}$$

where:

- $\sigma = \pi d^2$  is the effective cross-sectional area for spherical particles.
  - $n = \frac{N}{V} = \frac{p}{k_B T}$  is the number of particles per unit volume.
- The Knudsen number is an important dimensionless quantity which allows characterizing the boundary conditions of a fluid flow and it gives a numerical account of whether the continuum hypothesis can be applied. {3}

The expression for the Knudsen number is:

$$Kn = \frac{\lambda}{L}$$

where:

- $\lambda$  is the mean free path.
- $L$  is a characteristic length scale of the fluid mechanical system, such the chord of an airfoil or the diameter of a pipe.

Depending on the value of the Knudsen number, 3 different flow regimes are identified:

- If  $Kn < 0.01$ : The flow is in the viscous regime, and it behaves like a continuum. Traditional fluid dynamics equations (e.g., Navier-Stokes) are valid. The non-slip boundary condition is assumed.
- If  $0.01 < Kn < 1$ : The flow is in the transition regime, between continuum and rarefied regimes. Both molecular and continuum behaviors are significant, and models like the slip-flow model may be needed. In this case, the slip boundary condition is assumed.
- If  $Kn \gg 1$ : The flow is in the molecular regime, the mean free path is much larger than the system's characteristic length. The gas becomes rarefied, and molecular interactions dominate over continuum assumptions.

## Continuity equation

The continuity equation expresses the principle of mass conservation for a fluid in motion, ensuring that mass cannot spontaneously disappear or be created within a control volume.

In Computational Fluid Dynamics (CFD), the continuity equation is one of the primary equations solved to simulate fluid flows. Ensuring that numerical solutions satisfy the continuity equation is critical for accuracy in simulations.

Many CFD methods apply techniques to enforce continuity, such as:

- Pressure Correction Methods: Algorithms solve for pressure fields iteratively to satisfy the continuity equation in incompressible flows.
- Finite Volume Method (FVM): The continuity equation is applied at each control volume in the domain, ensuring mass conservation locally across the mesh.

Failure to satisfy the continuity equation in CFD can lead to unphysical results, such as artificial sources or sinks of mass, which can degrade the accuracy of simulations.

The continuity equation in fluid dynamics can be expressed in differential form as:

$$\frac{\partial \rho}{\partial t} + \nabla \cdot (\rho \vec{v}) = 0$$

where:

- $\rho$  is the density of the fluid (mass per unit volume),
- $\vec{v}$  is the velocity vector of the fluid,
- $\frac{\partial \rho}{\partial t}$  represents the time rate of change of density,
- $\nabla \cdot (\rho \vec{v})$  is the divergence of the mass flux (rate of mass flow per unit area).
- this equation states that any change in the density of a fluid within a control volume over time is balanced by the net flow of mass into or out of that volume.

The form of the continuity equation depends on whether the flow is compressible or incompressible:

- For compressible flows, where the density can vary with time and position (such as in gases under high-speed or variable temperature conditions), the general continuity equation applies in its full form.
- For incompressible flows, where density  $\rho$  is constant (often assumed in liquids or low-speed gas flows), the equation simplifies significantly. With constant density, the continuity equation becomes:

$$\nabla \cdot \vec{v} = 0$$

This simplified form implies that the fluid's velocity field is divergence-free. In other words, the net volume flux in and out of any region is zero, ensuring that the mass remains conserved. {4}

## Momentum Equation

It is essentially a reformulation of Newton's second law applied to fluid flow, describing how the velocity of a fluid changes in response to internal and external forces.

The momentum equation in the Navier-Stokes framework for an incompressible fluid is given by:

$$\frac{\partial(\rho\vec{v})}{\partial t} + \nabla \cdot (\rho\vec{v}\vec{v}) + \nabla p - \nabla \bar{\tau} = \rho\vec{f}$$

Where:

- $\rho$  is the density of the fluid (assumed constant for incompressible flow),
- $\vec{v}$  is the velocity vector,
- $\frac{\partial\vec{v}}{\partial t}$  is the unsteady term representing the time rate of change of velocity,
- $\nabla \cdot (\rho\vec{v}\vec{v})$  is the convective term representing the change in velocity due to fluid motion,
- $\nabla p$  is the pressure gradient term, which drives flow from high to low pressure,
- $\bar{\tau}$  is the stress tensor and  $\nabla \bar{\tau}$  represents the viscous diffusion term,
- $\rho\vec{f}$  is the external force term, which can include forces such as gravity or other body forces acting on the fluid. {4}

## Energy equation

It expresses the physical principles that energy is conserved by the first principle of thermodynamics.

Indeed, applying that to a control volume, it can be said that the Rate of change of the total energy in the control volume is the sum of the net heat flux towards the control volume and the work done per unit time on the control volume by volumetric and surface forces.

The energy equation in fluid dynamics can be expressed in differential conservative form as:

$$\frac{\partial E}{\partial t} + \nabla \cdot (E\vec{v}) = \rho\dot{\xi} - \nabla\dot{q} - \nabla \cdot (p\vec{v}) + \nabla \cdot (\bar{\tau} \cdot \vec{v}) + \rho\vec{f} \cdot \vec{v}$$

Where:

- $\dot{\xi}$  is the heat absorber per unit time and unit mass,
  - $\dot{q}$  is the heat flux due to thermal conduction where “k” is the conduction constant,
  - $E = e + \frac{|\vec{v}|^2}{2}$  is the total energy per unit volume as sum of internal energy e and kinetic energy,
  - $p\vec{v}$  work done by surface force of pressure,
  - $\bar{\tau} \cdot \vec{v}$  work done by surface force of shear stresses (viscosity dissipation),
  - $\rho\vec{f} \cdot \vec{v}$  work done by volumetric forces,
- 
- $\frac{\partial E}{\partial t} + \nabla \cdot (E\vec{v}) =$  Rate of change of the total energy in the control volume,
  - $\rho\dot{\xi} - \nabla\dot{q} =$  Volumetric heating and conduction heat flux,
  - $-\nabla \cdot (p\vec{v}) + \nabla \cdot (\bar{\tau} \cdot \vec{v}) + \rho\vec{f} \cdot \vec{v} =$   
= work done per unit time on the control volume by volumetric and surface forces.

The governing equations of fluid dynamics are a non-linear system of partial differential equations. They are not easy to solve and, currently, a general solution in closed form doesn't exist.

There are five governing equations of fluid dynamics: one equation for the conservation of mass, three for the momentum balance and one for the energy balance. However, if we count the unknowns that are present in the equations, we see that their number is seven:

- $\rho, u, v, w, p, e, T.$

Thus, we still need two equations to close the system. In typical aerodynamics applications, one can assume that the gas behaves like a perfect gas, so that the sixth equation is the perfect gas law:

$$p = \rho \frac{R}{M} T = \rho R^* T$$

A seventh equation that links the thermodynamics variables could be for a perfect gas the one which consider the specific heats as constant:  $e = c_v T.$

Now, the problem is a closed system but, unfortunately, there is not any analytical solution, only in some rare and simple cases. {4}

## 2.2. Discretization Methods

In Computational Fluid Dynamics (CFD), fluid behavior is governed by continuous equations that describe its flow. To numerically solve these equations, discretization techniques are applied to approximate them in a way that can be computed on a grid. Among the various discretization techniques, the Finite Difference Method (FDM), the Finite Volume Method (FVM), and the Finite Element Method (FEM) are widely used in CFD applications.

### 2.2.1. Finite Difference Method (FDM)

In numerical analysis, Finite Difference Method is a class of numerical techniques for solving differential equations by approximating derivatives with finite differences. It is commonly applied in fields like fluid dynamics, heat transfer, and wave propagation, where partial differential equations (PDEs) describe physical processes. {5}

#### Key concepts

- **Grid/Domain discretization:**

In FDM, the computational domain is divided into a grid made up of discrete points. These points are spaced at regular intervals in one, two, or three dimensions, depending on the problem.

- **Finite Difference Approximation:**

Instead of solving the continuous differential equations directly, FDM approximates the derivatives in the governing equations using finite difference formulas.

These are algebraic approximations of the derivative at a point, based on values at neighboring grid points.

There are different types of finite differences, such as:

- **Forward difference:**

It approximates the derivative using the current and next point. For example, the first derivative of a function  $f(x)$  can be approximated as:

$$\frac{df}{dx} \approx \frac{f(x + \Delta x) - f(x)}{\Delta x}$$

- **Backward difference:**

It uses the current and previous point.

For example, the first derivative of a function  $f(x)$  can be approximated as:

$$\frac{df}{dx} \approx \frac{f(x) - f(x - \Delta x)}{\Delta x}$$

- **Central difference:**

It uses the points on either side of the current point for better accuracy.

For example, the first derivative of a function  $f(x)$  can be approximated as:

$$\frac{df}{dx} \approx \frac{f(x + \Delta x) - f(x - \Delta x)}{\Delta x}$$

- **Formulation of the problem:**  
Once the domain is discretized and finite difference formulas are chosen, the continuous governing equations (e.g., fluid flow or heat transfer equations) are replaced with a set of algebraic equations. These equations relate the function's value at one grid point to its neighbors.
- **Boundary conditions:**  
Proper boundary conditions must be applied to the grid to define how the function behaves at the domain's edges. These can include fixed values (Dirichlet boundary conditions), gradients (Neumann boundary conditions), or more complex mixed conditions.
- **Solution of equations:**  
The system of algebraic equations resulting from the finite difference approximations is then solved using numerical methods, often iterative solvers, to find the values of the unknown variable (e.g., temperature, pressure, or velocity) at each grid point.
- **Time marching:**  
In transient (time-dependent) problems, FDM is used to march forward in time. Time derivatives are approximated similarly to spatial derivatives, and the solution is updated step-by-step.

## Advantages

- **Simplicity:**  
FDM is conceptually simple and easy to implement, making it a common starting point for learning numerical methods.
- **Structured Grids:**  
It works well on structured grids (i.e., grids with regular spacing), such as those used in simple geometries like rectangles or squares.
- **Efficiency:**  
For problems with simple geometry, FDM can be very computationally efficient.

## Limitations

- **Difficulty with complex geometries:**  
FDM is best suited for simple, regular domains. Handling complex, irregular shapes can be difficult and less accurate compared to other methods like the Finite Volume or Finite Element methods.
- **Less flexible with unstructured grids:**  
It does not handle unstructured grids (irregular meshes) easily, limiting its use in problems with irregular boundaries.



## Application areas

- **Heat transfer:**  
Solving the heat equation to predict temperature distributions over time.
- **Fluid dynamics:**  
Simple flow problems, particularly for structured grids.
- **Wave propagation:**  
Simulating waves in physics or engineering problems.

### 2.2.2. Finite Element Method (FEM)

The Finite Element Method is a general numerical method for solving partial differential equations (PDEs) in two or three space variables. To solve a problem, the FEM subdivides a large system into smaller, simpler parts called “finite elements”.

Initially designed for structural mechanics analysis, it has been adapted for use in fluid flow problems and it is suitable for modeling complex geometries.

#### Key concepts

- **Domain discretization:**  
In FEM, the computational domain (the physical space where the problem is defined) is divided into smaller, simpler shapes called **finite elements**. These elements can take forms such as triangles, quadrilaterals, tetrahedra, or hexahedra, depending on the geometry of the problem and whether it is two-dimensional (2D) or three-dimensional (3D).
- **Basis Functions:**  
Within each element, the solution to the problem is approximated using a set of basis functions (also called shape functions). These functions are usually simple polynomials, and they help approximate the unknown solution (e.g., displacement in structural mechanics or velocity in fluid flow) within the element.
- **Formulation of the problem:**  
The governing equations (such as those related to stress, heat, or fluid flow) are converted into a set of algebraic equations using the variational principle or weighted residual methods. This formulation ensures that the solution satisfies the physical laws (like conservation of energy or momentum) over each element.
- **Assembly:**  
Once the local equations for each finite element are set up, they are combined (or assembled) into a global system of equations that represents the entire problem.

- **Solution of equations:**  
The global system of equations, which is usually large but sparse (many zeros), is solved using numerical techniques to obtain the solution at discrete points (called nodes) across the domain.
- **Post-processing:**  
After solving, results such as stresses, temperatures, or fluid velocities can be interpolated within the elements and visualized. This step often involves plotting contours or gradients to understand the behavior of the system.

## Advantages

- **Flexibility with complex geometries:**  
FEM can handle complex, irregular shapes more easily than other methods like Finite Difference or Finite Volume.
- **Adaptivity:**  
FEM allows for adaptive mesh refinement, where the mesh can be locally refined in regions that require higher accuracy, improving the solution where needed.
- **Accuracy:**  
FEM can deliver high accuracy, especially when higher-order basis functions or adaptive refinement techniques are used.

## Limitations

In CFD (Computational Fluid Dynamics), FEM is less commonly used than the Finite Volume Method but is preferred in certain applications involving complex boundaries, solid mechanics, fluid-structure interaction, or when high precision is required.

### 2.2.3. Finite Volume Method (FVM)

The Finite Volume Method is a numerical technique used to solve partial differential equations (PDEs), especially those that represent conservation laws such as mass, momentum, and energy. It is one of the most used methods in Computational Fluid Dynamics (CFD) because of its ability to handle complex geometries and maintain conservation properties.

#### Key concepts

- **Domain discretization:**

In FVM, the computational domain (the space where the physical problem exists) is divided into small, non-overlapping regions called **control volumes**. These volumes can have regular or irregular shapes, depending on whether the grid is structured or unstructured.

- **Conservation law application:**

FVM is based on the integral form of the governing conservation equations. These equations, which may describe the conservation of mass, momentum, or energy, are applied to each control volume. The integral form ensures that fluxes across control volume boundaries are balanced, preserving physical quantities.

For example, for a conserved quantity  $\phi$ , the integral form of the conservation law over a control volume  $V$  is:

$$\frac{\partial}{\partial t} \int_V \phi \, dV + \int_S \mathbf{F} \cdot \mathbf{n} \, dS = \int_V Q \, dV$$

where  $\mathbf{F}$  represents the flux of  $\phi$  across the surface  $S$  of the control volume, and  $Q$  is a source term within the volume.

- **Flux calculation at control volume faces:**

The fundamental concept in FVM is that fluxes (e.g., mass, momentum, or energy transfer) are calculated at the faces between neighboring control volumes. By summing the fluxes entering and leaving a control volume, FVM ensures that the amount of a conserved quantity is balanced.

- **Converting to discrete equations:**

The governing equations are converted into algebraic equations by integrating the conservation laws over each control volume. This results in a system of equations that approximate the solution at discrete points (usually the centroids or nodes of the control volumes).

- **Boundary conditions:**

Appropriate boundary conditions must be applied at the edges of the computational domain. This can include specifying fixed values (Dirichlet conditions), specifying fluxes (Neumann conditions), or more complex boundary treatments for fluid or thermal problems.

- **Solving the equations:**

Once the algebraic system is assembled, numerical solvers are used to solve the equations, often using iterative methods, to obtain the values of the unknowns (e.g., pressure, velocity, temperature) within each control volume.

## Advantages

- **Conservation of physical quantities:**  
A major strength of FVM is that it inherently conserves physical quantities, such as mass, momentum, and energy, across control volumes. This is crucial for accurate simulations, particularly in fluid dynamics.
- **Adaptability to complex geometries:**  
FVM works well with both structured and unstructured grids, allowing it to handle irregular or complex geometries more effectively than methods like the Finite Difference Method (FDM).
- **Flexibility:**  
FVM is flexible enough to handle a wide variety of boundary conditions and can easily be applied to problems involving compressible and incompressible flows.

## Limitations

- **Lower order accuracy:**  
While FVM is robust and conserves fluxes, it can sometimes be less accurate than other methods like the Finite Element Method (FEM) when higher-order accuracy is required.
- **Complex implementation for advanced problems:**  
While the basic concepts of FVM are straightforward, handling complex physical phenomena (e.g., turbulence modeling) can require more advanced treatment and intricate numerical schemes

## Application areas

- **Heat transfer:**  
Solving conduction, convection, and radiation problems where energy conservation is essential.
- **Fluid dynamics:**  
Modeling fluid flow, particularly for complex geometries such as those found in automotive, aerospace, and chemical processing industries.  
In a CFD application, FVM might be used, as our interest, to simulate airflow over an FSAE car. The bodywork, the wings and surrounding air are represented as a mesh of control volumes. The Navier-Stokes equations (governing fluid flow) are applied to each control volume, and the flux of air (momentum, mass, and energy) is computed at the faces between volumes. This method ensures that the airflow's conservation properties, like momentum and mass balance, are maintained throughout the domain.
- **Combustion:**  
Simulating chemical reactions and heat release in combustion processes.

## 2.3. Turbulence Models

Turbulence models are mathematical tools employed in computational fluid dynamics (CFD) to estimate the impact of turbulence in fluid flows. Simulating turbulence across all scales—referred to as Direct Numerical Simulation (DNS)—is computationally impractical for most real-world scenarios. Therefore, turbulence models offer approximate solutions that preserve the key features of turbulent flows. Below there are some commonly used types of turbulence models.

### 1. Reynolds-Averaged Navier-Stokes (RANS) Models

The Reynolds-Averaged Navier-Stokes (RANS) approach involves time averaging the instantaneous Navier-Stokes equations to account for the effects of turbulence, allowing for the approximation of turbulent flows without directly resolving all turbulent fluctuations, which would be computationally prohibitive.

Reynolds decomposition refers to separation of the flow variable (like velocity  $\mathbf{u}$  or pressure  $\mathbf{p}$ ) into the mean (time-averaged) component  $\bar{\mathbf{u}}, \bar{\mathbf{p}}$  and the fluctuating component  $\mathbf{u}', \mathbf{p}'$ :

$$\begin{aligned} \mathbf{u}_i &= \bar{\mathbf{u}}_i + \mathbf{u}_i' \\ \mathbf{p}_i &= \bar{\mathbf{p}}_i + \mathbf{p}_i' \end{aligned}$$

where  $i$  is the direction. {6}

When this decomposition is applied to the Navier-Stokes equations and subsequently time-averaged, the Reynolds-Averaged Navier-Stokes equations, which govern the mean flow are obtained. For incompressible flows, the RANS equations in tensor form are expressed as follows:

$$\frac{\partial \bar{u}_i}{\partial x_i} = 0$$

$$\rho \left( \frac{\partial \bar{u}_i}{\partial t} + \bar{u}_j \frac{\partial \bar{u}_i}{\partial x_j} \right) = -\frac{\partial \bar{p}}{\partial x_i} + \mu \frac{\partial^2 \bar{u}_i}{\partial x_j \partial x_j} - \frac{\partial \overline{u_i' u_j'}}{\partial x_j}$$

where:

$\rho$  is the fluid density,

$\mu$  is the dynamic viscosity,

$\overline{u_i' u_j'}$  represents the Reynolds stress tensor.

The left-hand side of the second equation represents the change in mean momentum of a fluid element caused by the unsteadiness in the mean flow and the convection by the mean flow. This change is balanced by the isotropic stress due to the mean pressure field, the viscous stresses, and the Reynolds stresses which arises from the nonlinear interactions of the fluctuating velocity components, capturing the momentum transfer due to turbulence.

The challenge of RANS modelling is that it introduces more unknowns (Reynolds stresses) than there are equations. To close the system, turbulence models are introduced to approximate these Reynolds stresses.

The Boussinesq hypothesis assumes that Reynolds stresses are proportional to the mean rate of strain, analogous to molecular viscosity in laminar flows.

This assumption introduces a turbulent or eddy viscosity ( $\mu_t$ ) which models the transport of momentum by turbulent eddies, allowing for the Reynolds stresses to be expressed as:

$$\tau_{ij} = -\overline{\rho u'_i u'_j} = \mu_t \left( \frac{\partial \bar{u}_i}{\partial x_j} + \frac{\partial \bar{u}_j}{\partial x_i} \right) - \frac{2}{3} \rho k \delta_{ij}$$

Where  $k$  is the turbulent kinetic energy, defined as  $k = \frac{1}{2} \overline{u'_i u'_i}$ .

To estimate  $\mu_t$  and  $k$  two-equation models such as the  $k - \epsilon$  Model and  $k - \omega$  Model are commonly used. These models introduce transport equations for turbulent kinetic energy and dissipation rate/specific dissipation rate, allowing for the closure of the RANS equations.

- ***k - ε Model:***

- It is one of the most common models used in computational fluid dynamics (CFD).
- It is a two-equation model that gives a general description of turbulence solving two transport equations: the first transported variable is the turbulent kinetic energy ( $k$ ), the second transported variable is the rate of dissipation of turbulent kinetic energy ( $\epsilon$ ), which represents the rate at which turbulence energy is dissipated into heat.
- It has been tailored specifically for planar shear layers and recirculating flows, but it is the most widely used and validated turbulence model with applications ranging from free-shear layer flows with relatively small pressure gradients to confined flows where the Reynolds shear stresses are most important.

- ***k - ω Model:***

- It is a two-equation model that gives a general description of turbulence solving two transport equations: the first transported variable is the turbulent kinetic energy ( $k$ ), the second transported variable is the specific dissipation rate ( $\omega$ ), dissipation per unit turbulent kinetic energy.
- It is the most widely used and validated turbulence model with applications in adverse pressure gradient flows and near-wall regions.

- ***Spalart - Allmaras Model:***

- It is a one-equation model that solves a modelled transport equation for the kinematic eddy turbulent viscosity ( $\mu_t$ ).
- It is designed specifically for aerospace applications involving wall-bounded flows and has been shown to give good results for boundary layers subjected to adverse pressure gradients. It is also gaining popularity in turbomachinery applications.

## 2. Large Eddy Simulation (LES)

It is a mathematical model for turbulence used in computational fluid dynamics.

The principal idea behind LES is to improve the RANS approach and reduce the computational cost by:

- Solving the largest turbulent length scales.
- Ignoring the smallest length scales, which are the most computationally expensive to resolve, via low-pass filtering of the Navier–Stokes equations (which can be viewed as a time- and spatial-averaging).
- Modelling the effects of the smallest length scales on the flow field.

It gives better results rather than RANS in various applications like combustion, acoustics and simulations of the atmospheric boundary layer.

## 3. Detached Eddy Simulation (DES)

It is a mathematical model for turbulence used in computational fluid dynamics which combines elements of RANS and LES.

The idea is that areas close to solid boundaries, as well as those where the turbulent length scale is smaller than the maximum grid size, are handled using the RANS solution approach. When the turbulent length scale exceeds the grid size, the LES mode is applied to these regions. This approach reduces the grid resolution requirements compared to a full LES simulation, significantly lowering computational costs.

It is suitable for flows with complex boundary layers and large separation zones, like aerospace and automotive applications.

## 4. Direct Numerical Simulation (DNS)

It is a simulation in computational fluid dynamics (CFD) in which the Navier–Stokes equations are numerically solved without any turbulence model.

It provides the highest accuracy as no approximations are used for turbulence.

However, it is impractical for most industrial applications due to high computational cost, indeed, the whole range of spatial and temporal scales of the turbulence must be resolved. In particular, the spatial scales of the turbulence must be resolved from the smallest dissipative scales (Kolmogorov microscales), up to the integral scale  $L$ , associated with the motions containing most of the kinetic energy.

It is used for fundamental turbulence research and very small-scale problems.

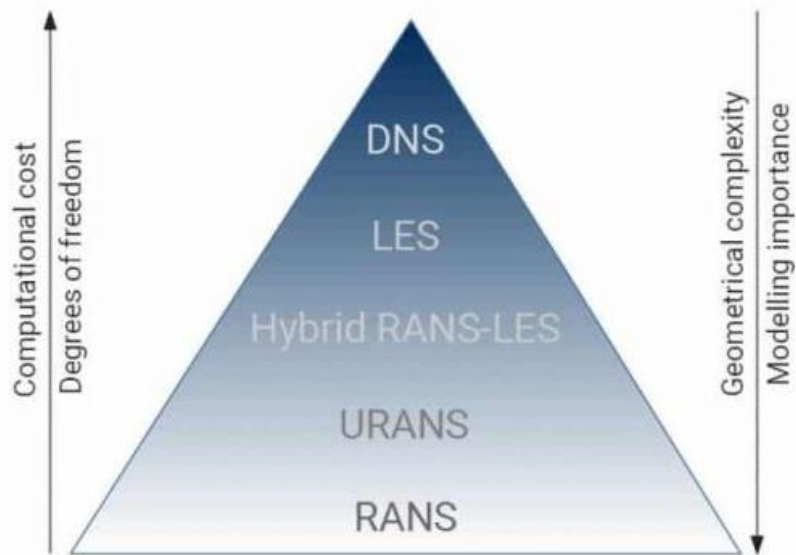


Figure 3.1 Turbulence models in CFD

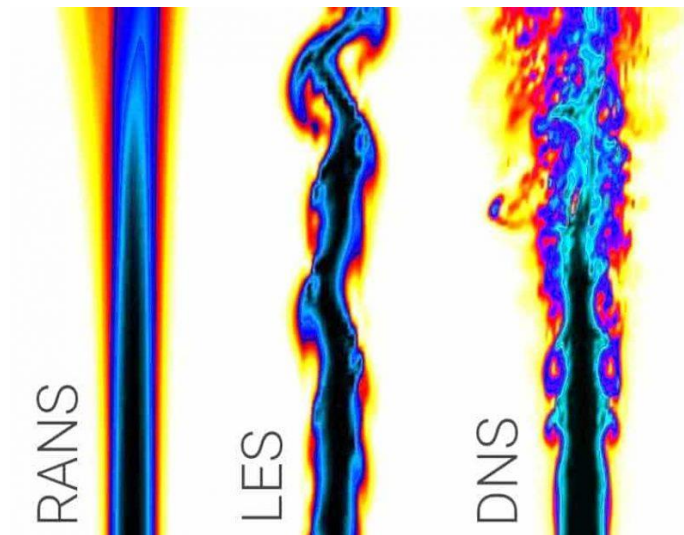


Figure 4.2 CFD modelling of a turbulent jet using different approaches



## 2.4. Types of Mesh

In CFD, a mesh is the partition of a computational domain into smaller discrete cells, in which are solved the discrete form of the governing equations of fluid. {7}

### 2.4.1. Cell shapes

The cell shape is classified according to whether the elements are 2D or 3D.

#### 2D cells:

- **Triangle:** This cell shape consists of 3 sides and is one of the simplest types of mesh. A triangular surface mesh is always quick and easy to create. It is most common in unstructured grids.
- **Quadrilateral:** This cell shape is a basic 4 sided. This kind of element is most common in structured grids, and it is usually excluded from being or becoming concave.

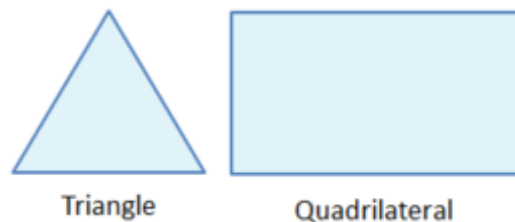


Figure 5.3 2D element cells

#### 3D cells:

- **Tetrahedron:** A tetrahedron has 4 vertices, 6 edges, and is bounded by 4 triangular faces.
- **Pyramid:** A quadrilaterally-based pyramid has 5 vertices, 8 edges, bounded by 4 triangular and 1 quadrilateral face. These are effectively used as transition elements between square and triangular faced elements and other in hybrid meshes and grids.
- **Triangular Prism:** A triangular prism has 6 vertices, 9 edges, bounded by 2 triangular and 3 quadrilateral faces. The advantage with this type of layer is that it resolves boundary layer efficiently.
- **Hexahedron:** A cuboid has 8 vertices, 12 edges, and 6 quadrilateral faces, making it a type of hexahedron. For the same cell amount, the accuracy of solutions in hexahedral meshes is the highest.

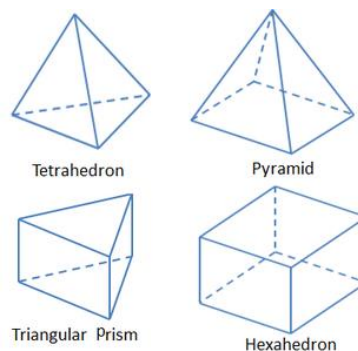


Figure 6.4 3D element cells

## 2.4.2. Grids classification

Mesh grids can be classified into the following categories.

### Structured Grids

Structured grids are characterized by consistent connectivity patterns.

In 2D, the elements can be quadrilaterals, while in 3D, they are typically hexahedra.

This grid model is very space-efficient because neighboring relationships are inherently defined by the grid's storage layout.

Compared to unstructured grids, structured grids offer advantages like improved convergence rates and enhanced resolution.

### Unstructured Grids

An unstructured grid is defined by its irregular connectivity, making it difficult to represent as a straightforward two- or three-dimensional array in computer memory.

This flexibility enables the use of various element types that the solver can handle.

Unlike structured meshes, where neighborhood relationships are implicit, unstructured grids require explicit storage of these connections, which can lead to higher space inefficiency.

Although storage needs for structured and unstructured grids are comparable within a constant factor, unstructured grids commonly use triangular elements in 2D and tetrahedral elements in 3D.

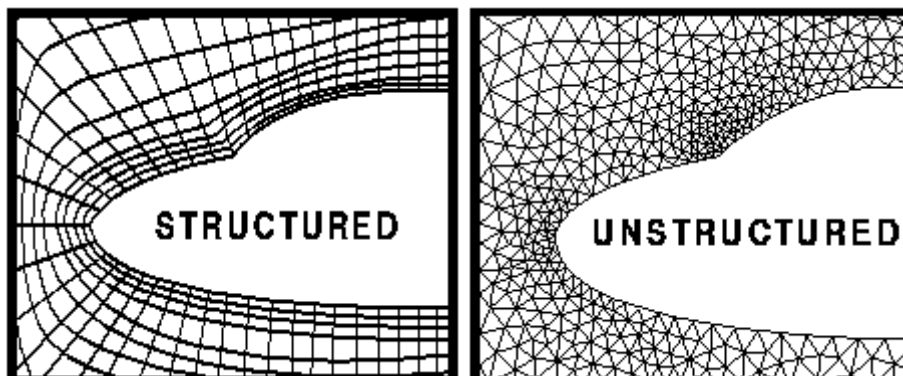


Figure 7.5 Structured and Unstructured Grids

### Hybrid Grids

A hybrid grid combines both structured and unstructured sections, integrating them efficiently. Regions of the geometry that are relatively regular can be covered with structured grids, while more complex areas use unstructured grids.

Hybrid grids can also be non-conformal, meaning grid lines are not required to align at the boundaries between blocks.

# 3. StarCCM+ Meshing

## 3.1. Method

The current meshing method is based on a 1<sup>st</sup> surface meshing phase on ANSA software, to export the volumes of the computational domain and then a 2<sup>nd</sup> phase which sees the replacement of the parts in the StarCCM+ model, a surface re-meshing and the volume meshing.

### 3.1.1. Trimmed cell mesher

In StarCCM+ model, one of the volumes meshers is the **Trimmed Cell Mesher**:

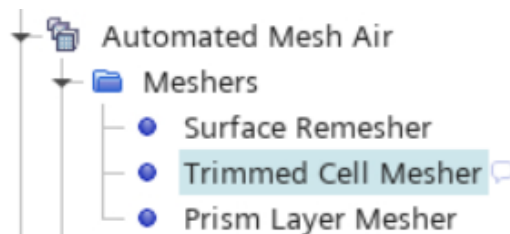


Figure 3.1 Trimmed Cell Mesher used in meshing operations

The Trimmed Cell Mesher delivers a robust and efficient technique for creating a high-quality grid, suitable for both simple and complex mesh generation tasks.

It combines multiple highly sought-after meshing characteristics within a single meshing strategy:

- predominantly hexahedral mesh with minimal cell skewness
- refinement that is based upon surface mesh size and other user-defined refinement controls
- surface quality independence
- alignment with a user specified coordinate system.

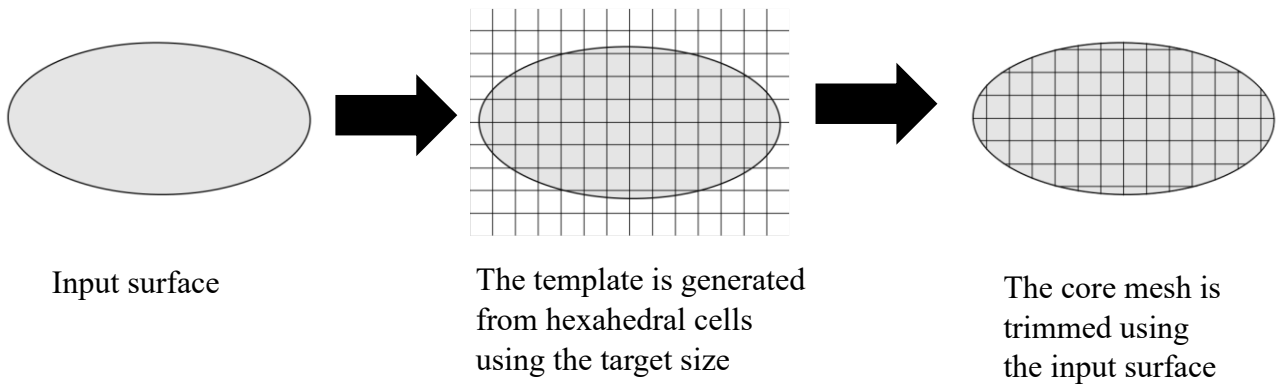
The Trimmed Cell Mesher is available for both the Parts-Based Meshing (PBM) and Region-Based Meshing (RBM) approaches.

The trimmer meshing model employs a template mesh made up of hexahedral cells at the specified target size, from which it cuts or trims the core mesh based on the initial input surface. This template mesh incorporates refinements that are dictated by the local surface mesh size and local refinement controls. The template can be oriented in any direction within a user-defined Cartesian coordinate system.

Growth parameters can be applied to manage the transition of mesh cell sizes from small to large, both at the surface and in the far field.

A maximum and/or minimum cell size can also be provided to define the upper and lower bounds for the cell sizes. {8}

The next sequence of images shows how a trimmed mesh is generated for an input surface in Simcenter STAR-CCM+:



**Default controls:**

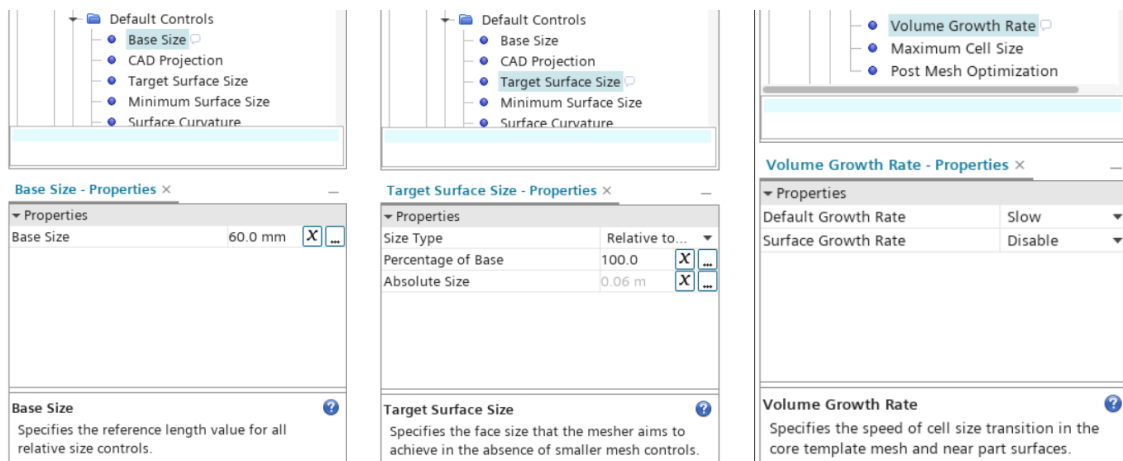


Figure 3.2 Parameters of the Trimmed Cell Mesher in the STAR-CCM+ model.

### 3.1.2. Polyhedral Mesher

In StarCCM+ model, also the Polyhedral Mesher is adopted as volume mesher.

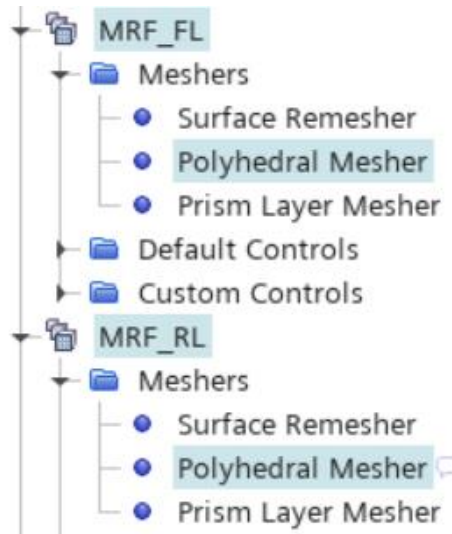


Figure 3.3 Polyhedral Mesher applied to Moving Reference Frame Regions

Polyhedral meshes provide a good solution for complex mesh generation problems.

The polyhedral cells have more faces (an average of 14) than tetrahedral or hexahedral cells, leading to fewer elements overall and thus potentially reducing computational demands.

Furthermore, they are particularly effective for handling highly intricate shapes because they can adapt well to complex boundaries.

#### Default controls:

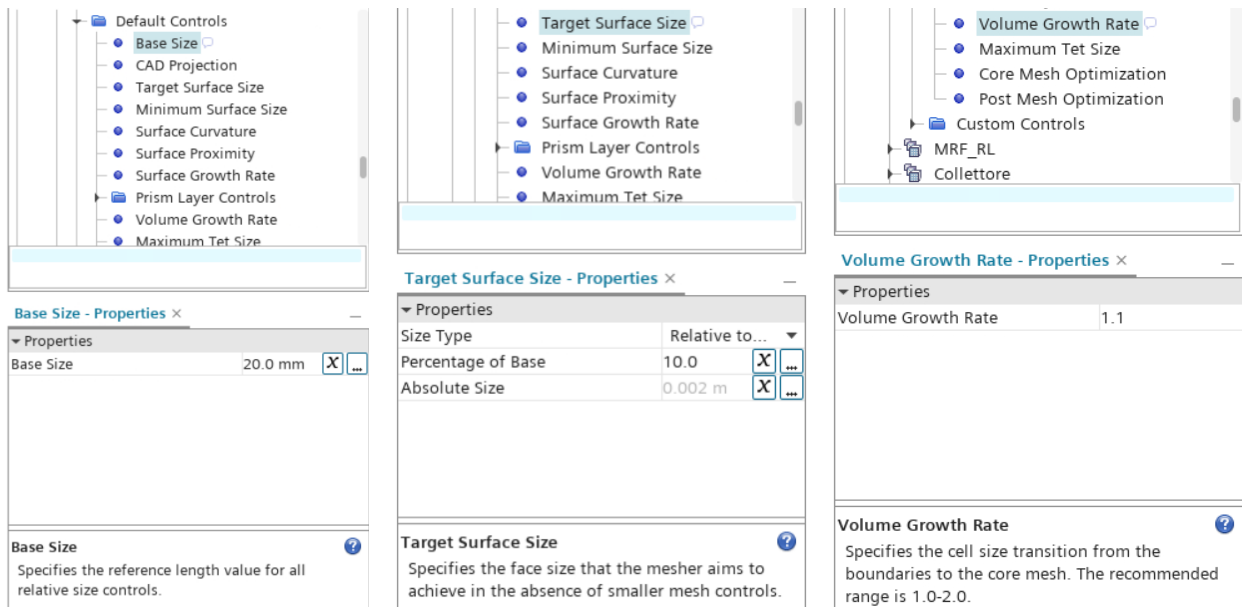
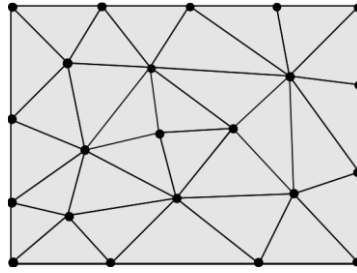


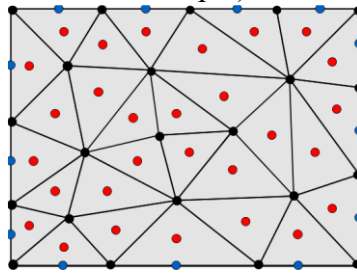
Figure 3.4 Parameters of the Polyhedral Mesher in the STAR-CCM+ model.

The next sequence of images shows how a polyhedral mesh is generated for an input surface in Simcenter STAR-CCM+:

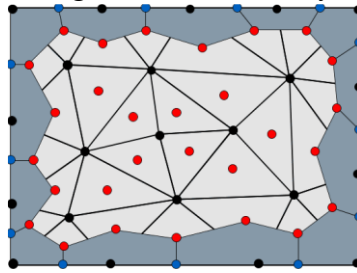
1. A tetrahedral mesh is generated for the input surface.



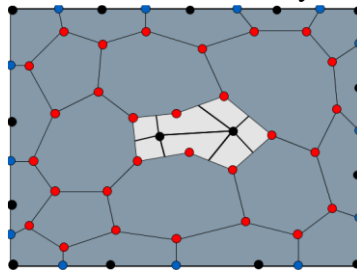
2. A dualization scheme is used to tag the center of the tetrahedral cells (red dots in this example), as well as the midpoints (blue dots in this example) on the boundary edges.



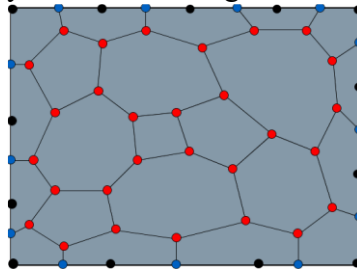
3. Polyhedral cells are generated, starting from the boundary edges.



4. Further polyhedral cells are generated from the outer layer.



5. The process goes on until all polyhedral cells are generated.



### 3.1.3. Prism Layer Mesher

In the StarCCM+ model, the **Prism Layer Mesher** is also adopted.

The prism layer mesh model, in conjunction with a core volume mesh, is employed to create orthogonal prismatic cells adjacent to wall surfaces or boundaries. This layer of cells is essential for enhancing the precision of the flow solution.

A prism layer is defined in terms of:

- Its thickness
- The number of cell layers within it
- The size distribution of the layers
- The function that is used to generate the distribution, either by geometric progression or hyperbolic tangent.

These general characteristics can be applied locally to specific part surfaces, regions, or boundaries, as well as within volumetric controls.

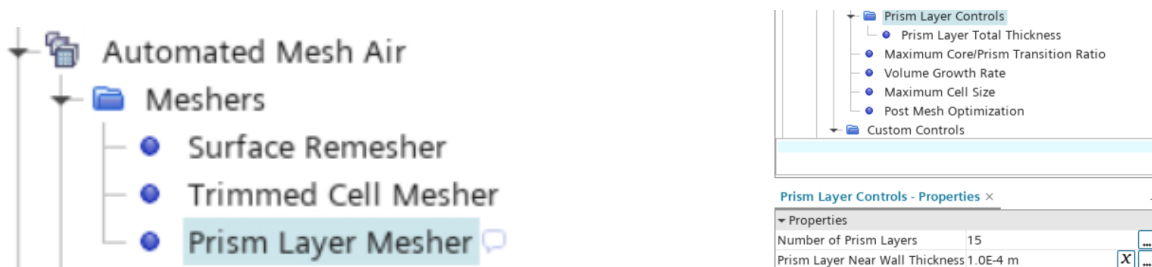


Figura 3.5 Prism Layer Mesher used in meshing operations

An example of a trimmed volume mesh of the front wing, displaying 15 prism layers near the wall surface, is illustrated below:

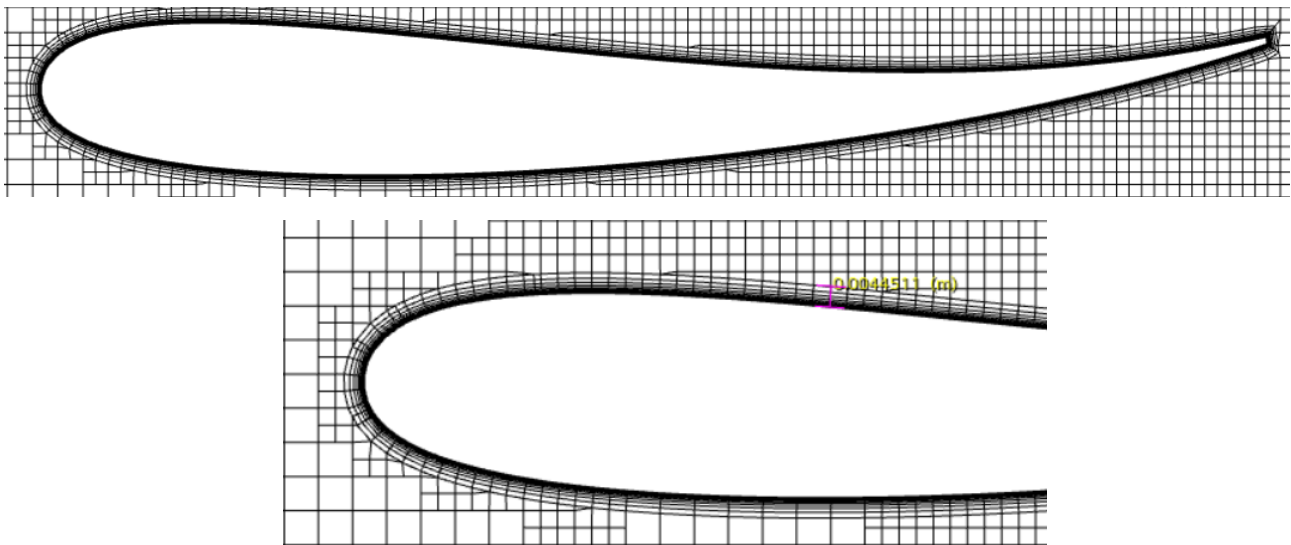


Figura 3.6 Example of prism layer built on the front wing mainplane of our FSAE car

## Prism Layer generation

1. Before the core volume mesh is created, a subsurface is generated at the specified prism layer thickness values, in effect “shrinking” (for internal flows) or “expanding” (for external flows) the starting surface.
2. The core mesh is built using this subsurface.
3. The prism layer mesh is then generated by extruding the cell faces from the core mesh back to the original starting surface.

## Key aspects of prism layer construction

The following properties govern the prism layer construction:

### 1. Number of prism layers

The number of prism layers parameter controls the number of cell layers that are generated within the prism layer on a part surface or boundary.

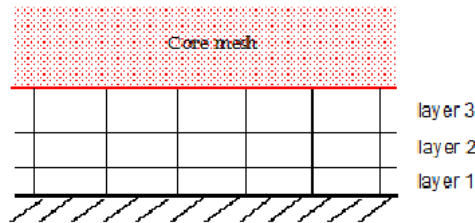


Figure 3.7 3 layers and core mesh example

The number of prism layers determines how well the near-wall region is resolved. More layers generally allow for better resolution of the boundary layer, especially the viscous sublayer in turbulent flows. However, too many layers can raise the computational cost.

Typically, a few layers (between 5 and 15) are utilized, depending on the complexity of the flow and the desired level of accuracy.

### 2. Prism layer total thickness

The prism layer thickness controls the total overall thickness of all the prism layers. It should be in relative or absolute size type.

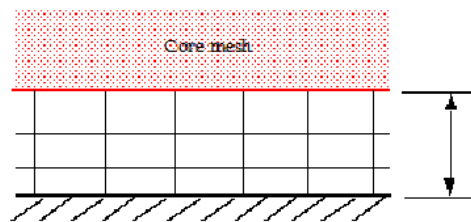


Figure 3.8 Total height of layers

The total thickness of the prism layers should cover the boundary layer region adequately. This ensures that all the relevant physics near the wall, including turbulent effects, are captured.



### 3. Prism layer stretching function

Prism layer stretching function is used to calculate the thickness of each cell layer within the prism layer.

The default StarCCM+ choice is the **Geometric Progression**:

- The cell layers are distributed using simple geometric relationships.
- An example of a prism layer that is constructed using 10 layers with geometric progression is given below, in which the prism layer stretching factor of 1.5 (default) is used for the entire prism layer.

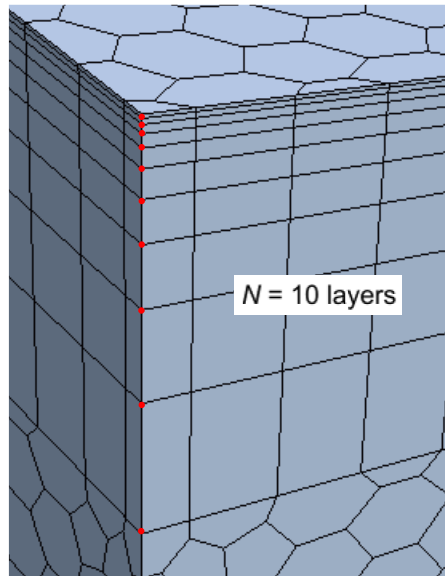


Figura 3.9 Geometric progression stretching function of 10 layers

### 4. Prism layer distribution mode

The distribution mode is important to use in specifying the relative size parameters that the stretching function requires.

In the model, the **Wall thickness** distribution mode is implemented: setting the thickness of the near wall cell layer results that the thicknesses of the remaining layers are distributed according to a calculated stretch factor. It is necessary to add the thickness of near wall prism layer.

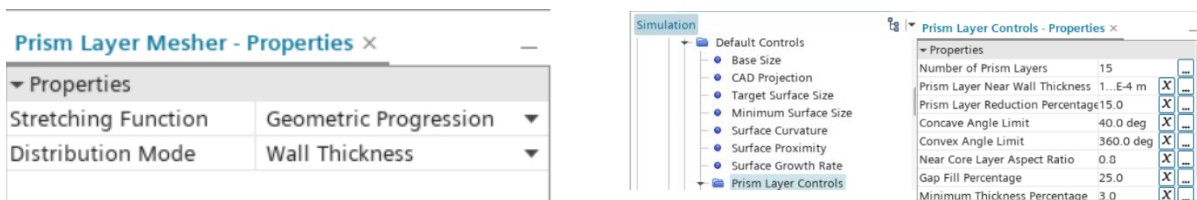


Figura 3.10 Prism layer settings in STAR-CCM+ Mesh model

## **The usefulness of Prism Layer Mesh**

### **1. Near wall resolution and improved accuracy**

Prism layers, providing an enhanced mesh density close to the wall, allow the solver to resolve near wall flow accurately, which is critical in determining not only the forces and heat transfer on walls, but also flow features such as separation.

Separation impacts integral outcomes such as drag or pressure loss, so, the accurate prediction of these flow behaviors depends on capturing the velocity and temperature gradients perpendicular to the wall. These gradients are much sharper in the viscous sublayer of a turbulent boundary layer than what would be indicated by using a coarse mesh. Utilizing a prism layer mesh allows for direct resolution of the viscous sublayer, assuming the turbulence model supports it (low  $y^+$  around 1). Alternatively, for coarser meshes, it enables the software to apply a wall function more precisely (high  $y^+$  over 30).

### **2. High aspect ratio cells**

Prism layers also enable the use of high-aspect-ratio cells, improving crossflow resolution without requiring excessive resolution along the flow direction.

### **3. Reduction of numerical diffusion**

Prism layers help mitigate numerical diffusion near the wall. Numerical diffusion is a discretization error that smooths out discontinuities and sharp gradients in a finite volume advection scheme. This error is minimized when the flow is aligned with the mesh. The use of prism layers greatly improves precision as a result.

### 3.2. Results

The mesh built on STAR-CCM+ has a total number of cells equal to 27186328.

Below are represented some interesting view of the mesh:

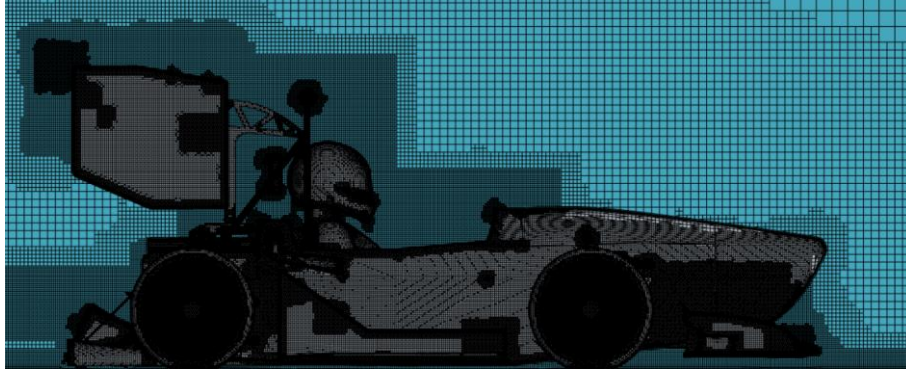


Figure 3.11 Full car side view

In figure 3.11 we can see that the mesh is very refined in the most important part of the car like the wheels, leading edge and trailing edge of the wings, sidepods ecc...

We can also note the shape of the size boxes used to make the mesh refinement.

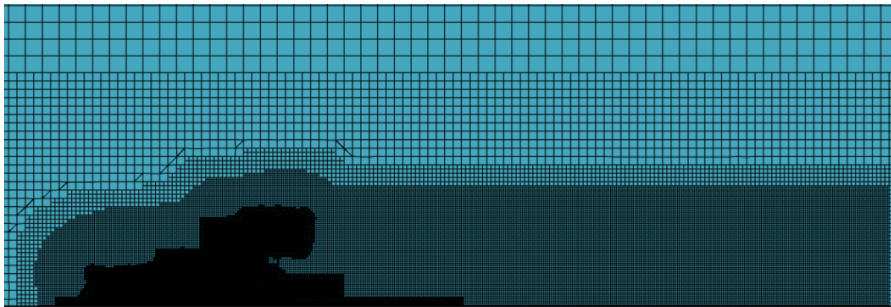


Figure 3.12 Full car and wake refinement

In figure 3.12 is highlighted the wake refinement extending from the rear wing to 10 m behind the car.

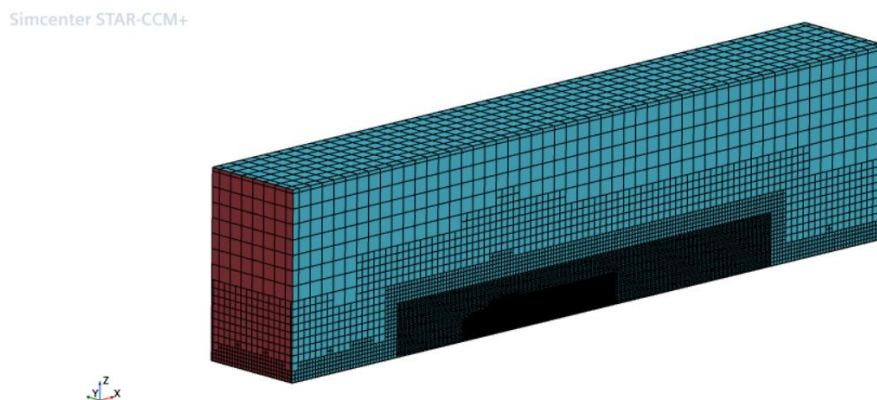



Figure 3.13 Computational domain

In figure 3.13 is represented the overall meshed computational domain, which has a symmetry shape to reduce the computational cost of the meshing and solving phases.

# 4. ANSA Meshing

## 4.1. Tool and Method

The mesh building process is based on the use of ANSA software, a commercial, advanced and multidisciplinary CAE pre-processing tool that provides all the necessary functionality for full-model build up, from CAD data to ready-to-run solver input file, in a single integrated environment.

The chosen meshing method is powered by the “Batch mesh” :

- It is a fully GUI driven tool available within ANSA, which performs automatic mesh generation on Geometry or FE through customizable meshing sessions and scenarios.
- It is often required to mesh specific areas of a Model with different meshing parameters
- The user creates Sessions within the Scenarios using the ANSA Batch Mesh Manager and assigns the respective parts, sub-assemblies or properties automatically to be meshed.

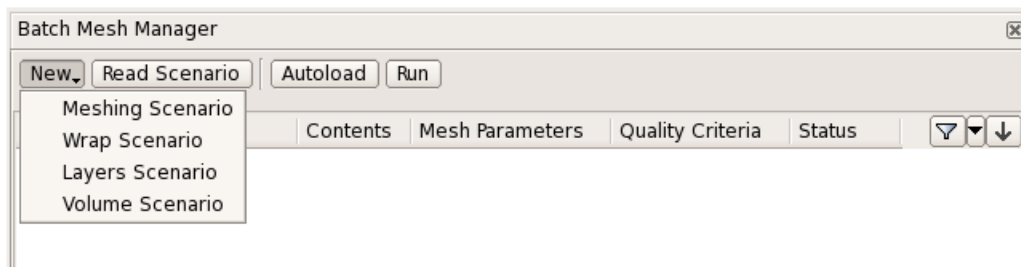


Figure 4.1 Batch Mesh Manager graphic interface

- For each separate Batch Meshing Session, the user has only to define (input/read) the following parameters:
  - **Mesh Parameters** contain all parameters needed for the mesh generation, requirements for the numerous features treatment tools as well as quality improvement settings.
  - **Quality Criteria** contain all the quality requirements that the created mesh has to respect. It also provides the capability to define threshold ranges.

- The ANSA Batch Mesh Tool gives the ability to control the following:
  - **Basic Mesh Requirements:**  
The type of the mesh to be created (Quad -Tria -Mixed), the order of the mesh (1st/2nd), the target element length alongside with requirements for the distortion distance or angle.
  - **Perimeters handling:** Automatic identification and treatment and de-featuring of perimeters, identification of significant features that need to be maintained (i.e. Maintain sharp edge ribs).
  - **Feature treatment:** The following features are automatically identified and can be treated with special treatment available for each case:
    - a. **Fillets** can be sharpened or meshed with specific element rows according to the user request. Local element length for each range can also be specified, as well as different treatment for concave and convex fillets.
    - b. **Chamfers** can be split or sharpened.
    - c. **Flanges 2D** are meshed with the required rows of elements for a specific width-range or with a local target element length.
    - d. **Holes 2D:** Distinction between Round, Oval, Rectangular holes. The user using diameter ranges can fill or ask for a specific hole diameter, set the number of Nodes and create zones of elements.
    - e. **Holes 3D:** Like with holes, tube treatment can also be applied on openings of 3D parts.
    - f. **Special Perimeters** like sharp, leading or free edges can be joined or excluded from joining, given a specific nodal distribution, or create zones with offset. {9}
  - **Refinement boxes:** If there is need for a local mesh refinement, the user is able to create a refinement box. Entities or region of entities in this box are meshed according to the refinement box's special requirements.  
In this way ANSA ensures both the mesh refinement as well as the smooth transition of the mesh flow.
  - **CFD and STL Mesh:** All settings required for the creation of mesh respectively for CFD-Models. This includes all parameters for the mesh generation and treatment of the entities.
  - **Layers creation** over shell mesh.
  - **Volume meshing:** After the shell mesh is complete the Batch Mesh can automatically generate the solid mesh of volumes.
  - **Quality Improvement Settings:** For the correction of elements that violate the Quality Criteria.

The first version of the Batch Mesh has the following characteristics:

| Name  | Contents  | Color        | Mesh Parameters | Quality Criteria |
|---|-----------|--------------|-----------------|------------------|
| <input checked="" type="checkbox"/> <b>Surface_Mesh</b> | <b>72</b> |              |                 |                  |
| <input checked="" type="checkbox"/> Contact Patch       | 2         | Red          | CFD parameters  | StarCCM+         |
| <input checked="" type="checkbox"/> MNS                 | 15        | Purple       | CFD parameters  | StarCCM+         |
| <input checked="" type="checkbox"/> Diffuser            | 7         | Light Green  | CFD parameters  | StarCCM+         |
| <input checked="" type="checkbox"/> Rad                 | 5         | Green        | CFD parameters  | StarCCM+         |
| <input checked="" type="checkbox"/> Car                 | 27        | Pink         | CFD parameters  | StarCCM+         |
| <input checked="" type="checkbox"/> Wings               | 11        | Light Purple | CFD parameters  | StarCCM+         |
| <input checked="" type="checkbox"/> Ground              | 1         | Purple       | CFD parameters  | StarCCM+         |
| <input checked="" type="checkbox"/> Domain              | 4         | Pink         | CFD parameters  | StarCCM+         |
| <input type="checkbox"/> Default_Session                | 0         | Dark Purple  | CFD parameters  | StarCCM+         |
| <input checked="" type="checkbox"/> <b>Prism_Layers</b> | <b>58</b> |              |                 |                  |
| <input checked="" type="checkbox"/> Layers Condotti     | 7         | Orange       | CFD parameters  | StarCCM+         |
| <input checked="" type="checkbox"/> Rad                 | 1         | Red          | CFD parameters  | StarCCM+         |
| <input checked="" type="checkbox"/> Layers Car          | 51        | Light Green  | CFD parameters  | StarCCM+         |
| <input checked="" type="checkbox"/> Inlets-Outlets      | 3         | Brown        | CFD parameters  | StarCCM+         |
| <input checked="" type="checkbox"/> Road                | 1         | Purple       | CFD parameters  | StarCCM+         |
| <input type="checkbox"/> Default_Session                | 0         | Light Green  | CFD parameters  | StarCCM+         |
| <input checked="" type="checkbox"/> <b>Volume_Mesh</b>  | <b>0</b>  |              |                 |                  |
| <input checked="" type="checkbox"/> air                 | 0         | Brown        | CFD parameters  | StarCCM+         |
| <input checked="" type="checkbox"/> MRF_RL              | 0         | Orange       | CFD parameters  | StarCCM+         |
| <input checked="" type="checkbox"/> MRF_FL              | 0         | Light Green  | CFD parameters  | StarCCM+         |
| <input checked="" type="checkbox"/> collettore          | 0         | Light Green  | CFD parameters  | StarCCM+         |
| <input checked="" type="checkbox"/> mod123              | 0         | Blue         | CFD parameters  | StarCCM+         |
| <input checked="" type="checkbox"/> radiator            | 0         | Grey         | CFD parameters  | StarCCM+         |
| <input checked="" type="checkbox"/> rad_nozzle          | 0         | Light Green  | CFD parameters  | StarCCM+         |
| <input type="checkbox"/> mod3                           | 0         | Blue         | CFD parameters  | StarCCM+         |
| <input type="checkbox"/> Default_Session                | 0         | Yellow       | CFD parameters  | StarCCM+         |

Figure 4.2 Scenarios and Sessions setted in the first version of Batch Mesh

- Surface Mesh Scenario:
  - 1<sup>st</sup> order tria elements.
  - Sharp edge, Leading edge, Trailing edge recognition in “Car”, “MNS”, “Diffuser” and “Wings” Sessions.
- Prism Layers Scenario:
  - Low  $y^+$  approach.
  - 4 layers in “Condotti” Session.
  - 9 layers in “Car” Session.
  - 3 layers in “Road” Session.
- Volume Mesh Scenario:
  - Hexa Interior algorithm:
 

This function creates a volume mesh from a combination of a Cartesian hexa mesh (aligned to the global or a local user defined coordinate system) inside the main volumes and a transition zone to the surface mesh, with a blend of tetra and pyramid elements.

The main criticality occurred in the construction of the prism layers, which was interrupted and the batch mesh did not advance.

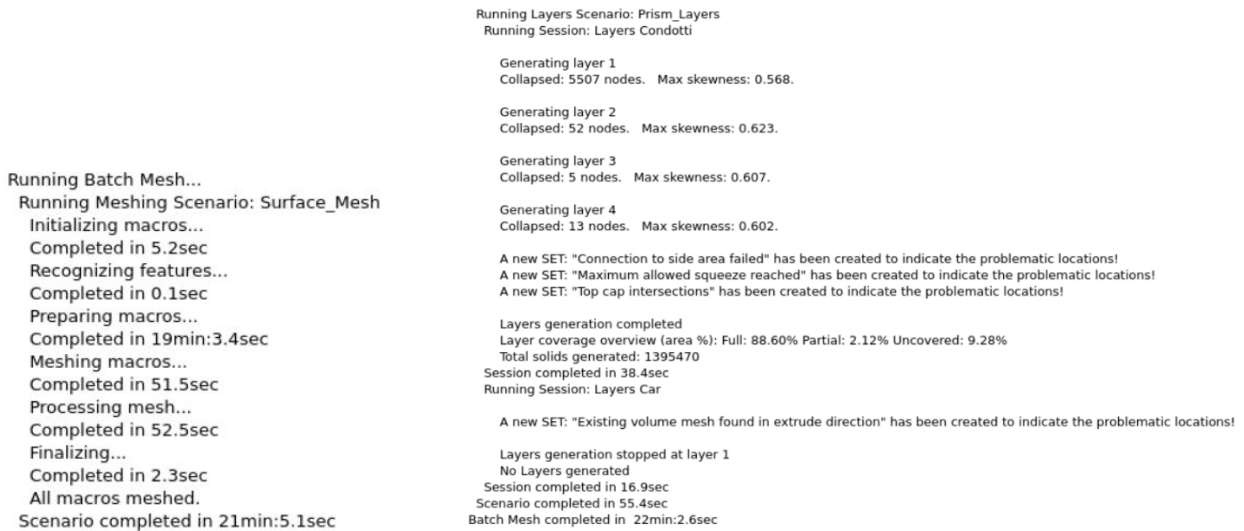


Figure 4.3 Interruption of the Batch Mesh execution during Prism Layers scenario

To fix the problem and to improve the meshing quality, changes were made:

- **Correction of geometric errors and improvement of the global topology of the model, in order to increase its quality also from a meshing perspective.**
  - A local curvature peak was noted on some surfaces in the front area of the car. This led to greater refinement in the meshing phase, so, geometric conditions of this kind were avoided as much as possible by correcting the critical areas with the "surface, reduce" algorithm.

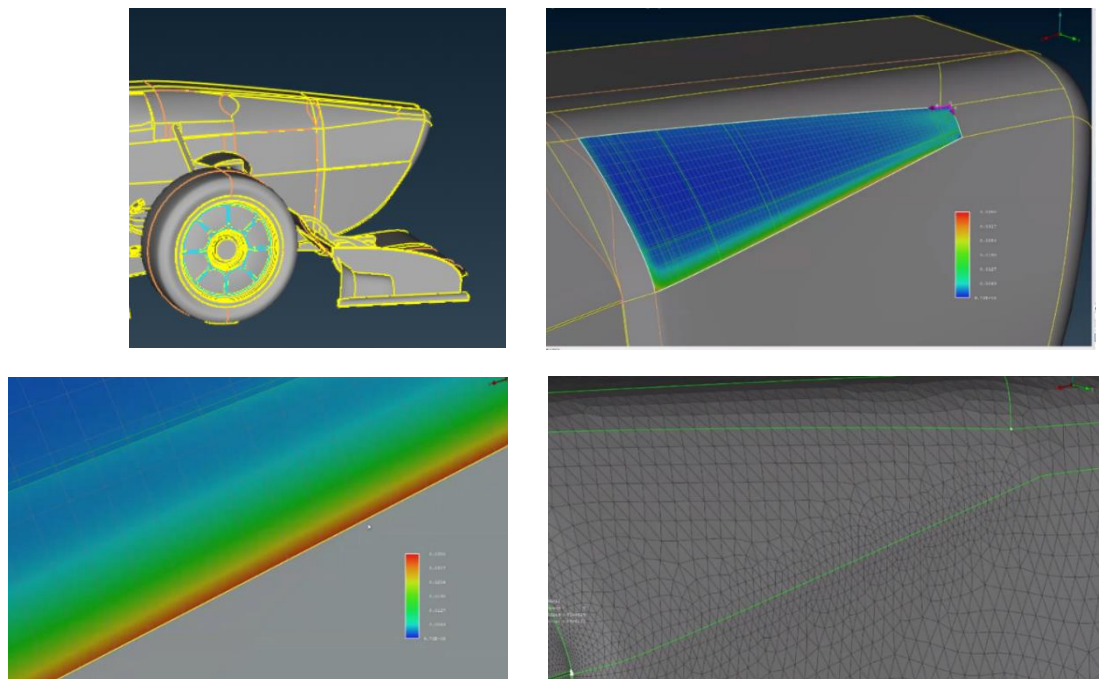


Figure 4.4 Fixing of peaks of local curvature

- The inlet-outlet interfaces of the “radiator nozzle”, “module nozzle”, and “col\_airscoop” rested on the edge of the geometry and were moved 3mm inwards, to give the layers the opportunity to project onto the interface.

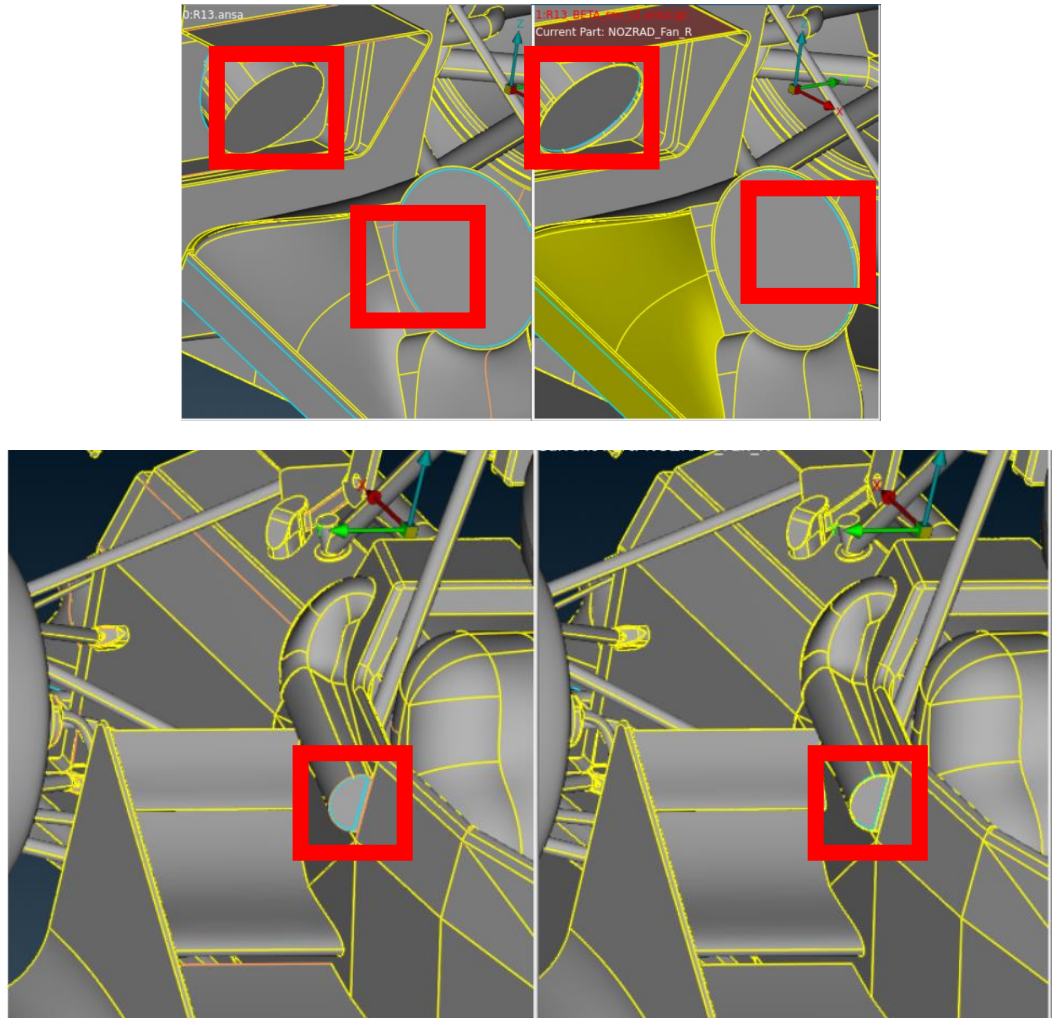


Figure 4.5 Movement of Inlet/outlet interfaces

This was a critical situation because layers must be built both inside and outside the duct. The mesher would encounter a singularity and would not understand where to perform the extrusion. The prisms that would be generated would be of very poor quality.



- The interfaces of the MRFs have been moved inwards.

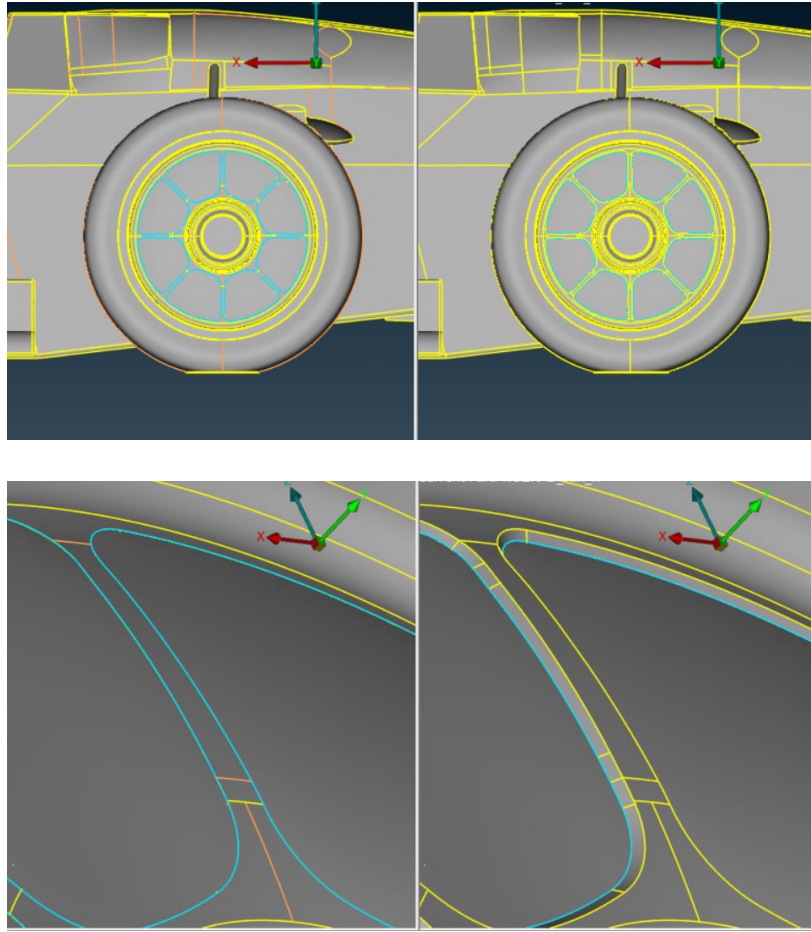


Figure 4.6 Movement of MRFs interfaces

This was done because, by positioning the interface on the external part, an area with an accentuated edge was created and this area was seen by ANSA as a source of proximity.

Proximity caused a densification of mesh elements and a deterioration in quality. Moving the face inward increased the angle on the outer edge and, therefore, the proximity area is improved.

- **Addition of Size Field (based on size boxes) to refine the mesh in volume areas of particular interest.**

In ANSA software, the user can implement additional mesh size controls in shell and volume mesh in two ways:

- Basic way via Size Boxes.
- Advanced way via Size Field (that includes Size Boxes).

These functions influence all CFD manual surface and volume meshing operations and CFD Batch Meshing (the latter case as in this thesis project, the Size Field refinement has the priority on Batch Mesh settings).

Size Boxes are generated in the CFD Decks from the group “Size Boxes”.

Main functions are DECK→SIZE BOXES →NEW and LIST.

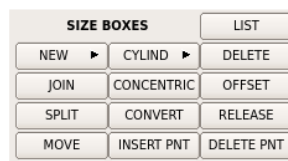


Figure 4.7 Size Boxes panel

By default, a new Size Box is set as “Controlled by Size Field=YES”, which means that they must be loaded in a Size Field.



Figure 4.8 Controlled by Size Field option

More advanced size control can be achieved via the function “Octree” → “Size Field” Create a New Size Field and Edit its card. Add new Size Rules to construct a combination of different sizing functions. Every rule can have different constant or variable size distributions in the Parameters card.

Size Field rules can be:

- Closed surface: PIDs from iso-surface results
- Surface offset: PIDs that are offset and swept
- Cylinder: radial and axial 3D Curve sources
- Sphere: 3D Point sources
- Size Boxes: as described above, set Controlled by Size Field=YES

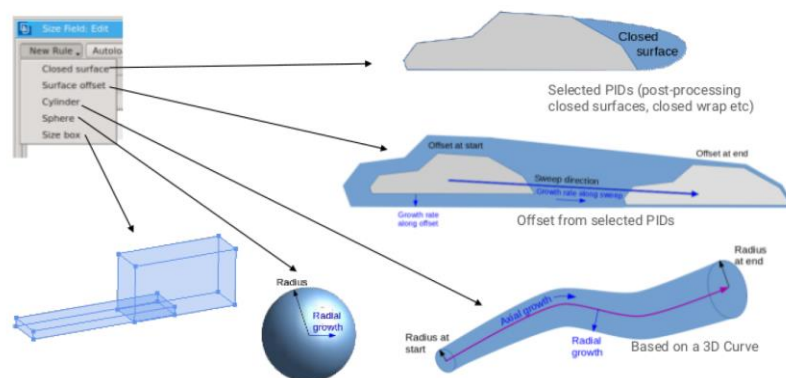


Figure 4.9 Size Field rules

Once the Size Field is set up the user can press “Build” so that ANSA calculates it. {9}

For this project, the choice was to build Size Fields with Size Boxes rule, to be sure to incorporate and detect all the turbulent structures that arise downstream of the car components and avoid irregularities. This is a good recommendation in open-wheels cars (Formula categories). In particular:

- The “wake” size box, as named, is built to refine the mesh around and behind the car to better capture the turbulent eddies and understand the wake structure.
- The “ground” size box is built to refine the mesh near the zones like the front wing, sidepods and diffuser. All these components work in ground-effect because they are really close to the ground so a well mesh refinement is needed.
- The “rear\_wing” size box, as named, is built to refine the mesh in a specific aerodynamic component which is crucial in the downforce generation due to its surface dimension, high position, and multi-element wing construction.

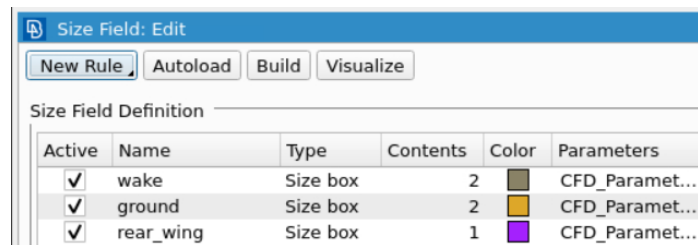


Figure 4.10 Size Field

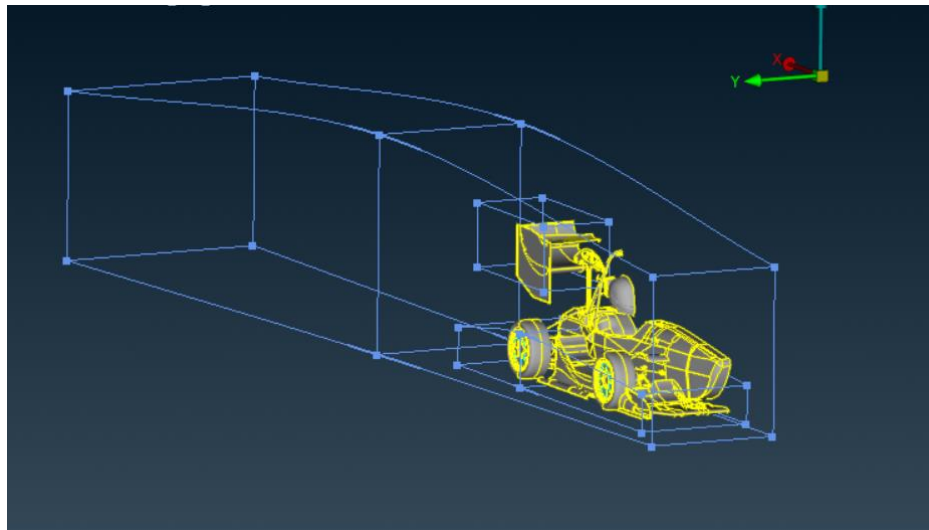


Figure 4.11 Representation of refinement Size Boxes

An important recommendation is that the Size Boxes should not be tangential to the geometry but must go a little further, especially on the plane of symmetry (if there is one). This is because, in case of tangency of the box, it is not guaranteed that the refinement will be carried out as the box could rest on the plane of symmetry and/ or other geometries, creating interference. The purpose of Size Boxes is to capture a portion of geometry and make sure that in this area are set limits for the size of surface and volumetric mesh. Therefore, after the construction of Size Boxes is applied an offset by the appropriate command.

- **Quality criteria are changed.**
  - Automotive\_y+1\_StarCCM is a template generated in ANSA v24 with USFs tool which is useful for FSAE applications.

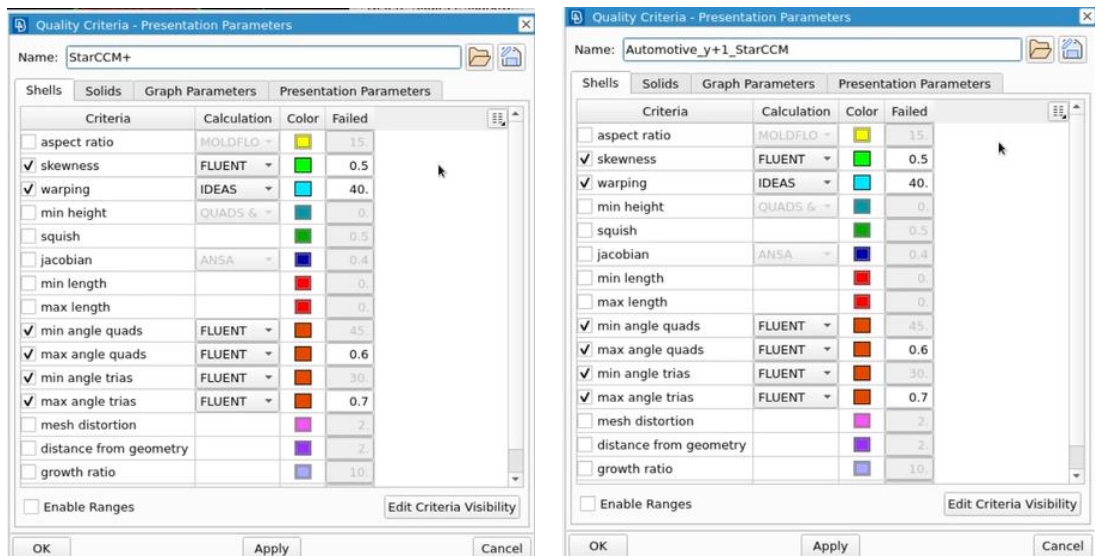


Figure 4.12 Automotive\_y+1\_StarCCM quality criteria enable in USFs of ANSA v24

- **Revision of the Batch Mesh Scenario for the surface mesh, with changes to the treatments applied to the Features (the leading-edge recognition was limited to "Wings" and "Diffuser" sessions because in the rest of the car is unnecessary).**

- **Reorganization of the Batch Mesh Scenario for prism layers, to reduce mesh generation times.**

- The generation of prism layers in ANSA occurs in parallel (using all the CPU) so, having separate sessions, delays mesh generation.  
Furthermore, if the layers were made in multiple sessions, ANSA does not guarantee that, if there were communicating parts between the various sessions (e.g. the ground connected to the contact patch) the mesh connects to the interface in a compliant manner.  
There would be no guarantee of continuity between the volume layers of the car and the road.

| Prism_Layers    |    | 58 |                |          |
|-----------------|----|----|----------------|----------|
| Layers Condotti | 7  |    | CFD parameters | StarCCM+ |
| Rad             | 1  |    | CFD parameters |          |
| Layers Car      | 51 |    | CFD parameters | StarCCM+ |
| Inlets-Outlets  | 3  |    | CFD parameters |          |
| Road            | 1  |    | CFD parameters |          |

| Prism_Layers |    | 56 |                |                     |
|--------------|----|----|----------------|---------------------|
| Car          | 56 |    | CFD parameters | Automotive_y+1_S... |
| Rad          | 1  |    | CFD parameters |                     |
| Condotti     | 5  |    | CFD parameters |                     |
| Road         | 1  |    | CFD parameters |                     |

Figure 4.13 Prism layers Scenario setted in the second version of Batch Mesh

- **Revision of Batch Mesh Scenario for volumes, to improve mesh quality.**

- Tetra Rapid algorithm (in “MRFs” and “Collettore” sessions, because there is no advantage to use Hexa Interior where volumes have to rotate).  
The Tetra Rapid algorithm gives tetrahedral mesh (and pyramid elements, if the surface mesh contains quad elements). It is most suited for geometries of thick volumes or large domains with significant variation in length of the surface mesh (say more than 2 orders of magnitude). Such geometries are mainly found in CFD applications.
- Hexa interior algorithm (useful when the air flows in a main direction, furthermore, it needs enough space because it starts from the surfaces and then moves inside the volume, creating first the tetrahedrons, then the pyramids and then the hexa, which must have space to grow).

- **Revision of Batch Mesh Scenario for layers and volume, to fix mesh problems.**

- "Fix Quality" was activated in all sessions, having verified that it only takes 3 minutes and manages to correct almost all problems

```
Running fix quality on created solids :
Fixing Solids Quality. layers + volume mesh fix quality
Trying to fix 133 violating and neighboring elements...
Fix Solids Quality results: fixed 131, skipped 0, moved 74 nodes, maximum movement= 0.37506, average movement= 0.02846
Worst quality values of violating elements:
Skewness : 85.411184
Completed in 2min:59.1sec
```

Figure 4.14 Time taken by the "fix quality" visible in the log of mesh operation

## 4.2. Results

The meshing process resulted in about 80 million cells with only 2 elements off.

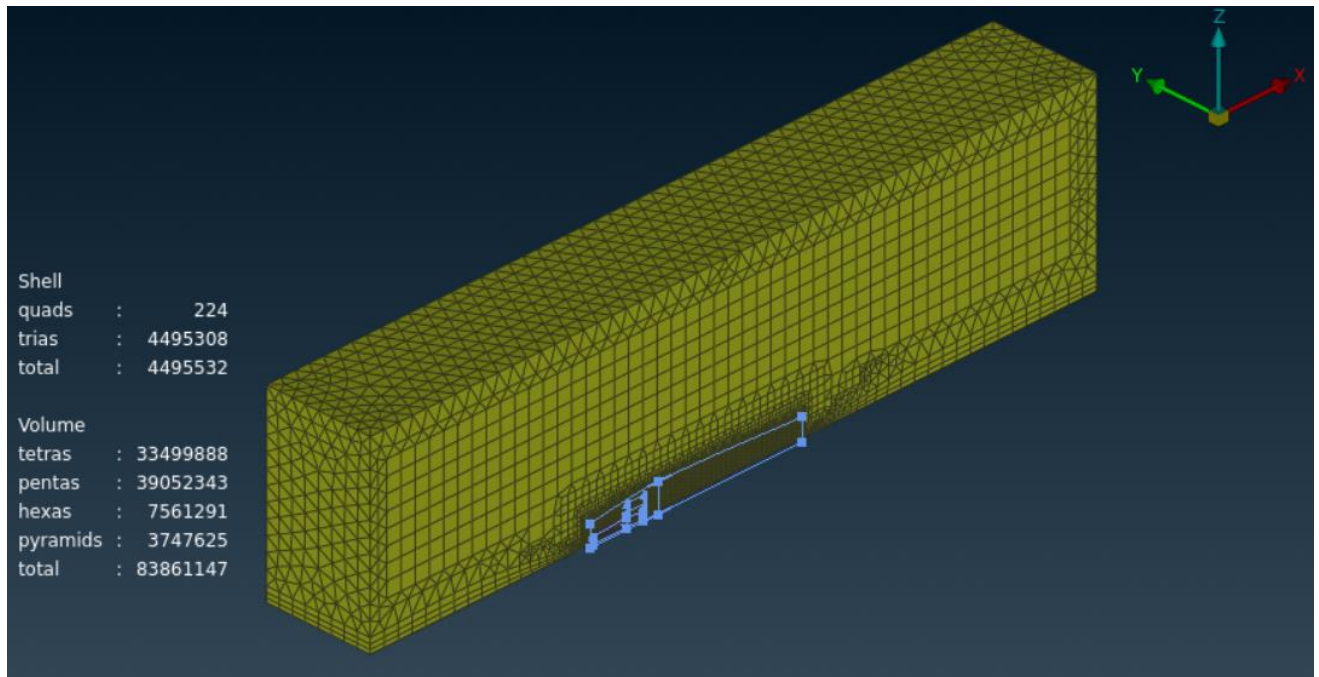


Figure 4.15 Computational domain

In figure 4.15 is represented the overall meshed computational domain, which has a symmetry shape to reduce the computational cost of the meshing and solving phases.

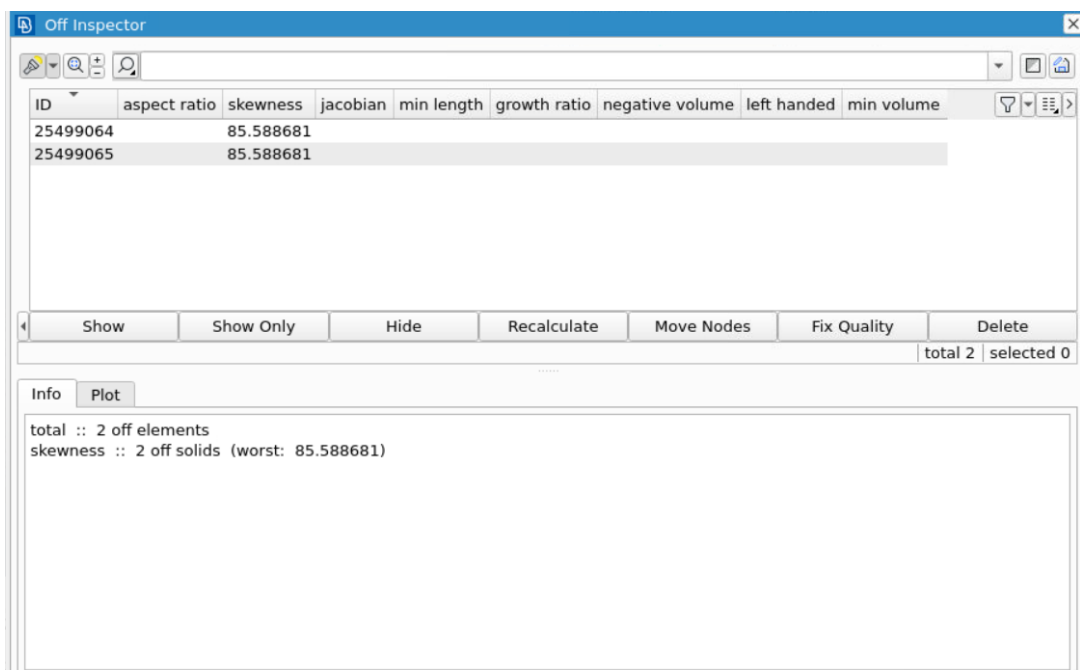


Figure 4.16 Off Inspector tool

Figure 4.16 represents the only 2 off elements about skewness quality criteria in ANSA mesh.

Subsequently, the conversion into polyhedra was performed, using these steps:

- MESH → Volumes → Conv2Poly (with default settings).
- USFs → SetQualityCriteria → STAR-CCM+ | y+1 | Polyhedral mesh=Conv2Poly  
This step is very important in order to disable some criteria which could slow down the quality control with polyhedral mesh and/or obtain a number of off elements which is higher than reality.
- MESH → Volumes → Improve → Fix quality

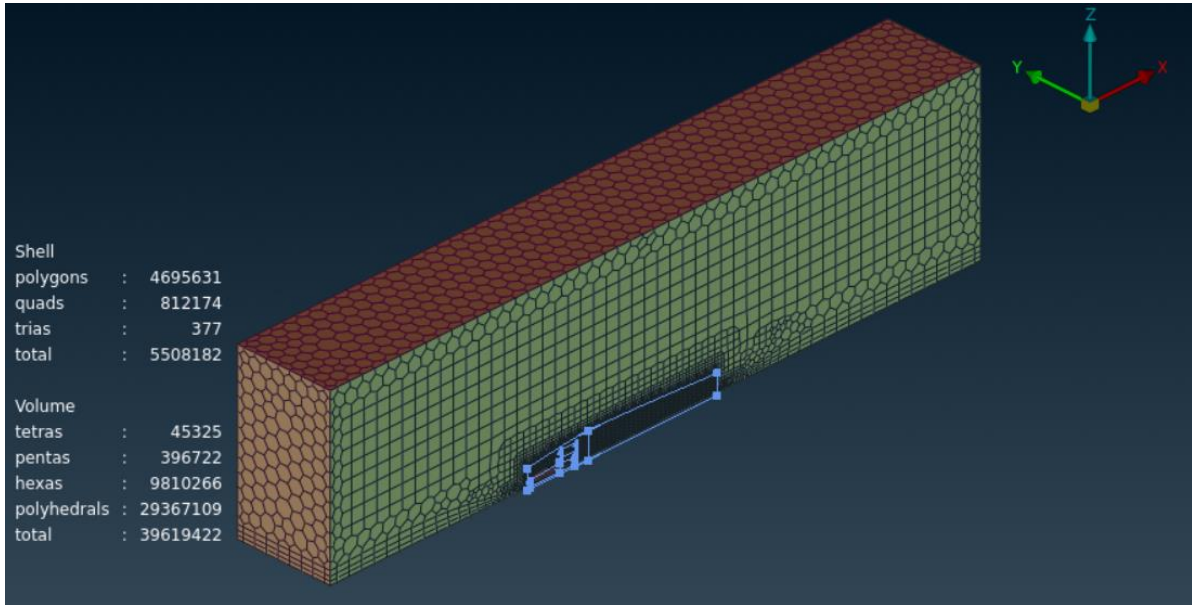


Figure 4.17 Computational domain

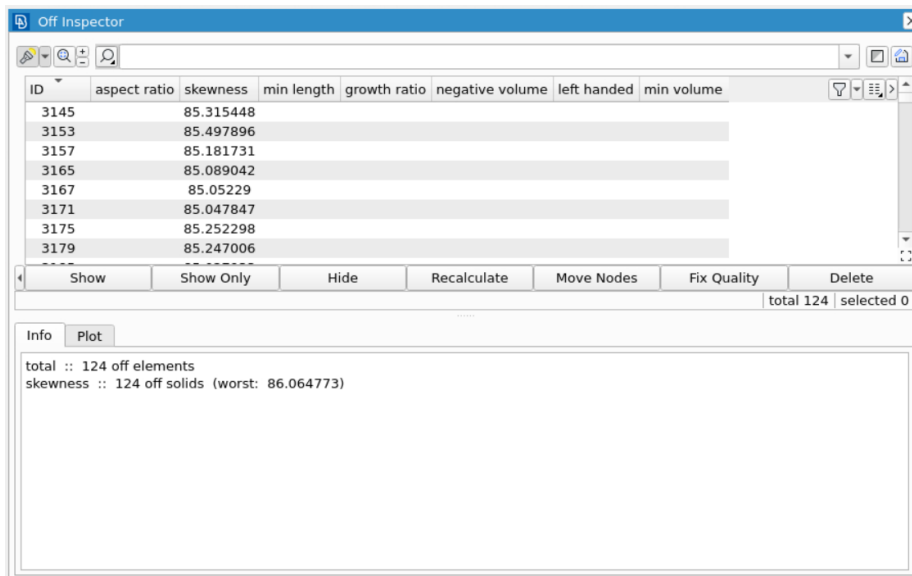


Figure 4.18 Off Inspector tool

Figure 4.17 and 4.18 shows that the result of polyhedral conversion was very positive:

- 52.7 % of cells reduction,
- around 1300 off elements corrected in less than a minute, leaving only 124 cells off (with skewness just above 85) located in non-critical areas.

# 5. Comparisons

## 5.1. Meshes Comparison

Generally, a poor-quality volume mesh can result in a significant reduction and efficiency of the obtained CFD results, so it is fundamental to check the validity of the mesh and get statistics on the mesh quality.

To check the overall validity and quality of the volume mesh and to compare the StarCCM+ mesh with the ANSA Meshes, some histogram plots based on important parameters were made.

These parameters are:

- Cell skewness angle
- Face validity metric
- Cell quality metric
- Volume change metric
- Chevron quality indicator

### Skewness angle

The cell skewness angle is a proper indicator of the mesh quality and suitability.

To understand its meaning, we consider the following 2D representation of two adjacent cells, which are separated by a mutual face.

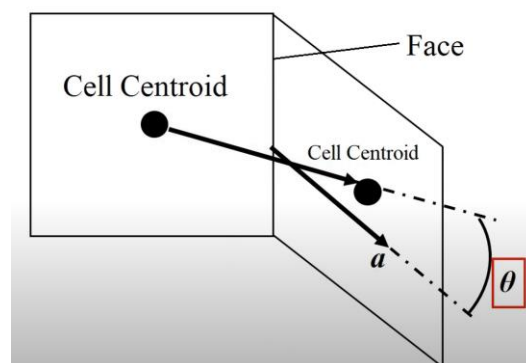


Figure 5.1 Skewness Angle representation

The skewness angle  $\theta$  is the angle between the face area vector (face normal) represented by “a”, and the vector connecting the two cells centroid.

If  $\theta = 0$ : it's the best situation with an orthogonal mesh.

To reduce the influence on the CFD results, it is recommended to keep the skewness angle  $< 85^\circ$ .



## R13 STAR-CCM+ Mesh

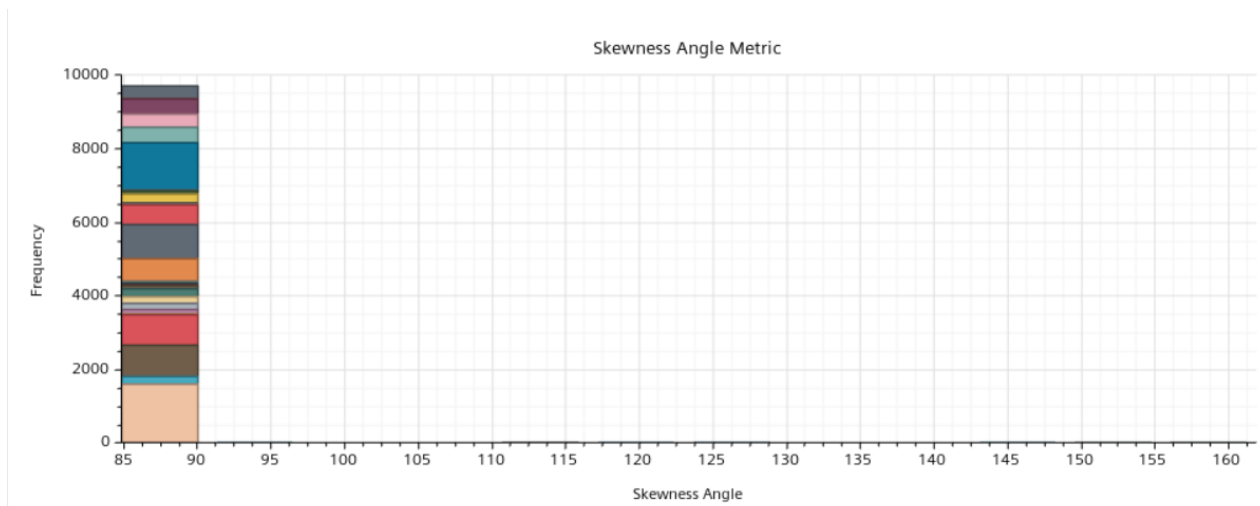


Figure 5.2 R13 STAR-CCM+ Mesh Skewness angle histogram plot

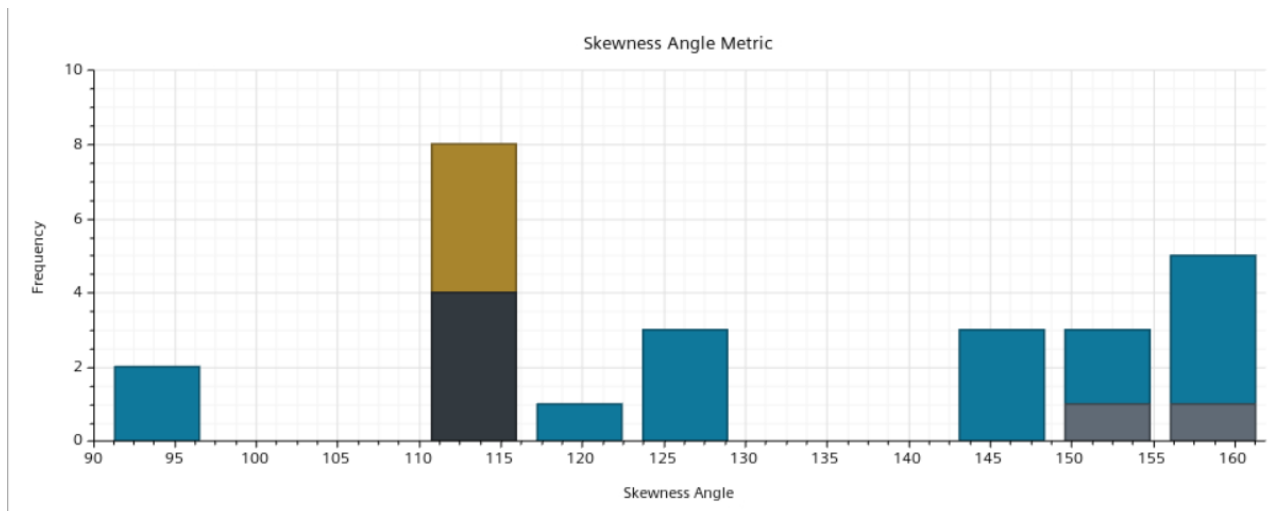


Figure 5.3 R13 STAR-CCM+ Mesh number of cells off recommended skewness angle limit

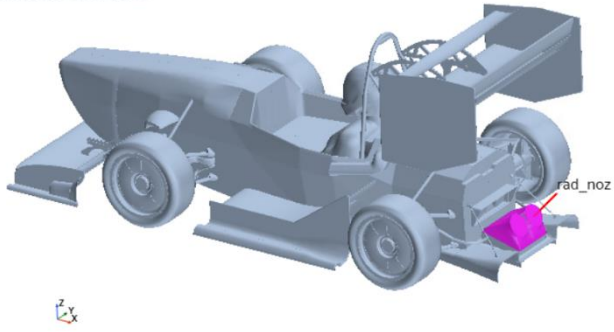
Figure 5.2 and 5.3 highlight the number of cells off relative to the quality criterion of the mesh skewness angle. In particular, the following details are shown:

- 9688 cells have skewness angle values between  $85^\circ$  and  $90^\circ$ .
- 25 cells have skewness angle values that exceed  $90^\circ$ .

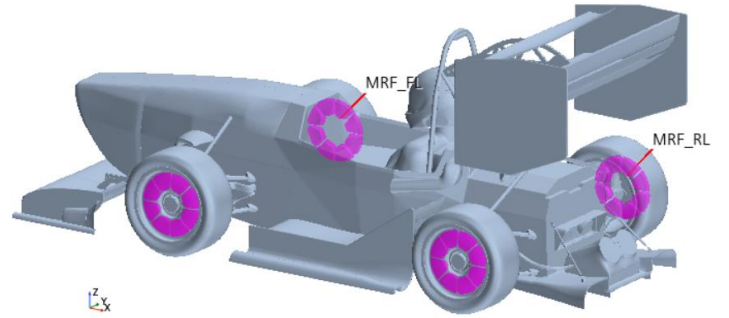
The most critical areas are those highlighted in figure 5.4:

- Moving reference frames have 1535 cells off with an  $87^\circ$  midpoint.
- Rad\_noz has 2649 cells off with an  $87^\circ$  midpoint.
- Radiator has 8 cells off with a midpoint of  $113^\circ$ .

Simcenter STAR-CCM+



Simcenter STAR-CCM+



Simcenter STAR-CCM+

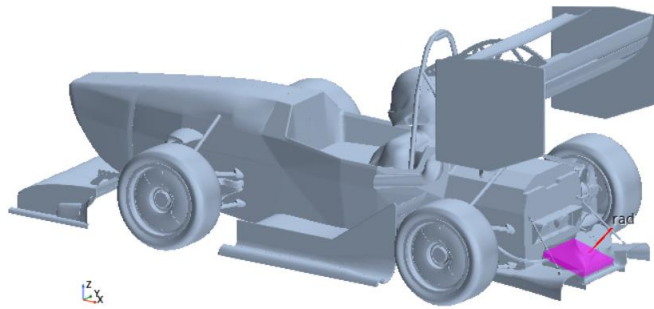


Figure 5.4 R13 STAR-CCM+ Mesh Skewness Angle critical areas

From these results we can understand that there are some areas of the car that have a mesh with cells that do not meet the skewness angle criterion and therefore can be improved.

## R13 ANSA Mesh

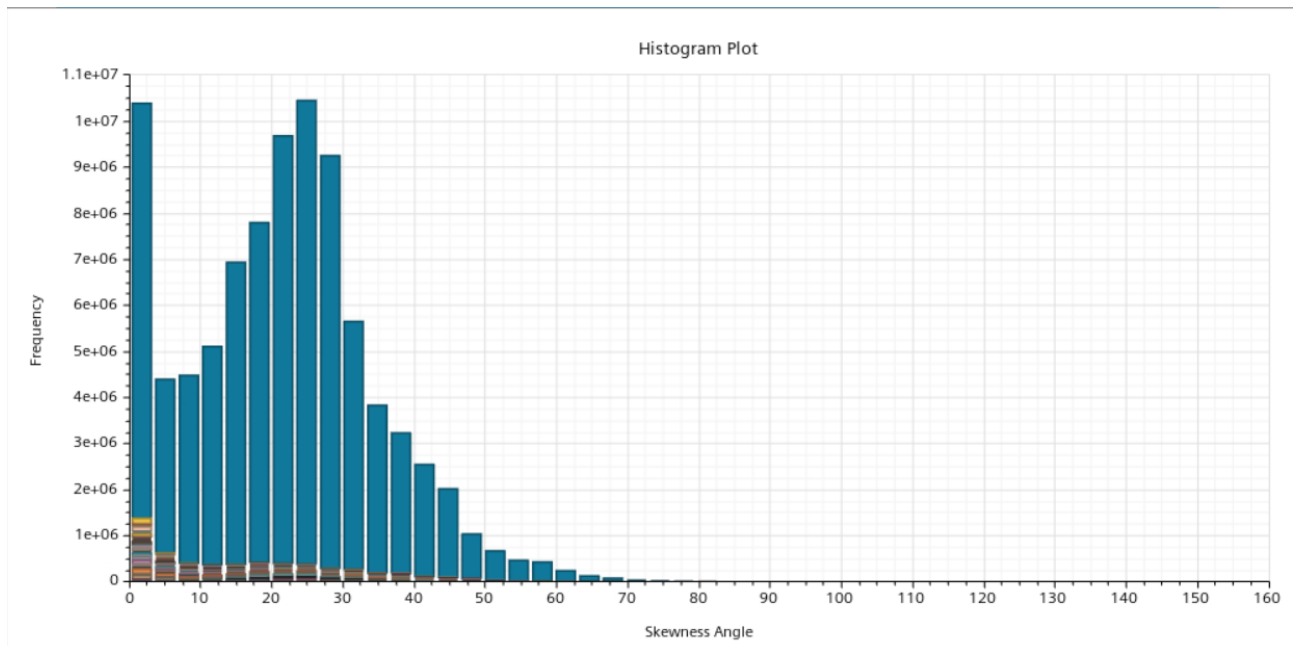


Figure 5.5 R13 ANSA Mesh Skewness Angle histogram plot

Figure 5.5 highlights the improvement achieved by using the ANSA mesh.

The mesh does not have any off cells from the skewness angle criterion, with values below 85°.

In particular, it can be noted that

- 39 MLN of cells (about 50% of the total) have skewness angle values < 20°.
- 63 MLN of cells (about 75% of the total) have skewness angle values < 30°.
- 75.6 MLN of cells (about 90 % of the total) have skewness angle values < 40°.

These results certify the quality of the new mesh and the big improvement with respect to STAR-CCM+ mesh.

## R13 ANSA Mesh Conv2Poly

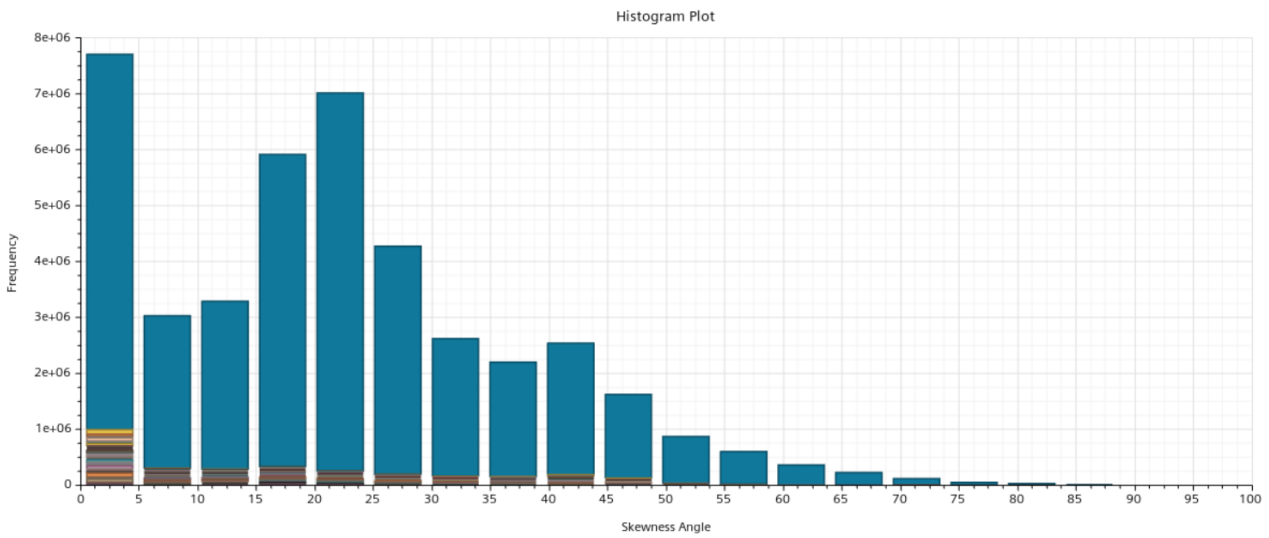


Figure 5.6 R13 ANSA Mesh Conv2Poly Skewness Angle histogram plot

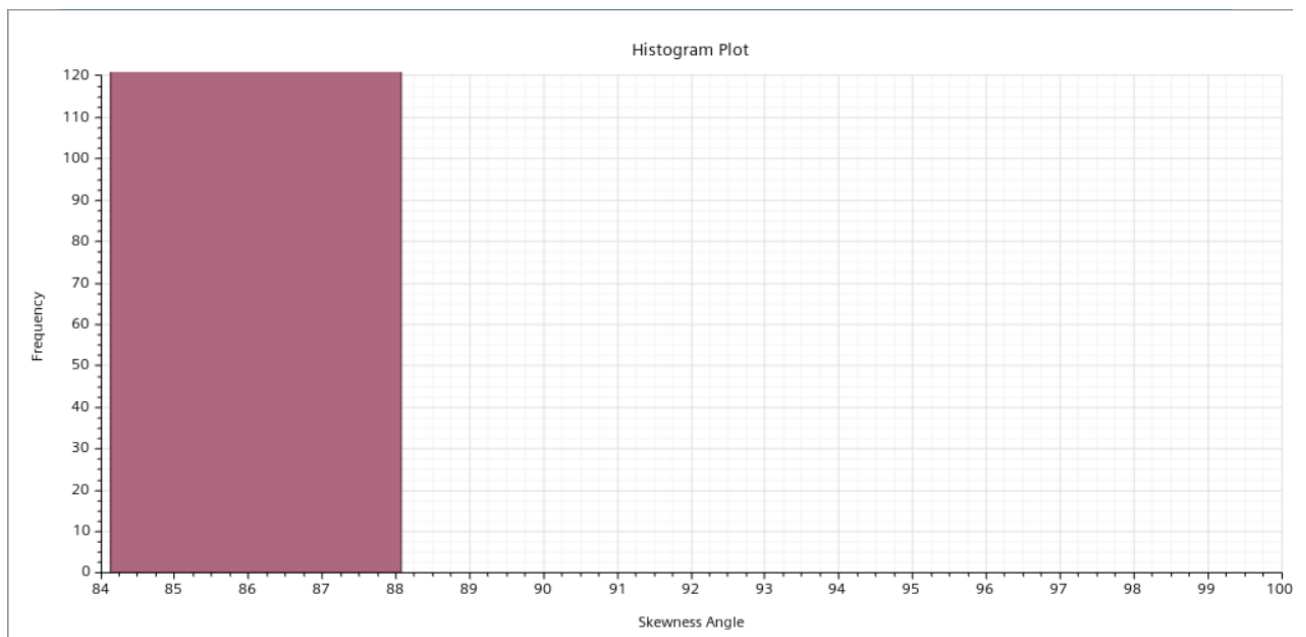


Figure 5.7 R13 ANSA Mesh Conv2Poly number of cells off recommended skewness angle limit

Figure 5.6 and 5.7 highlights the improvement achieved by using the ANSA mesh also with the polyhedral conversion.

We note that the ANSA Mesh Conv2Poly has:

- 35.9 MLN of cells (about 90 % of the total) with skewness angle values  $< 40^\circ$ .
- Only the radiator region with 120 cells off and skewness angle midpoint equal to 86.091.

These results certify the quality of the polyhedral mesh also and the improvement with respect to STAR-CCM+ mesh.

## Face validity

It is a measure of correctness of the face normal relative to cell centroid to which they are attached. In the picture below are represented a good quality cell (on the left side) with the face normals are pointing outwards with respect to the cell centroid, and a bad quality cell (on the right side) with one or more face normal are pointing toward the cell centroid.

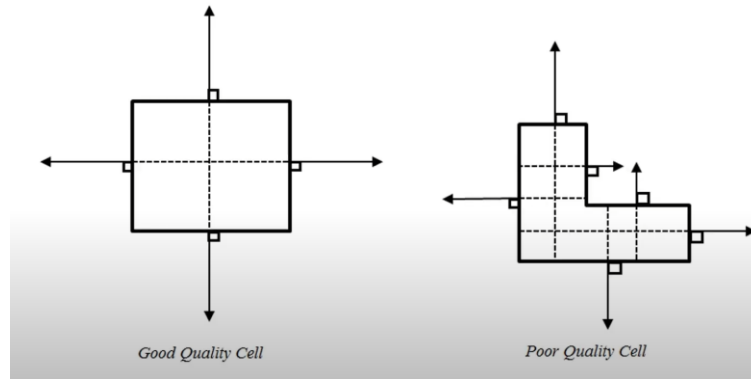


Figure 5.8 Face Validity representation

A face validity of 1.0 is an indication of a good quality cell. Values smaller than 0.5 indicate negative volume mesh and must be avoided.

## R13 STAR-CCM+ Mesh

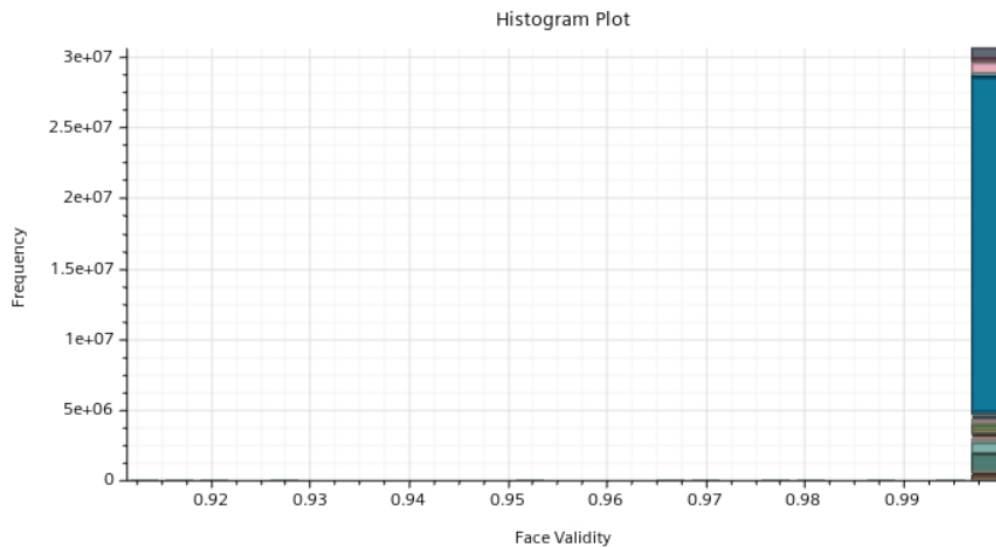


Figure 5.9 R13 STAR-CCM+ Mesh Face Validity histogram plot

The figure 5.9 represents the number of cells relative to the face validity quality criterion in the STAR-CCM+ mesh. In detail we can see how the cells have a good quality because their face validity midpoint is equal to 0.998, so really close to the ideal value of 1.

## R13 ANSA Mesh

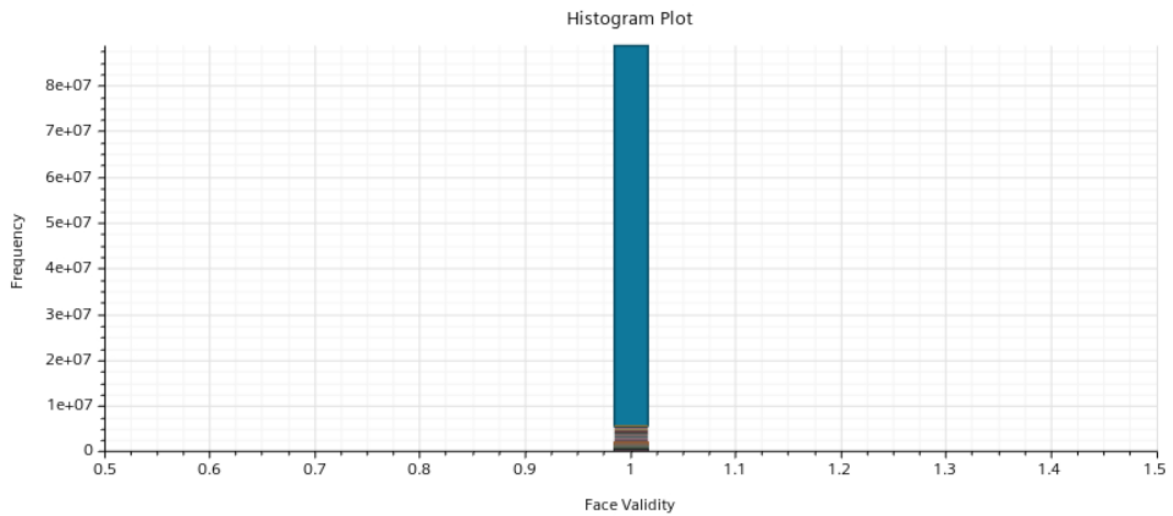


Figure 5.10 R13 ANSA Mesh Face Validity histogram plot

The figure 5.10 represents the number of cells relative to the face validity quality criterion in the ANSA mesh.

In particular, we can see how all the cells in the computational domain exceptional quality have because their face validity midpoint is equal to the ideal value of 1, so, all face normal are correctly pointing away from the cell centroid.

## R13 ANSA Mesh Conv2Poly

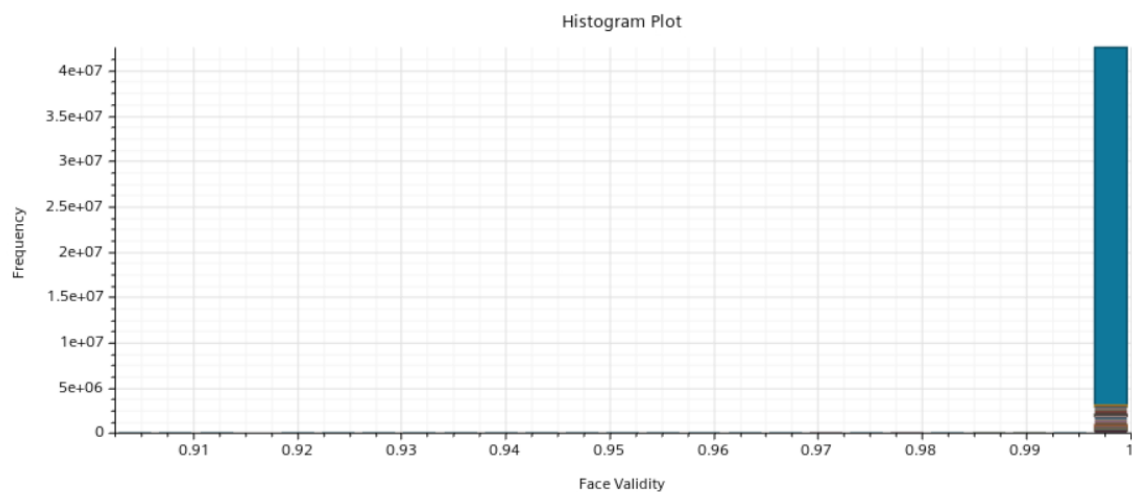


Figure 5.11 R13 ANSA Mesh Conv2Poly Face Validity histogram plot

The figure 5.11 represents the number of cells relative to the face validity quality criterion in the ANSA mesh with polyhedral conversion. In detail we can see how the cells have a good quality, like which of STAR-CCM+ mesh. Indeed, their face validity midpoint is equal to 0.998, so really close to the ideal value of 1.

## Cell quality metric

Cell quality is a metric that is determined from the relative geometric distribution of the cell centroids of the face neighbor cells and of the orientation of the cell faces. Generally flat cells with highly non-orthogonal faces have a low cell quality. As an example, these figures below show a good quality cell (on the left side) and a bad quality cell (on the right side).

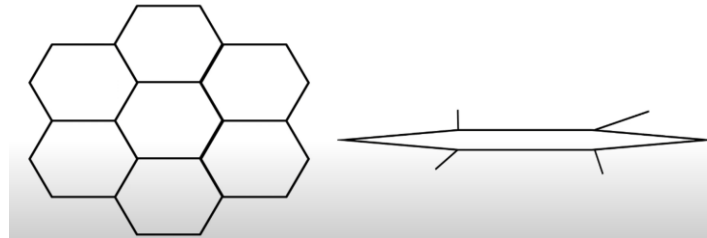


Figure 5.12 Cell Quality representation

A cell with a quality of 1.0 is considered perfect (a cubic cell is an example of such a perfect cell) and a cell with poor quality has a cell quality approaching zero. Cells with a quality less than  $1e-5$  are considered degenerated.

## R13 STAR-CCM+ Mesh

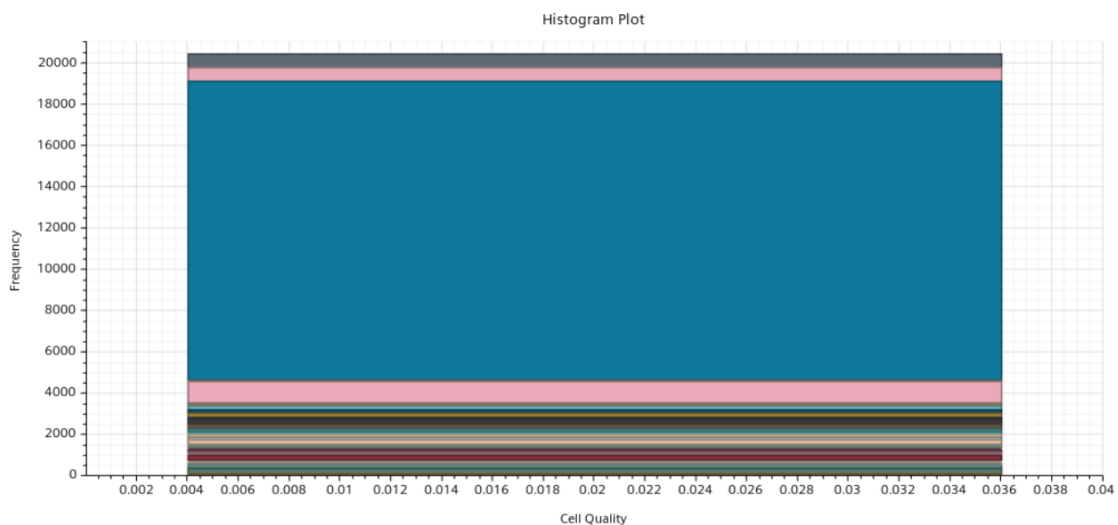


Figure 5.13 R13 STAR-CCM+ Mesh Cell Quality metric histogram plot

Figure 5.13 represent the cells of STAR-CCM+ mesh in relation to the cell quality metric. It can be seen that:

- None of the cells of the mesh is degenerated because their values are bigger than  $1e-5$ .
- There are some regions of interest as the moving reference frames and the endplates of the front wing which have low values of cell quality. In these regions the minimum value is equal to 0.004 and the midpoint is 0.02.

From these results we can understand that there are some areas of the car that have a mesh with cells that could be improved from the cell quality point of view.

## R13 ANSA Mesh

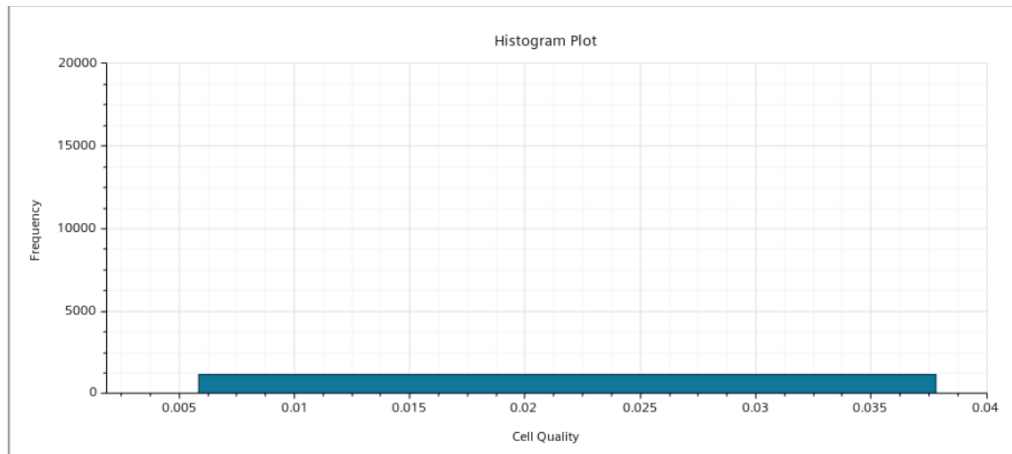


Figure 5.14 R13 ANSA Mesh Cell Quality metric histogram plot

The figure 5.14 represents the number of cells relative to the cell quality criterion in the ANSA mesh. It can be seen that:

- None of the cells of the mesh is degenerated because their values are bigger than  $1e-5$ .
- The regions of moving reference frames and front wing endplate don't show anymore low values of cell quality.
- The minimum value of this metric in all the domain has increased to 0.006, 50% bigger than STAR-CCM+ mesh.
- The overall number of cells which have low values of cell quality went drastically down with respect to STAR-CCM+ mesh (from 20000 to 1000, all located outside of the car).

These results certify the quality of the new mesh and the big improvement with respect to STAR-CCM+ mesh.

## R13 ANSA Mesh Conv2Poly

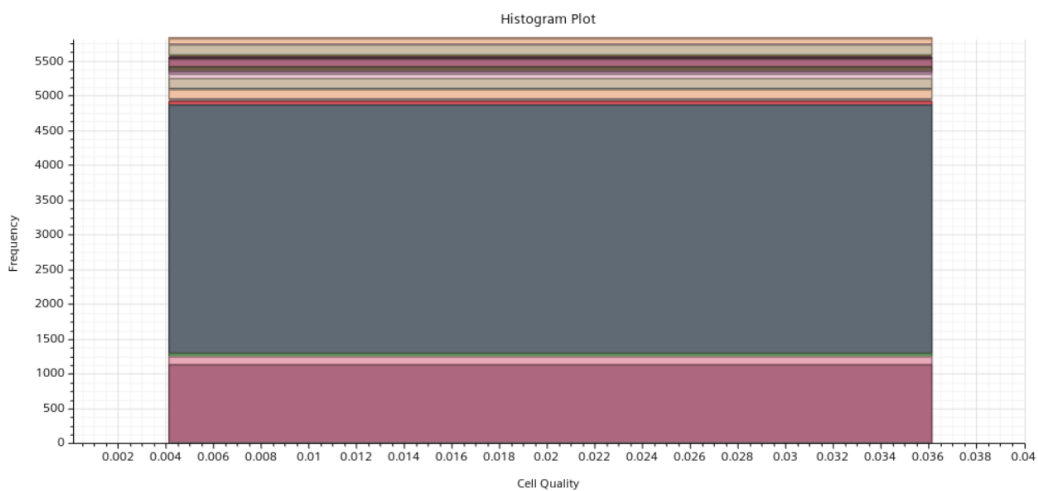


Figure 5.15 R13 ANSA Mesh Conv2Poly Cell Quality metric histogram plot



Figure 5.15 represents the number of cells relative to the cell quality criterion in the ANSA mesh with polyhedral conversion.

It can be seen that:

- None of the cells of the mesh is degenerated because their values are bigger than  $1e-5$ .
- The minimum value of cell quality metric in all the domain is very similar to which of STAR-CCM+ mesh (0.004).
- The overall number of cells which have low values of cell quality have decreased with respect to STAR-CCM+ mesh (from 20000 to 5500).

These results certify the quality of the polyhedral mesh also and the improvement with respect to STAR-CCM+ mesh.

### Volume Change metric

It evaluates the ratio of the volume of a cell to the largest volume of its neighboring cells.

As an example, this figure below shows a good quality cell (on the left side) and a bad quality cell (on the right side).

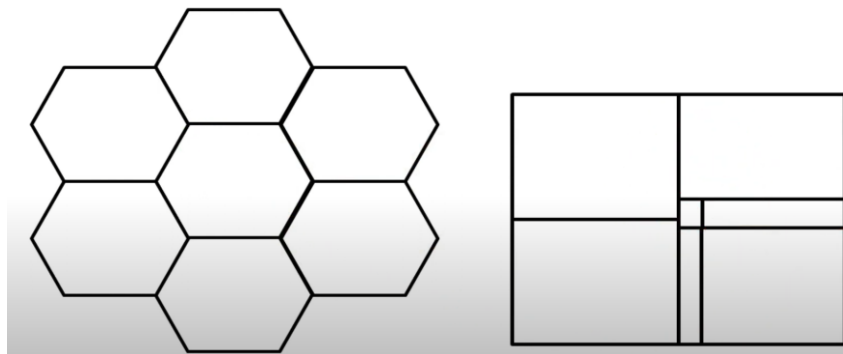


Figure 5.16 Volume Change representation

Sharp variations of the cell volumes in a vicinity of a cell can cause serious inaccuracies and instabilities in the solver.

Cells with poor quality are those with a volume change of 0.01 or less.

## R13 STAR-CCM+ Mesh

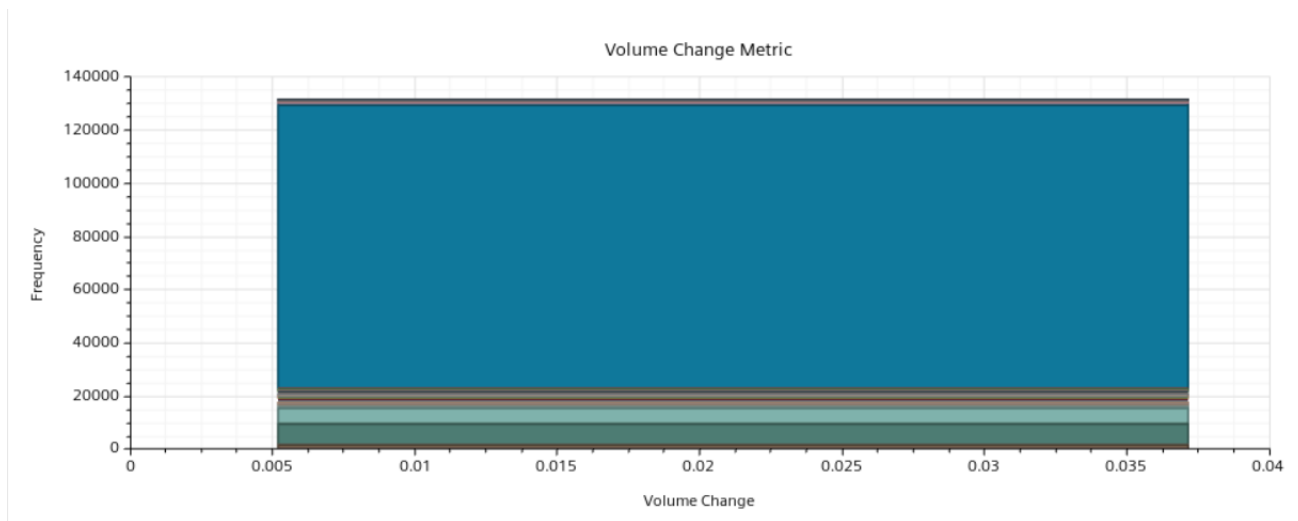


Figure 5.17 R13 STAR-CCM+ Mesh Volume Change metric histogram plot

Figure 5.17 represents the cells of STAR-CCM+ mesh in relation to the volume change quality metric. It can be seen that:

- The midpoint volume change value is equal to 0.02, so this is not critical for the cell quality.
- There are some regions of interest, highlighted in the figure 5.18 below (“collettore”, battery modules and the nozzle of radiator) which have low values of volume change. In these regions the minimum value is equal to 0.005.
- The overall number of cells with low volume change quality is about 131000.

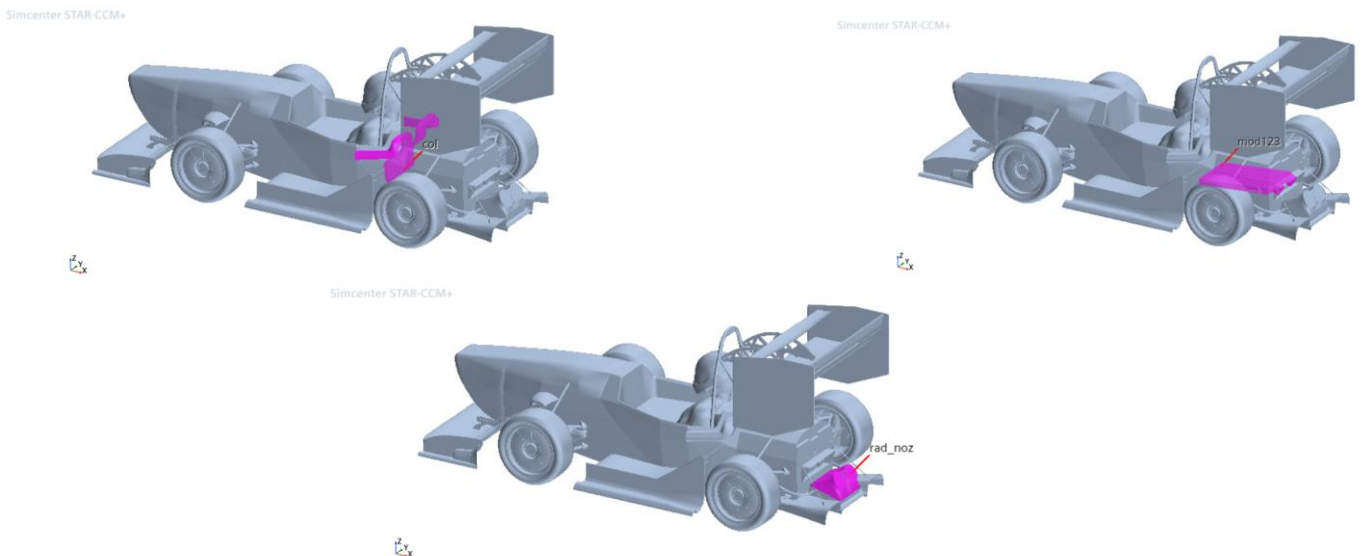


Figure 5.18 R13 STAR-CCM+ Mesh Volume Change areas of interest

## R13 ANSA Mesh

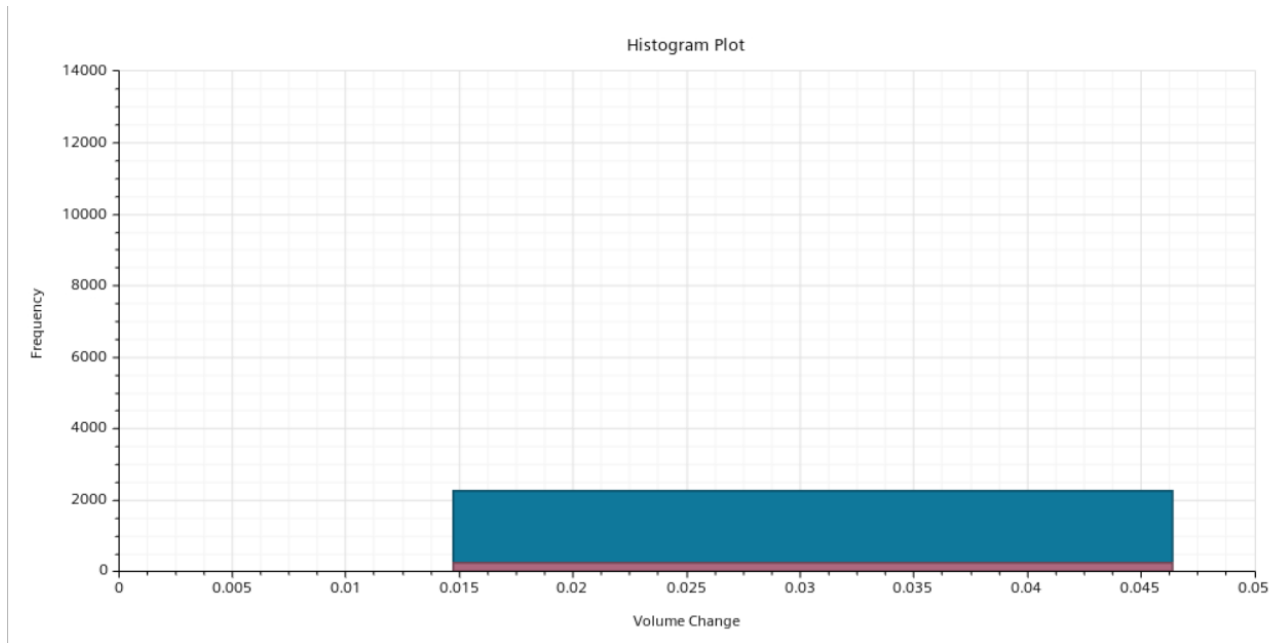


Figure 5.19 R13 ANSA Mesh Volume Change metric histogram plot

The figure 5.19 represents the number of cells relative to the cell quality criterion in the ANSA mesh. It can be seen that:

- None of the cells of the mesh is degenerated because their midpoint volume change value is bigger than 0.01.
- The regions of “collettore”, battery modules and the nozzle of radiator don’t show anymore low values of volume change.
- The minimum value of this quality metric in all the domain has increased to 0.014, almost three times bigger than STAR-CCM+ mesh.
- The overall number of cells which have low values of cell quality went drastically down with respect to STAR-CCM+ mesh (from 131000 to 2253, mostly located outside of the car).

These results certify the quality of the new mesh and the big improvement with respect to STAR-CCM+ mesh.

## R13 ANSA Mesh Conv2Poly

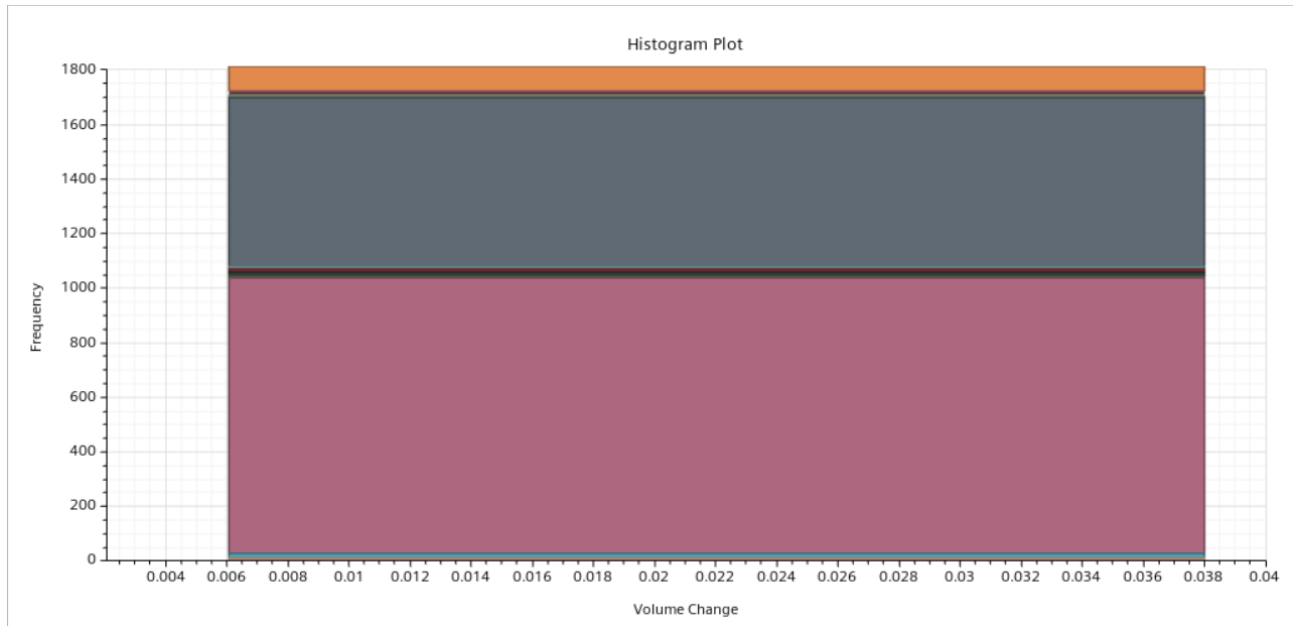


Figure 5.20 R13 ANSA Mesh Conv2Poly Volume Change metric histogram plot

The figure 5.20 represents the number of cells relative to the volume change criterion in the ANSA mesh with polyhedral conversion.

It can be seen that:

- None of the cells of the mesh is degenerated because their values are bigger than  $1e-5$ .
- The minimum value of cell quality metric in all the domain is slightly bigger to which of STAR-CCM+ mesh (0.006).
- The overall number of cells which have low values of cell quality have decreased with respect to STAR-CCM+ mesh (from 131000 to 1812).

These results certify the quality of the polyhedral mesh also and the improvement with respect to STAR-CCM+ mesh.

### Chevron quality

It associates a value of 1 to cells in which the line joining the cell centers (of two adjacent cells) does not pass through the common face. A value of 0 is attributed to every other cell.

For instance, the figure below shows a normal and a chevron cell.

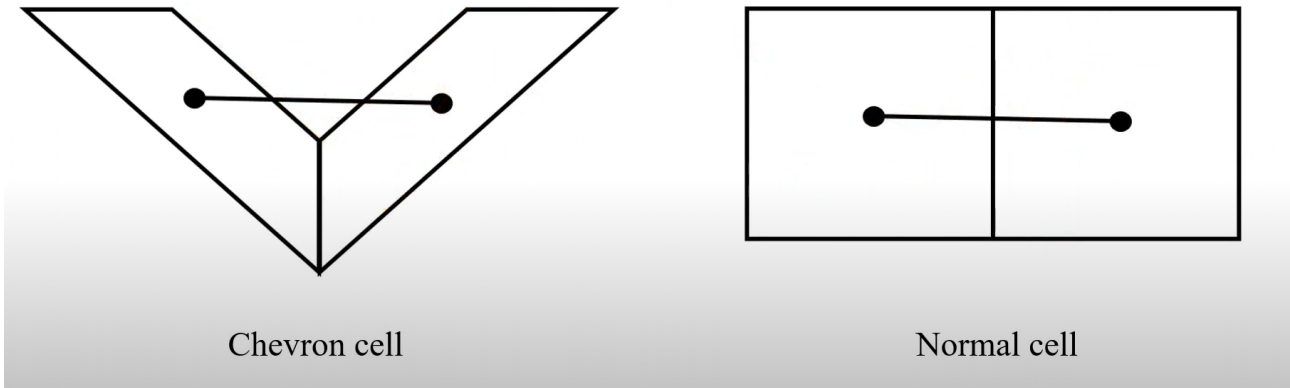


Figure 5.21 Chevron Quality cell representation

These cells are considered bad cells because they affect the accuracy and robustness in the calculation of the convective fluxes.

### R13 STAR-CCM+ Mesh

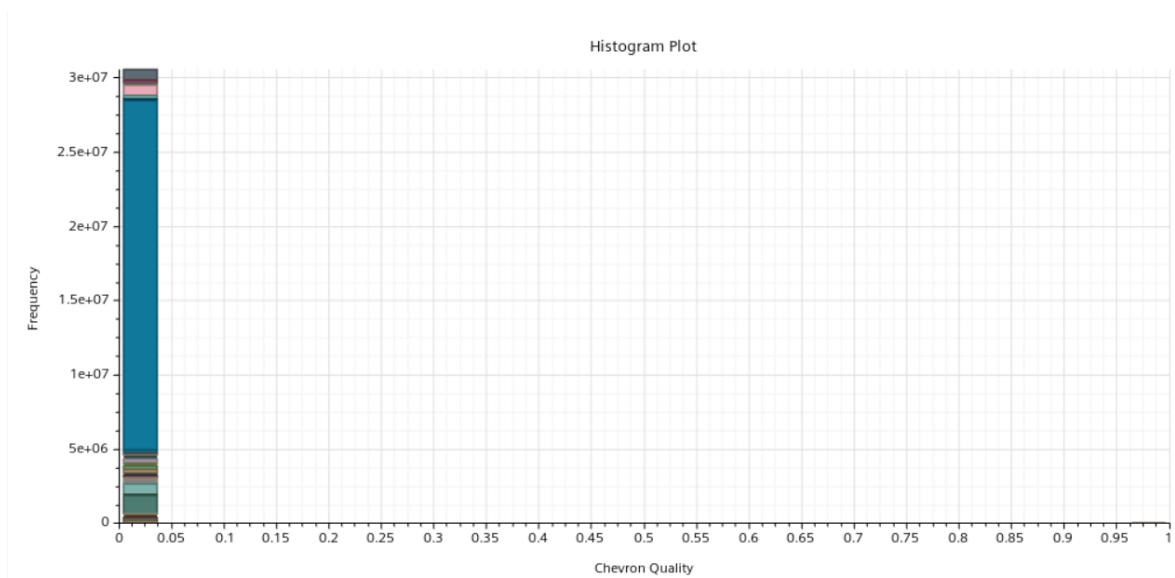


Figure 5.22 R13 STAR-CCM+ Mesh Chevron Quality metric histogram plot

## R13 ANSA Mesh

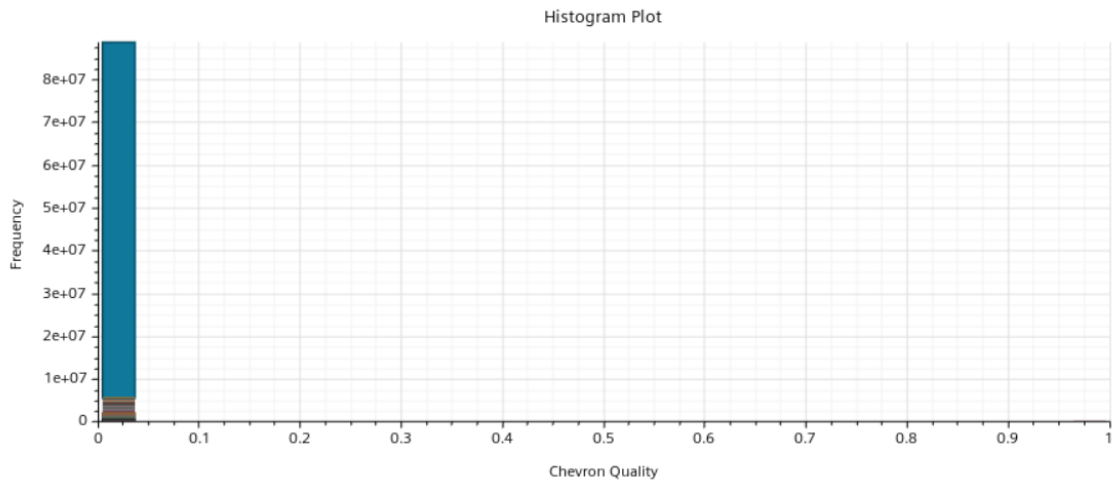


Figure 5.23 R13 ANSA Mesh Chevron Quality metric histogram plot

## R13 ANSA Mesh Conv2Poly

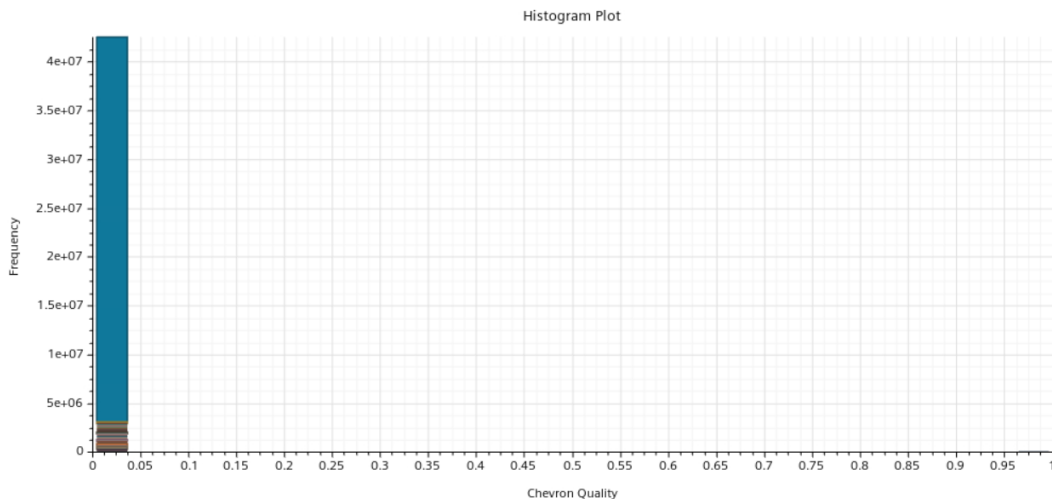


Figure 5.24 R13 ANSA Mesh Conv2Poly Chevron Quality metric histogram plot

Looking at figures 5.22, 5.23, 5.24, we can see how all the 3 built mesh have cells with Chevron quality indicator equals to 0.02, so there are no degenerated and critical areas related to this quality metric.

At the end of meshes comparison, we can say that there was a big improvement especially in the parameters like skewness angle, cell quality and volume change metrics and the goodness in the other metrics remained strong.

These factors allow us to say that the ANSA meshes enhanced the STAR-CCM+ mesh on the cells quality point of view and they produced cells with better accuracy. This last aspect will be rediscovered in the simulations based on these meshes even if we need experimental test to validate it.

## 5.2. Simulations Comparison

The comparison is between the 3 simulations (R13-R13 ANSA Mesh- R13 ANSA Mesh Conv2Poly) and it consist into the analysis of residuals plots, drag coefficients plots, lift coefficients plots, skin friction coefficients scenes and pressure coefficients scenes, to determine the effectiveness of the new ANSA mesh to produce convergent and stable simulations, capturing the main turbulence phenomena around the car and leading to good results.

### 5.2.1. Plots

In computational fluid dynamics (CFD), most fluid flow problems are inherently non-linear and involve unstable phenomena like turbulence. To solve these problems, iterative methods are employed to progressively refine the solution until "convergence" is achieved.

Convergence refers to the point where the solver addresses a discretized version of the governing and turbulence equations for each mesh cell. The residual in each cell represents the degree to which the discretized equation is satisfied.

As the solution progresses, a semi-logarithmic graph is generated to track the residuals associated with each governing equation (such as mass, momentum, and energy conservation).

Residuals are a key indicator of convergence in iterative solutions, as they quantify the error in solving the system of equations. Specifically, they represent the local imbalance of a conserved variable within each control volume.

In an iterative numerical solution, the residual will never be exactly zero. However, the lower the residual value is, the more numerically accurate the solution. For CFD, roots mean square residual levels of :

- 1E-4 are loosely converged.
- 1E-5 are well converged.
- 1E-6 are tightly converged.

For complicated problems, however, it's not always possible to achieve residual levels as low as 1E-6 or even 1E-5 so the convergence criterion should change in which that the normalized unscaled residuals should drop of 1E-3.

In general, a good residuals plot has several characteristics to identify: the key elements are decreasing lines and downward slopes, residuals should always decrease.

In the next pages are represented the Residuals plots, the lift coefficient plots, and the drag coefficient plots to compare the convergence of the simulations and the numerical results.

The lift coefficient (negative due to the reference system) and drag coefficient, are related to a reference surface equals to  $1.0 \text{ m}^2$ .

## R13 Simulation

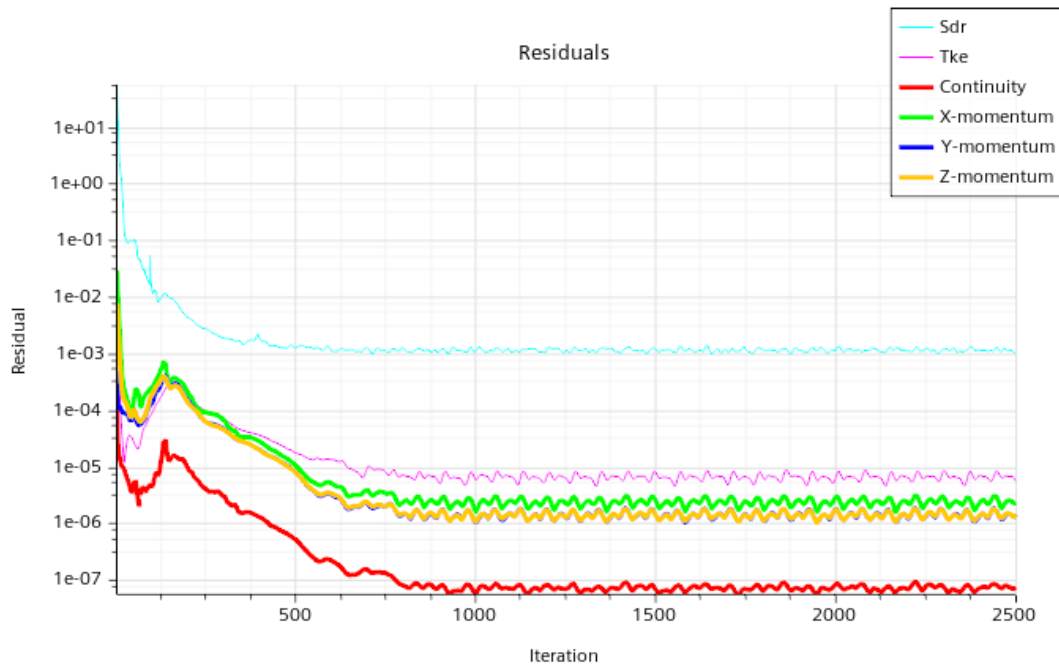


Figure 5.25 R13 Simulation Residuals

Figure 5.25 represents the convergence behavior of various residuals in R13 simulation, plotted against the number of iterations.

Each residual is color-coded and labeled in the legend:

- Sdr (light blue): The specific dissipation rate residual.
- Tke (magenta): The turbulent kinetic energy residual.
- Continuity (red): The residual of the continuity equation, which represents the mass conservation of the system.
- X-momentum (green), Y-momentum (blue), and Z-momentum (orange): The residuals of the momentum equations along each respective coordinate axis.

About overall convergence behavior we can say that the early stages (up to approximately 500 iterations) show rapid decreases in residuals across all equations, which is a common indication of initial convergence where the solver quickly resolves major imbalances. Afterward, each residual either plateaus or decreases gradually, indicating that the simulation is reaching a steady-state solution. The plot reveals that the Sdr and Tke residuals plateau earlier, while the continuity and momentum equations continue to converge to lower magnitudes, though with some oscillations.

The minor fluctuations observed in the momentum and Tke residuals are typical in complex flows where turbulence and recirculation may cause small residual fluctuations, but they remain within acceptable bounds for steady-state solutions.



In this simulation, the values of CL.A and CD.A are multiplied by a factor 2 in the reports, monitors and plots, thanks to the «account for idealization» option in STAR-CCM+, which considers the symmetry of the model.

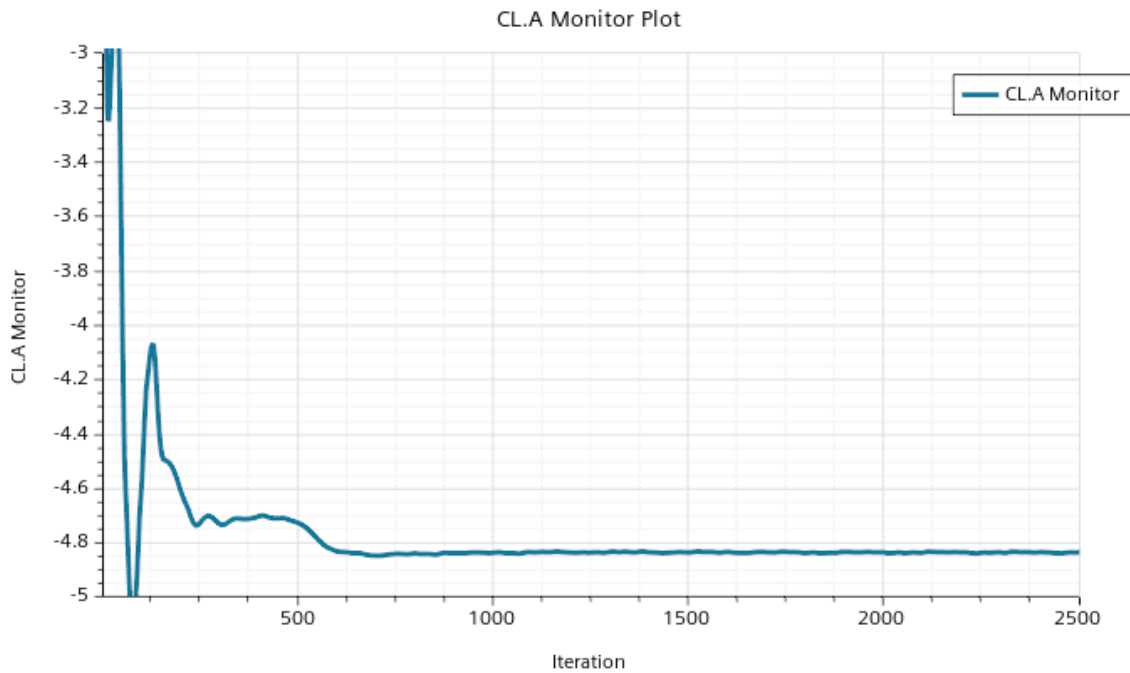


Figure 5.26 R13 Simulation Lift Coefficient monitor plot

Figure 5.26 Represents the lift coefficient (related to a reference area) monitor plot as a function of iterations of R13 simulation.

Overall, the CL.A Monitor Plot illustrates three main behavioral phases:

- period of instability (0-150 iterations), in which the CL.A values exhibit substantial fluctuations from -3 to -5.
- period of adjustment in which the CL.A values decreases to reach a value around -4.80 by about 550 iterations.
- period of small fluctuations where the CL.A is stabilized around a mean value of -4.84 and, at the end of the simulation CL.A equals to -4.836.

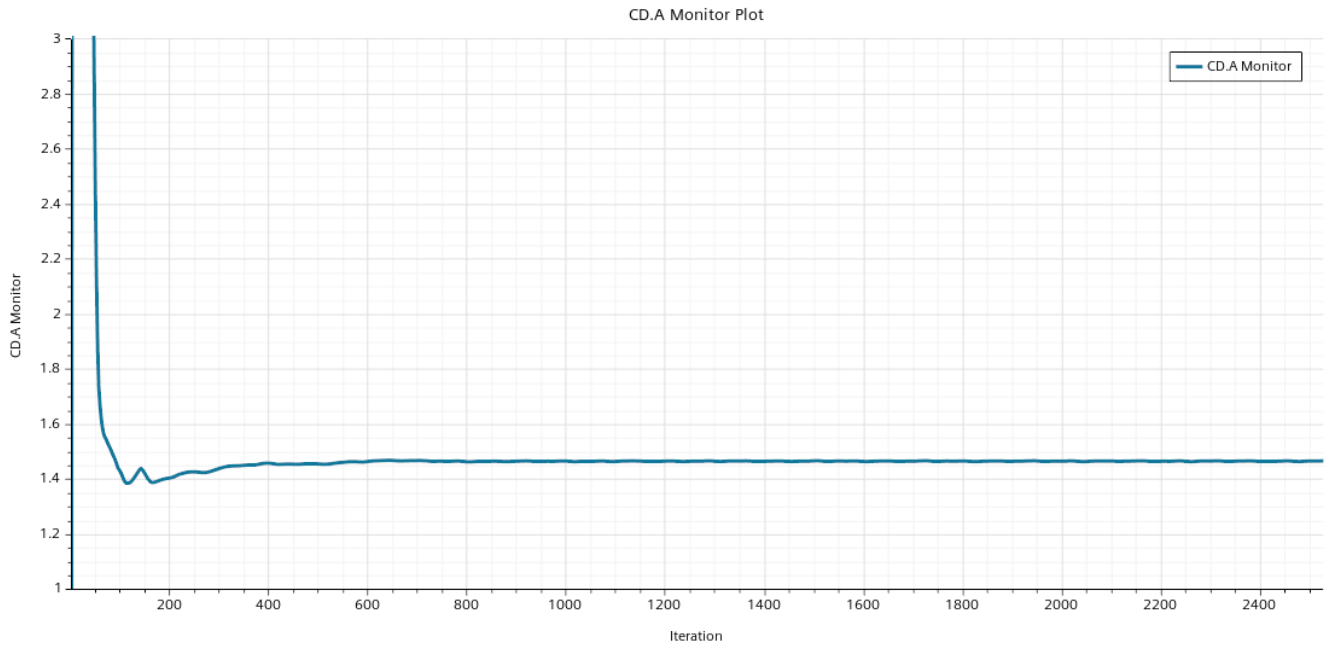


Figure 5.27 R13 Simulation Drag Coefficient monitor plot

Figure 5.27 Represents the drag coefficient (related to a reference area) monitor plot as a function of iterations of R13 simulation.

Overall, the CD.A Monitor Plot illustrates three main behavioral phases:

- period of high degrowth (0-160 iterations), in which the CD.A values exhibit substantial fall from 3 to 1.4.
- period of small fluctuation in which the CD.A try to find a stable value around 1.45 by about 400 iterations.
- period of stabilization where the CD.A are stabilized around a mean value of 1.46 and, at the end of the simulation CD.A equals to 1.465.

## R13 ANSA Mesh simulation

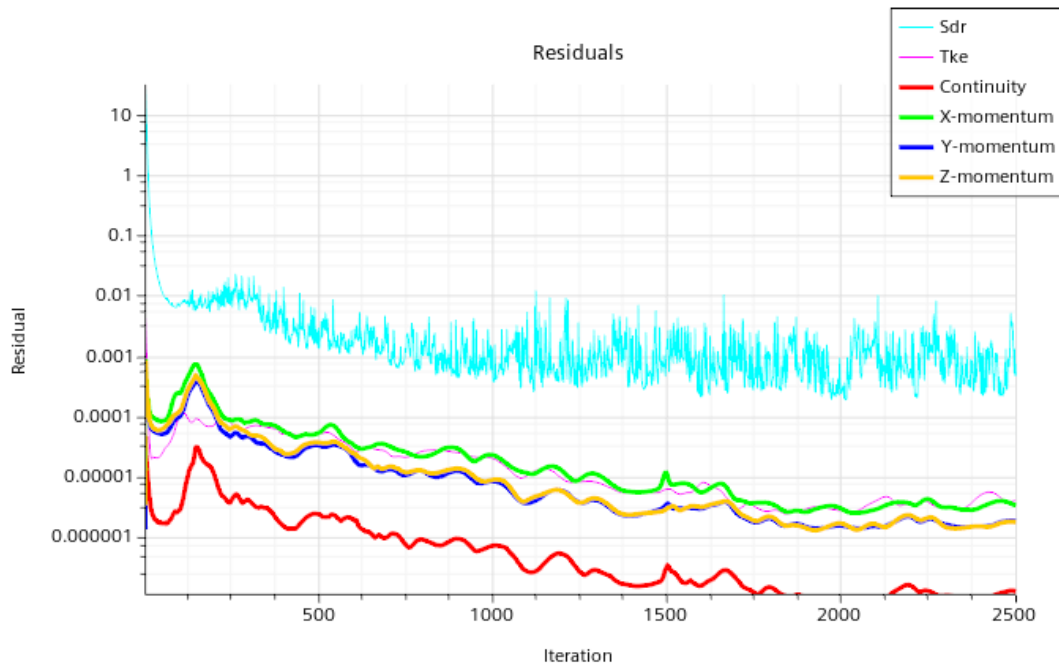


Figure 5.28 R13 ANSA Mesh Simulation Residuals

Figure 5.28 represents the convergence behavior of various residuals in R13 ANSA Mesh simulation, plotted against the number of iterations.

Each residual is color-coded and labeled in the legend as explained before.

About overall convergence behavior we can say that the continuity and momentum residuals, which are typically critical for assessing solution accuracy, have reduced to values near or below  $10^{-5}$  meeting standard convergence criteria in CFD simulations. The turbulence-related residuals (Sdr and Tke) show higher final values and fluctuations, which is common for turbulent flow simulations. The plateauing of these residuals around  $10^{-3}$ ,  $10^{-4}$  respectively, is often a practical limit for turbulence equations and is acceptable for steady-state simulations.

Given that the core residuals (continuity and momentum) have reached low values, the simulation can likely be considered converged and reliable for extracting flow characteristics.

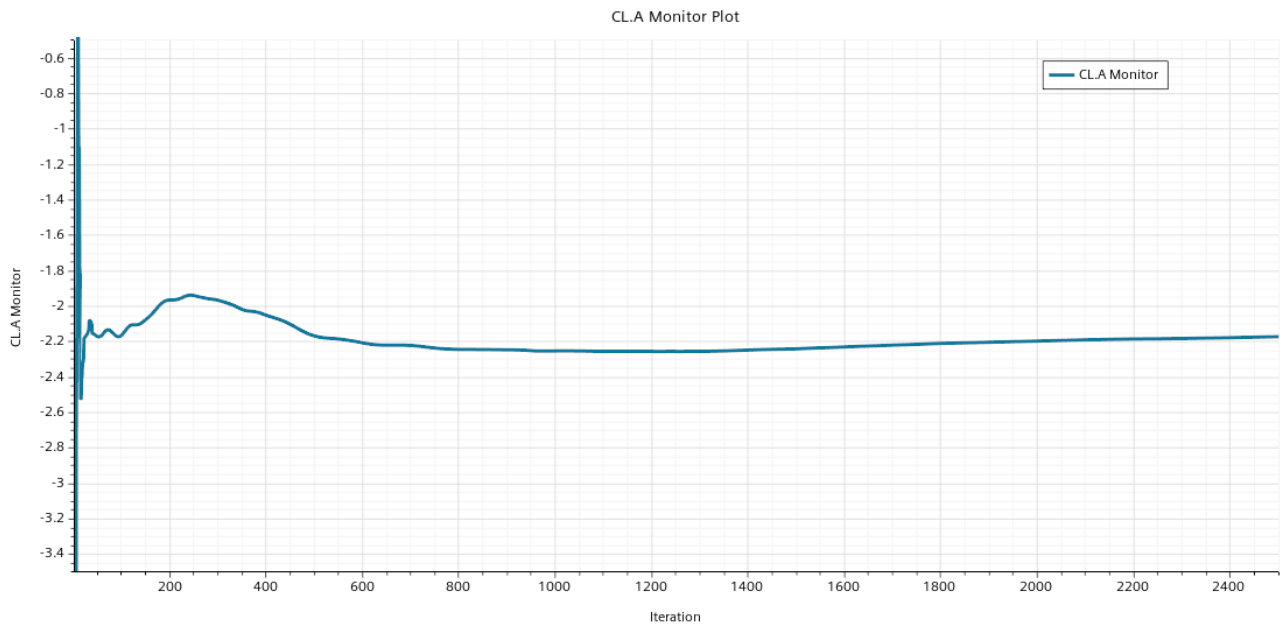


Figure 5.29 R13 ANSA Mesh Simulation Lift Coefficient monitor plot

Figure 5.29 Represents the lift coefficient (related to a reference area) monitor plot as a function of iterations of R13 ANSA mesh simulation.

Overall, the CL.A Monitor Plot illustrates three main behavioral phases:

- an initial period of instability (0-200 iterations), in which the CL.A values exhibit substantial fluctuations.
- followed by convergence to a relatively stable configuration, in which the CL.A values enter a period of relatively steady decline, where they stabilize and reach a value around -2.20 by about 600 iterations.
- and finally, a slight upward drift that suggests a small deviation from the previously CL.A values but it is quite a convergent plot with variations of hundreds of orders and a final CL.A equals to -2.174 (to be multiplied by two to take into account the fact that the simulation is carried out in symmetry, therefore with half of the car).

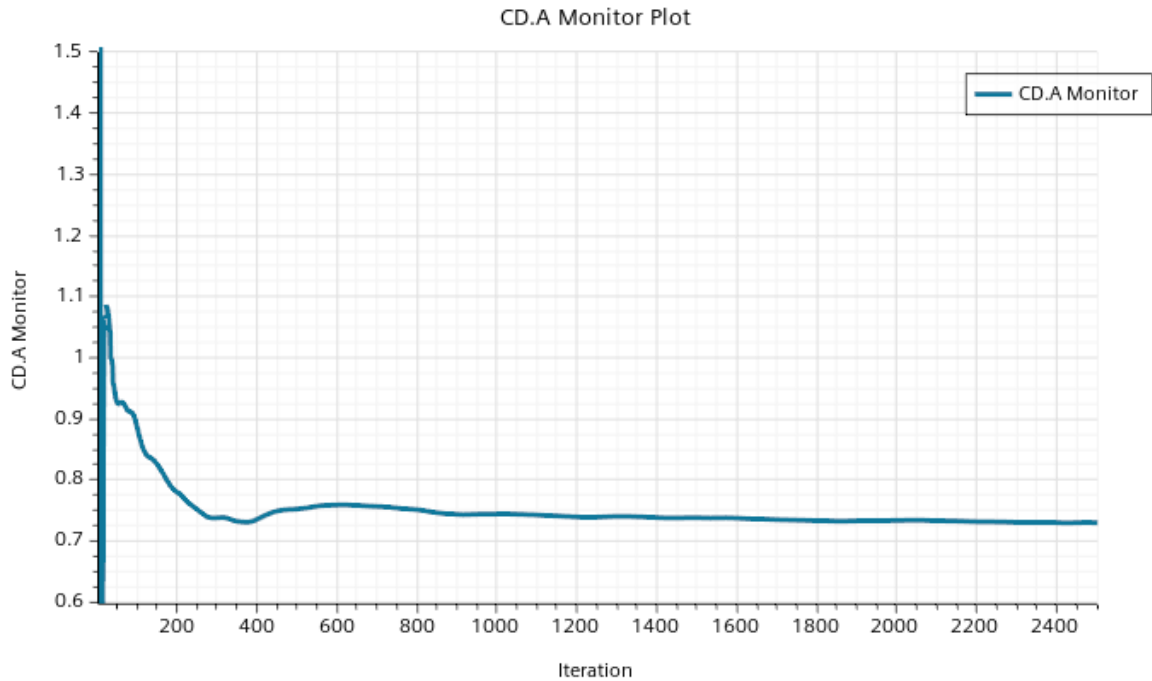


Figure 5.30 R13 ANSA Mesh Simulation Drag Coefficient monitor plot

Figure 5.30 Represents the drag coefficient (related to a reference area) monitor plot as a function of iterations of R13 ANSA mesh simulation.

Overall, the CD.A Monitor Plot illustrates three main behavioral phases:

- an initial period of instability (0-200 iterations), in which the CLA values exhibit high values and a rapid reduction.
- followed by an intermediate fluctuation and stabilization phase in which, after the initial decline, the CD.A values experience a slight rebound, rising from around 0.73 up to about 0.75 between 200 and 400 iterations. This fluctuation stabilizes by around 600 iterations, where the CDA values begin a downward trend again.
- and finally, a gradual improvement and convergence, indeed from 600 iterations onward, the CD.A values exhibit a slow, steady decline, reducing from approximately 0.74 to around 0.73 over the remaining iterations up to 2400 (the final value has to be multiplied by two to take into account the fact that the simulation is carried out in symmetry, therefore with half of the car).

## R13 ANSA Mesh Conv2Poly simulation

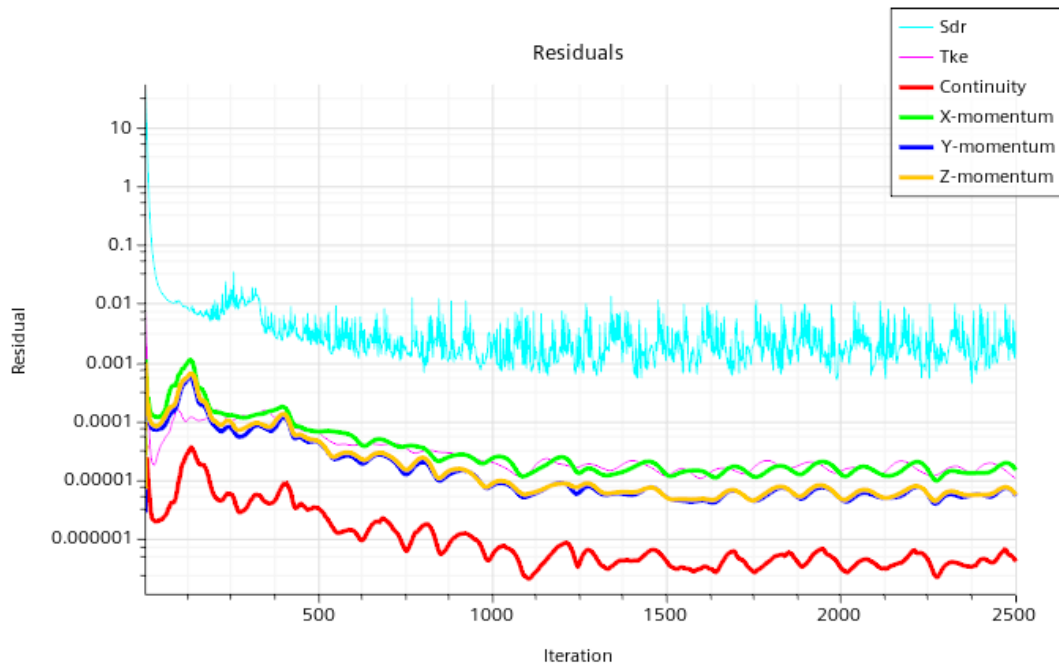


Figure 5.31 R13 ANSA Mesh Conv2Poly Simulation Residuals

Figure 5.31 represents the convergence behavior of various residuals in R13 ANSA Mesh Conv2Poly simulation, plotted against the number of iterations.

Each residual is color-coded and labeled in the legend as explained before.

About overall convergence behavior we can say that the continuity and momentum residuals, which are typically critical for assessing solution accuracy, have reduced to values near or below  $10^{-6} - 10^{-5}$  meeting standard convergence criteria in CFD simulations.

The turbulence-related residuals (Sdr and Tke) show higher final values and fluctuations, which is common for turbulent flow simulations. The plateauing of these residuals around  $10^{-2}, 10^{-4}$  respectively, is often a practical limit for turbulence equations and is acceptable for steady-state simulations.

Given that the core residuals (continuity and momentum) have reached low values, the simulation can likely be considered converged and reliable for extracting flow characteristics.

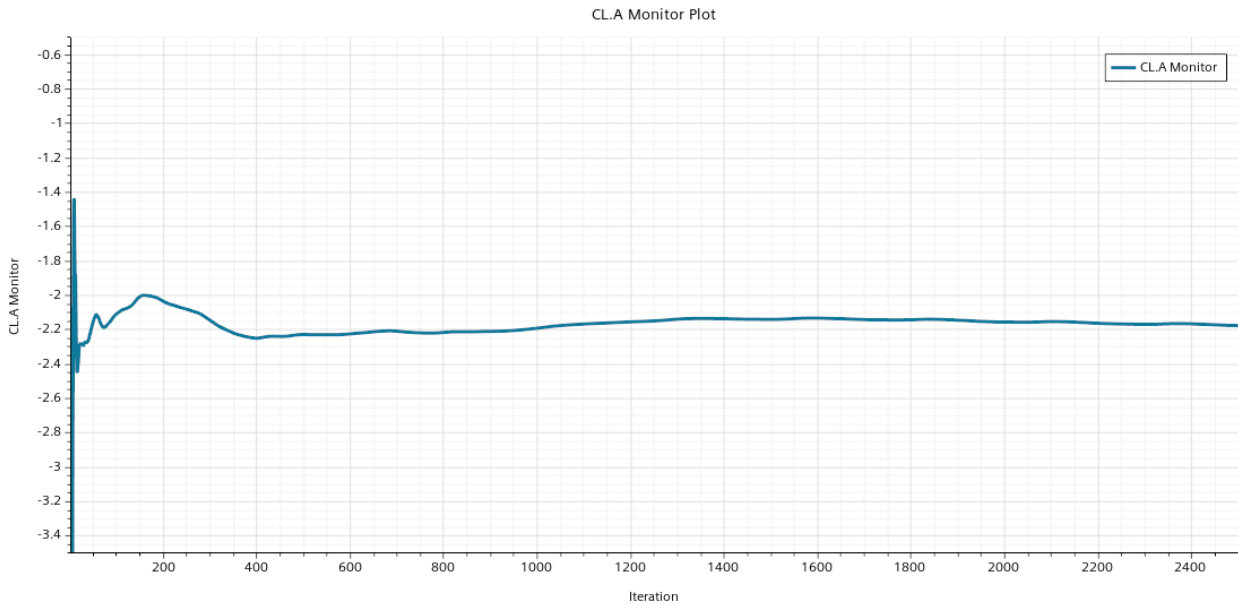


Figure 5.32 R13 ANSA Mesh Conv2Poly Simulation Lift Coefficient monitor plot

Figure 5.32 represents the lift coefficient (related to a reference area) monitor plot as a function of iterations of R13 ANSA mesh Conv2Poly simulation.

Overall, the CL.A Monitor Plot illustrates 4 main behavioral phases:

- an initial period of instability (0-200 iterations), in which the CL.A values exhibit high values, a rapid reduction and a subsequent growth to reach a value of -2.
- followed by an intermediate decrease phase in which, the CL.A values experience a decrease from -2 to -2.25 between 200 and 400 iterations.
- then there is a phase with a slight rebound of the CL.A, rising from around -2.25 up to about -2.17
- and finally, a gradual stabilization and convergence around -2.18 mean value, with a final CL.A equals to -2.178 (to be multiplied by two to consider the fact that the simulation is carried out in symmetry, therefore with half of the car).

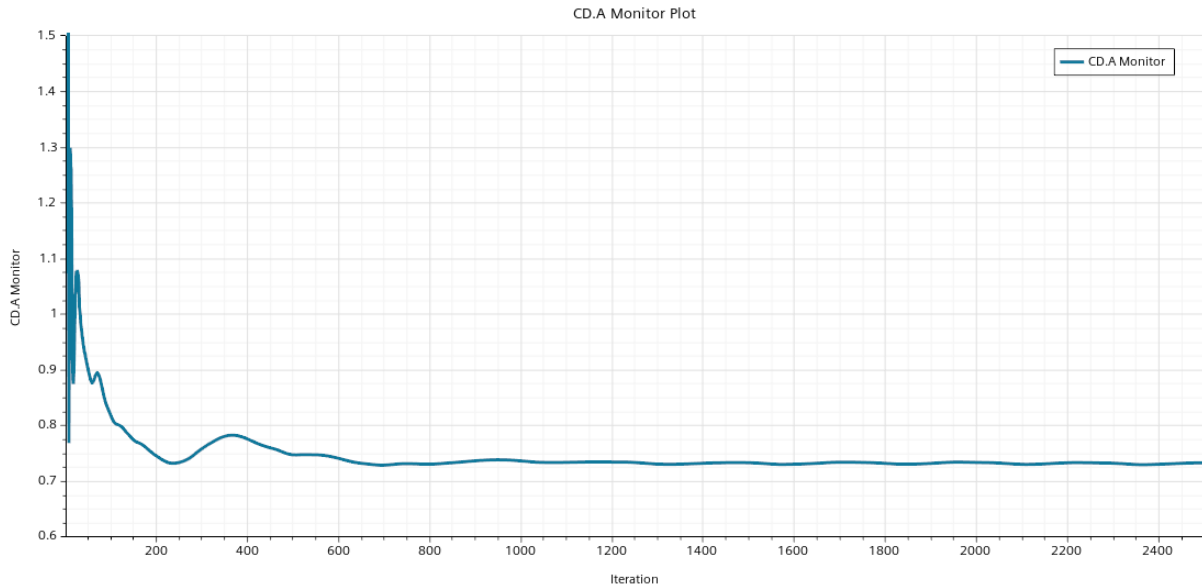


Figure 5.33 R13 ANSA Mesh Conv2Poly Simulation Drag Coefficient monitor plot

Figure 5.33 represents the drag coefficient (related to a reference area) monitor plot as a function of iterations of R13 ANSA mesh Conv2Poly simulation.

Overall, the CD.A Monitor Plot illustrates 4 main behavioral phases:

- an initial period of instability (0-50 iterations), in which the CLA values exhibit high values and a rapid reduction.
- followed by an import decrease between the 50 and 200 iterations in which CD.A values goes from 1.05 to 0.74.
- after that there is and intermediate fluctuation and stabilization phase in which, the CD.A values experience a slight rebound, rising from around 0.74 up to about 0.78 between 200 and 400 iterations.
- and finally, a gradual degrowth and convergence, indeed from 450 iterations onward, the CD.A values exhibit a slow, steady decline, reducing from approximately 0.78 to around 0.732 over the remaining iterations up to 2400 (the final value has to be multiplied by two to take into account the fact that the simulation is carried out in symmetry, therefore with half of the car).



## **Final considerations**

### **1) Overall convergence**

Simulations with ANSA meshes generally show low residuals and good stability in momentum and continuity variables, indicating a numerical convergence comparable to the R13 simulation. This suggests that the simulation conditions (such as meshing or solver parameters) produce good performance.

### **2) Sdr residual**

Simulations with ANSA meshes show an oscillatory behavior of the Sdr residual. However, the values are quite low, and the results are not critical.

### **3) Recommendations**

Given the residual behavior, the simulations with ANSA mesh appears generally accurate for most variables, but the Sdr residual requires attention. It may be beneficial to explore different settings for the turbulence model or further refine the mesh to obtain a more stable solution.

### 5.2.2. Skin Friction Coefficient

The skin friction coefficient  $C_f$  is a dimensionless quantity that represents the ratio of wall shear stress  $\tau_w$  to the dynamic pressure of the flow. It is defined as:

$$C_f = \frac{\tau_w}{\frac{1}{2} \rho U_\infty^2}$$

where:

- $\tau_w$  = wall shear stress, the tangential force exerted by the fluid on the surface per unit area.
- $\rho$  = fluid density.
- $U_\infty$  = freestream velocity of the fluid.
- $\frac{1}{2} \rho U_\infty^2$  = dynamic pressure, which is a measure of the kinetic energy of the flow.

The skin friction coefficient is critical in understanding aerodynamic drag produced by surfaces interacting with the flow. Drag consists of two primary components:

- Pressure drag (due to flow separation and pressure differentials).
- Friction drag (due to viscous forces between the fluid and the surface).

Since skin friction drag is directly proportional to the wall shear stress,  $C_f$  gives engineers insight into how much energy is being lost due to the interaction of the fluid with the surface at the boundary layer and which are the regions of possible flow separation.

The accuracy of the  $C_f$  computation depends heavily on mesh quality near the surface, especially in the boundary layer.

Once STAR-CCM+ computes the skin friction coefficient, it can be visualized as:

- **Scalar Fields:**  $C_f$  values are often plotted as contour maps on the surface of the geometry, showing the distribution of friction along the surface. These plots help identify areas of high shear stress, flow separation, and regions of turbulent flow.
- **Streamlines:** Flow structures such as vortices or flow detachment points can be correlated with local changes in  $C_f$  helping to improve designs by minimizing separation or reducing drag in these areas.
- **Line Plots:** to evaluate how  $C_f$  changes spatially.

These are the main reasons why the skin friction coefficient is a good parameter to make the simulations comparison with the goal to evaluate the goodness of the new ANSA meshes.

Into the next pages are represented the  $C_f$  scalar fields obtained by the simulations.

## R13 Simulation

Simcenter STAR-CCM+

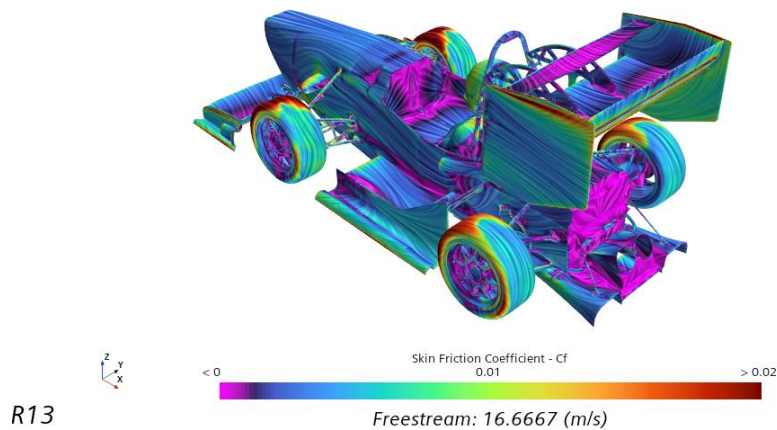


Figure 5.34 R13 Simulation Skin Friction Coefficient Full car top rear view

Figure 5.34 represents the skin coefficient scalar field on the car surface, in R13 simulation with a top rear view. Examining it in detail, many separation regions could be identified:

- In the rear wing area, the  $C_f < 0$  is in the beam-wing portion and in the backside of the two supports.
- In the sidepod area, separation is highlighted near the monocoque attachment and in the external initial concave part.
- In the back of the car, separation is found at the end of the monocoque, in the nozzle of the radiator and on a portion on top of the diffuser.
- In the cockpit area, there is separation in the steering wheel zone.
- In the wheels area, separation is evidence in the rims zone.

Simcenter STAR-CCM+

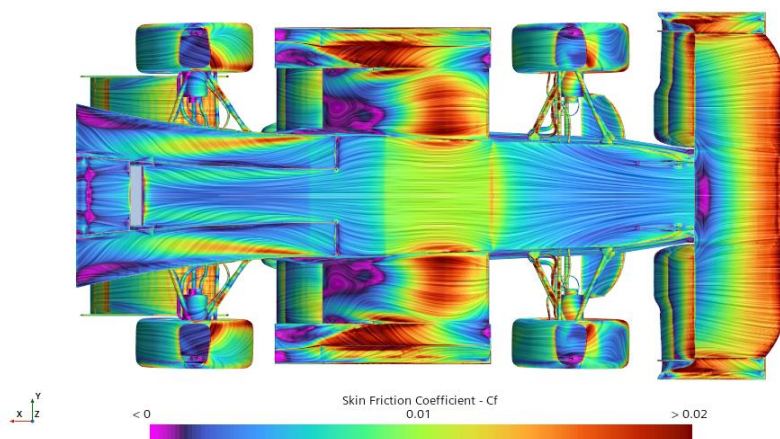


Figure 5.35 R13 Simulation Skin Friction Coefficient Full car bottom view

Figure 5.35 represents the skin coefficient scalar field on the car surface, in R13 simulation, with a bottom view. The most critical areas in terms of separation are the end external portion of the diffuser, the end internal zone of the sidepods (near the monocoque), the end concave portion of the sidepods, the end central portion of the main profile of the front wing.

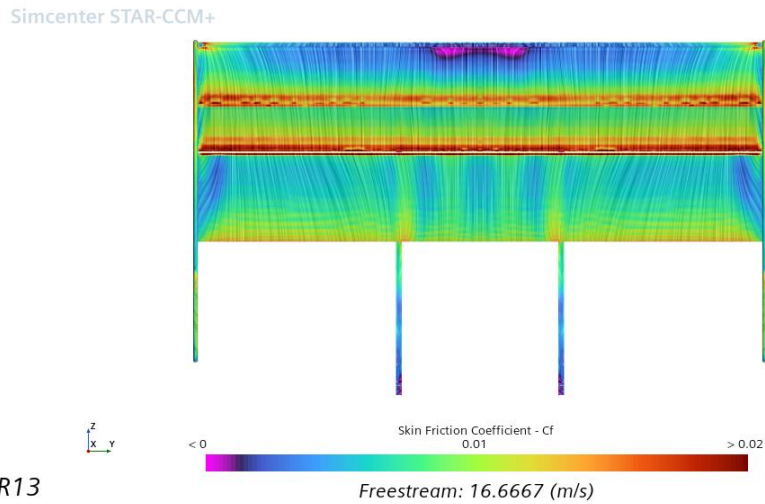


Figure 5.36 R13 Simulation Skin Friction Coefficient Rear wing rear view

Figure 5.36 represents the skin coefficient scalar field on rear wing surface, in R13 simulation, with a rear view.

The most critical area in terms of separation is the central portion of the upper flap, in which it can be seen as a magenta area, representing a zone of negative value of the skin friction coefficient.

Other low values regions of  $C_f$  are in the dorsal portion of the main profile of the rear wing, near the endplates (blue zones) and the lower part of the supports.

## R13 ANSA Mesh Simulation

Simcenter STAR-CCM+

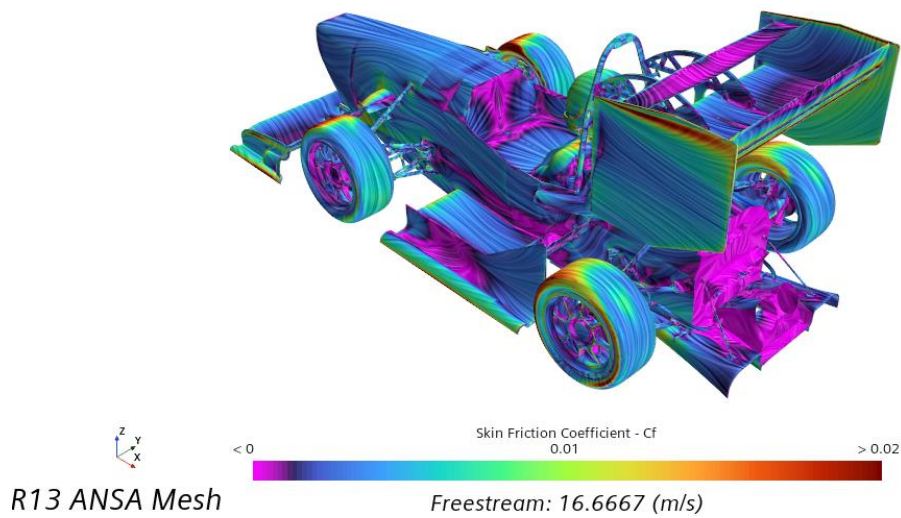


Figure 5.37 R13 ANSA Mesh Simulation Skin Friction Coefficient Full car top rear view

Figure 5.37 represents the skin coefficient scalar field on the car surface, in R13 ANSA Mesh simulation with a top rear view.

Examining it in detail, many separation regions could be identified:

- In the rear wing area, the  $C_f < 0$  is in the beam-wing portion and in the backside of the two supports.
- In the sidepod area, separation is highlighted near the monocoque attachment and in the external initial concave part. Comparing with R13 Simulation, these portions are larger, so the flow is more detached from the car surface.
- In the back of the car, separation is found at the end of the monocoque, in the nozzle of the radiator and on a portion on top of the diffuser.
- In the cockpit area, there is separation in the steering wheel zone.
- In the wheels area, separation is evidence in the rims zone.

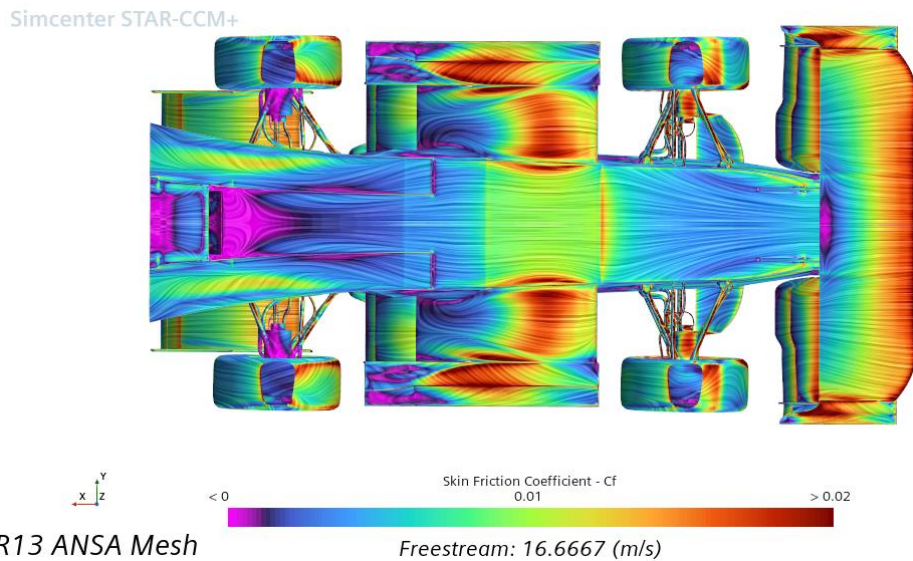


Figure 5.38 R13 ANSA Mesh Simulation Skin Friction Coefficient Full car bottom view

Figure 5.38 represents the skin coefficient scalar field on the car surface, in R13 ANSA Mesh simulation, with a bottom view.

The differences with R13 Simulation are:

- In the diffuser area in which the separation has moved into the centre.
- In the sidepods area in which the separation at the end internal zone of the sidepods (near the monocoque) is diminished but the separation in the end concave portion is larger.
- In the rear suspensions the separation is larger.

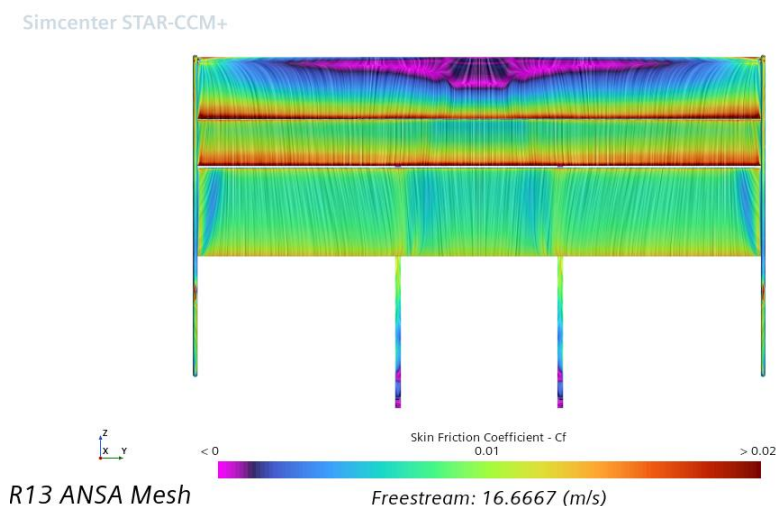


Figure 5.39 R13 ANSA Mesh Simulation Skin Friction Coefficient Rear wing rear view

Figure 5.39 represents the skin coefficient scalar field on rear wing surface, in R13 ANSA Mesh simulation, with a rear view.

The central portion of the upper flap shows the negative value of the skin friction coefficient and a wider area with respect to R13 simulation. This indicates a possible bigger separation zone. As R13 simulation, the dorsal portion of the main profile of the rear wing (near the endplates, blue zones) and the lower part of the supports have low values regions of  $C_f$ .

## R13 ANSA Mesh Conv2Poly Simulation

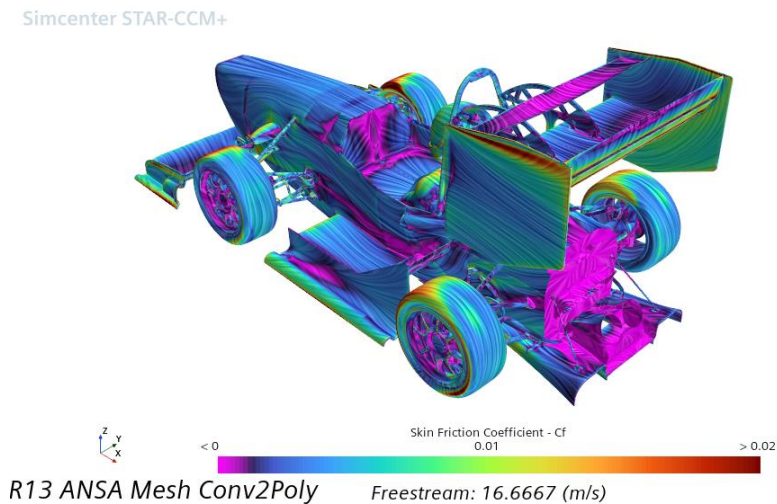


Figure 5.40 R13 ANSA Mesh Conv2Poly Simulation Skin Friction Coefficient  
Full car top rear view

Figure 5.40 represents the skin coefficient scalar field on the car surface, in R13 ANSA Mesh Conv2Poly simulation with a top rear view.

Examining it in detail, many separation regions could be identified:

- In the rear wing area, the  $C_f < 0$  is in the beam-wing portion and in the backside of the two supports.
- In the sidepod area, separation is highlighted near the monocoque attachment and in the external initial concave part. Comparing with R13 Simulation, these portions are larger, so the flow is more detached from the car surface. Comparing with R13 ANSA Mesh Simulation the external concave part has a smaller area of  $C_f < 0$ .
- In the back of the car, separation is found at the end of the monocoque, in the nozzle of the radiator and on a portion on top of the diffuser.
- In the cockpit area, there is separation in the steering wheel zone.
- In the wheels area, separation is evidence in the rims zone.

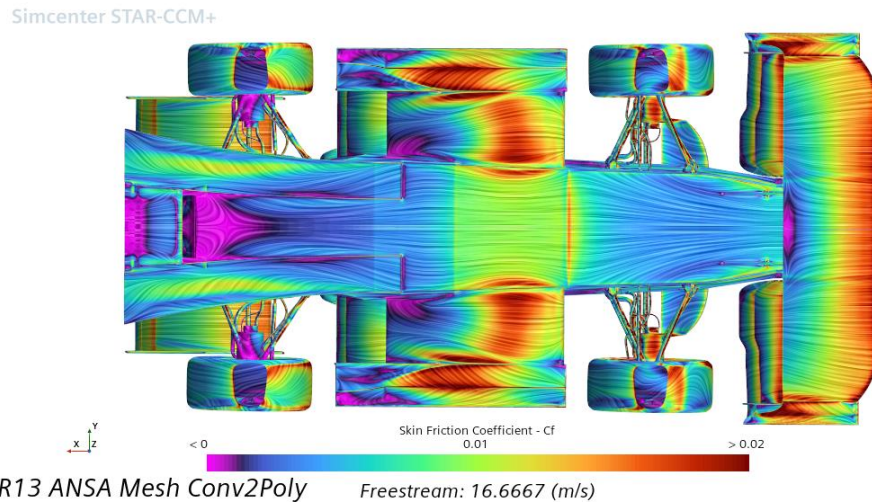


Figure 5.41 R13 ANSA Mesh Conv2Poly Simulation Skin Friction Coefficient Full car bottom view

Figure 5.41 represents the skin coefficient scalar field on the car surface, in R13 ANSA Mesh Conv2Poly simulation, with a bottom view.

The skin friction scalar field is quite like which in R13 ANSA Mesh Simulation except in the internal zone of sidepods in which the magenta area is slightly bigger.

The differences with R13 Simulation are:

- In the diffuser area in which the separation has moved into the centre.
- In the sidepods area in which the separation at the end internal zone of the sidepods (near the monocoque) is diminished but the separation in the end concave portion is larger.
- In the rear suspensions the separation is larger.

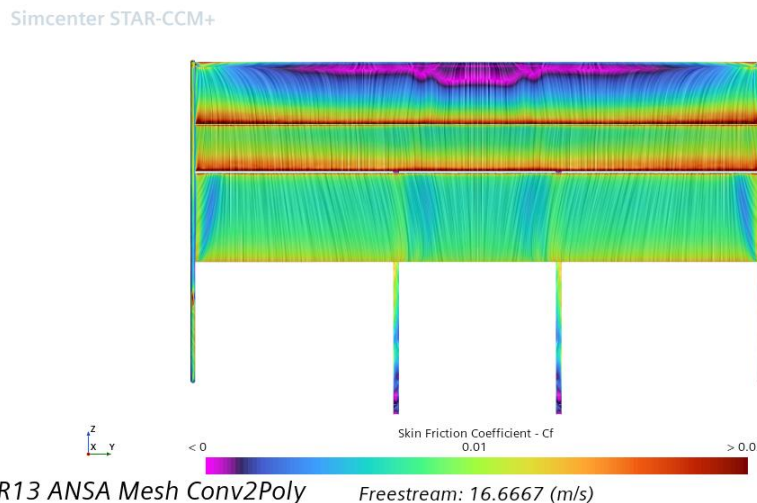


Figure 5.42 R13 ANSA Mesh Conv2Poly Simulation Skin Friction Coefficient Rear wing rear view

Figure 5.42 represents the skin coefficient scalar field on rear wing surface, in R13 ANSA Mesh simulation, with a rear view.

The central portion of the upper flap shows the negative value of the skin friction coefficient.

This area is wider with respect to R13 simulation (and it indicates a possible bigger separation zone) but slightly narrower than R13 ANSA Mesh simulation.

As R13 simulation, the dorsal portion of the main profile of the rear wing (near the endplates) and the lower part of the supports have low values regions of  $C_f$ .



## **Final considerations**

### **1) Differences**

In the simulations with ANSA meshes, in the third flap of the rear wing and on the sidepods, the magenta region is bigger, and this indicates possible bigger flow separation. This could explain the lower value of  $C_l$  in these simulations compared to R13 simulation.

### **2) Similarities**

Looking all the simulations, for example the rear wing (rear view) and full car (bottom view) representations, it is known as the overall  $C_f$  distribution is similar, with flow attachment in most part of the car and the almost the same separation regions (especially in the simulations with ANSA mesh).

### **3) Conclusions and recommendations**

Thanks to skin friction coefficient scenes we can say that the simulations with ANSA meshes have very similar results. Looking into detail they have some differences of flow separation with the R13 simulation and, having a better quality than the STAR-CCM+ mesh we expect the results to be better than the R13 simulation, but this should be validated with wind tunnel tests.

### 5.2.3. Pressure Coefficient

The pressure coefficient  $C_p$  is a dimensionless number that represents the relative pressure at a point on an object's surface, normalized by the dynamic pressure of the flow and it is defined as:

$$C_p = \frac{p - p_\infty}{\frac{1}{2} \rho U_\infty^2}$$

Where:

- $p$  is the local pressure at the point of interest on the surface,
- $p_\infty$  is the free-stream pressure (pressure of the undisturbed flow far from the object),
- $\rho$  is the fluid density,
- $U_\infty$  is the free-stream velocity of the flow.

In the field of aerodynamics, the pressure coefficient plays an essential role by allowing engineers and researchers to examine pressure distribution across surfaces, which is directly linked to the aerodynamic forces acting on an object. Specifically:

- **Lift and Drag Estimation:** The pattern of  $C_p$  along the surface of an airfoil or wing can be used to calculate lift and drag forces. Lift is largely generated from differences in  $C_p$  between the upper and lower surfaces of the wing.
- **Flow Behavior:** Variations in  $C_p$  reflect different flow conditions, like areas of high or low pressure, possible points of flow separation, and stagnation points. This information helps pinpoint where flow might separate from the surface, contributing to drag or reducing lift.
- **Design Optimization:** Studying  $C_p$  assists engineers in adjusting shapes to improve performance, whether by minimizing drag or maximizing lift, based on specific design goals.

In StarCCM+, this coefficient can be directly computed and visualized across surfaces of interest with color maps in which:

- **High Positive  $C_p$  (Red):** These are high-pressure regions, commonly found at stagnation points where the flow comes to a stop (such as at the leading edge of an airfoil or the front end of a vehicle). These zones increase drag.
- **Low or Negative  $C_p$  (Blue):** Low-pressure areas, often located on the upper surface of an airfoil or along curved sections, which contribute to lift. Negative  $C_p$  values indicate accelerated flow over the surface, generating suction.
- **Flow Patterns and Gradients:** Smooth transitions in  $C_p$  suggest steady flow, while abrupt changes point to areas with intense turbulence, flow separation, or shock waves, especially in transonic or supersonic conditions.
- **Flow Separation:**  $C_p$  maps can highlight separation points, where pressure begins to rise after a low-pressure zone, signalling that the flow is losing momentum and detaching from the surface.

Into the next pages are represented the  $C_p$  scalar fields into 3D obtained by the simulations.

## R13 Simulation

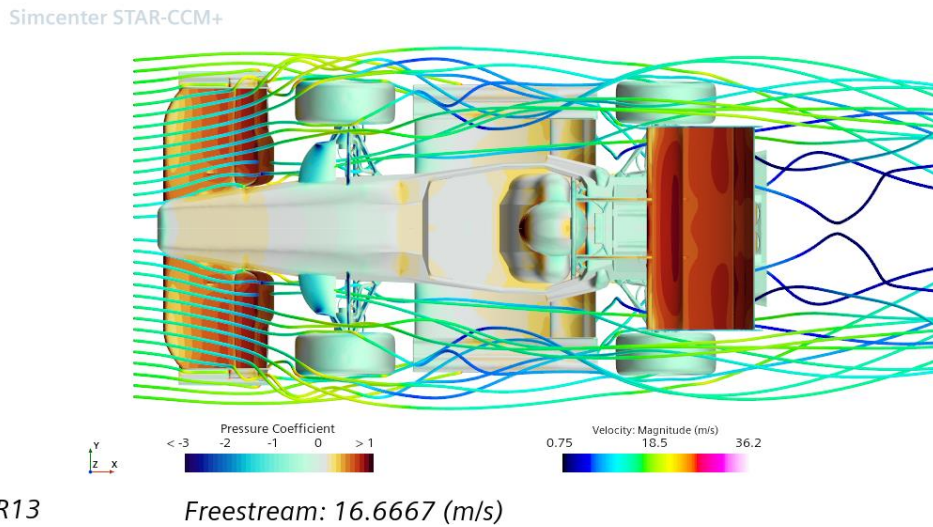


Figure 5.43. R13 Simulation Pressure Coefficient and Velocity Magnitude Full car streamlines top view

Figure 5.43 represents the pressure coefficient distribution over the car surface, in R13 simulation, with a top view and the streamlines course around the vehicle.

High-pressure zones (orange/red areas) appear mainly on the front wing and rear wing. Another high-pressure area is the stagnation point in the front part of the helmet.

The streamlines represent the airflow around the car:

- Smooth airflow can be seen around the body of the car, with minimal disruption until the rear wing.
- High curvature of streamlines is present near the wheels and the rear wing, indicating strong aerodynamic interaction.
- The wake behind the car indicates a reduction in velocity and increased turbulence.

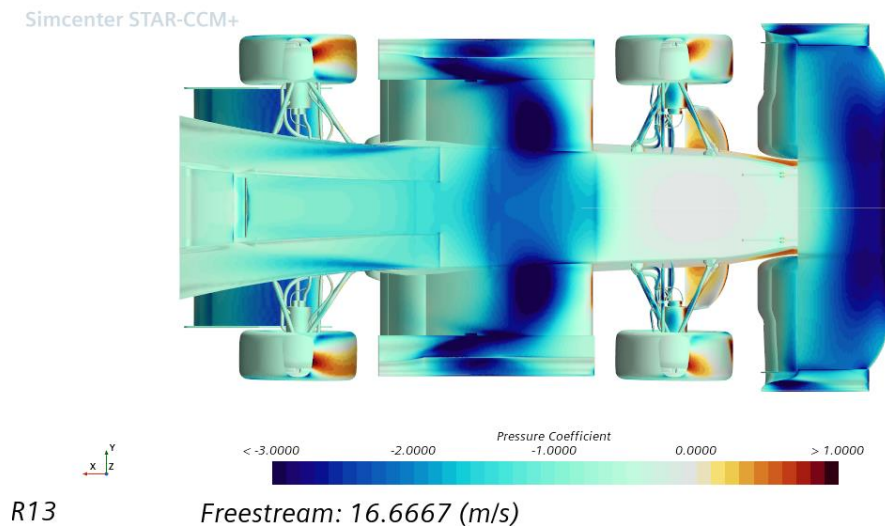


Figure 5.44 R13 Simulation Pressure Coefficient Full car bottom view

Figure 5.44 represents the pressure coefficient distribution over the surface of the car, in R13 simulation, with a bottom view.

High pressure zones can be identified near to:

- Leading surfaces of the vehicle, such as the front face (nose area).
- Tires and nose wings, where the airflow stagnates and causes a buildup of pressure.

These zones contribute significantly to aerodynamic drag (especially the tires), as the high-pressure areas resist forward motion.

Low pressure zones can be identified near to the bottom surfaces of the vehicle, especially along:

- The main profile of the front wing.
- Sidepods.
- Rear wing.

These zones contribute significantly to downforce generation due to suction phenomenon which is generated with flow acceleration and depression.

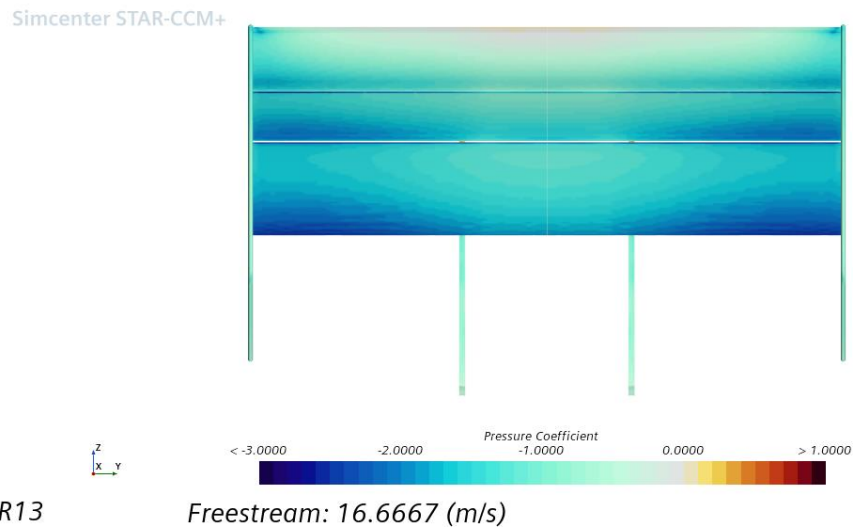


Figure 5.45 R13 Simulation Pressure Coefficient Rear wing rear view

Figure 5.45 represents the pressure coefficient distribution over the rear wing surface, in R13 simulation, with a rear view.

We note that the dorsal portions of the main profile and the second flap produce the largest depression areas of the rear wing.

There are also two big suction zones near the endplates and an high pressure zone on the upper part of the third flap.

### R13 ANSA Mesh Simulation

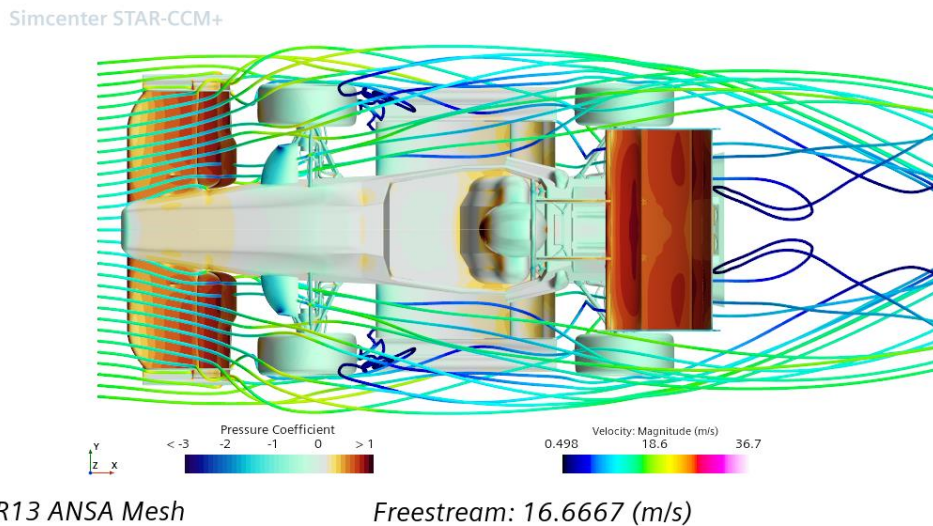


Figure 5.46 Full car streamlines top view

Figure 5.46 represents the pressure coefficient distribution over the car surface, in R13 ANSA Mesh simulation, with a top view and the streamlines course around the vehicle.

High-pressure zones (orange/red areas) appear mainly on the front wing and rear wing. Another high-pressure area is the stagnation point in the front part of the helmet.

The streamlines represent the airflow around the car:

- Smooth airflow can be seen around the body of the car, with minimal disruption until the rear wing.
- High curvature of streamlines is present near the wheels and the rear wing, indicating strong aerodynamic interaction.
- The wake behind the car indicates a reduction in velocity and increased turbulence.

The comparison with figure 5.43 leads to say that:

- We have similar flow paths around the car.
- Slight changes in streamline density and curvature, particularly near the sidepods, the wheels and rear wing, suggest slight differences in the computational mesh.
- Figure 5.46 compared to figure 5.43 shows a marginally higher maximum velocity (36.7m/s vs 36.2m/s).
- Figure 5.46 with respect figure 5.43 may reflect improved meshing techniques, leading to more refined results (e.g., higher velocity magnitudes and altered wake patterns).

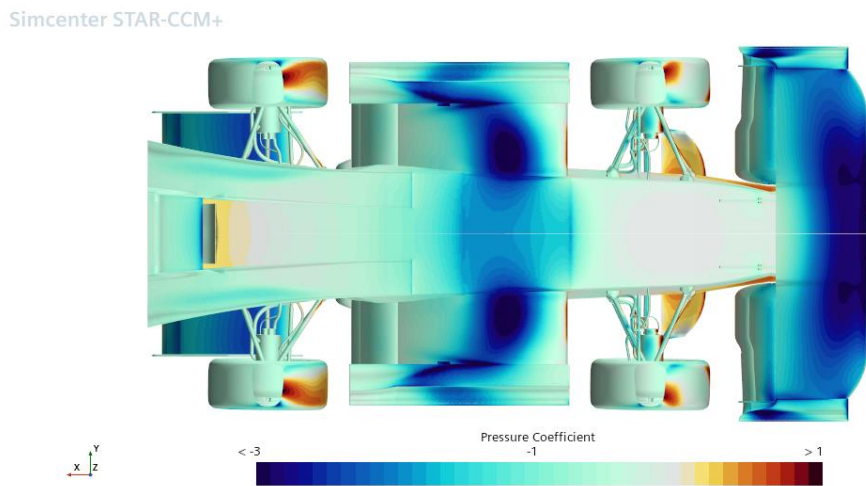


Figure 5.47 Full car bottom view

Figure 5.47 represents the pressure coefficient distribution over the surface of the car, in R13 ANSA Mesh simulation, with a bottom view.

High pressure zones can be identified near to the same regions of R13 simulation:

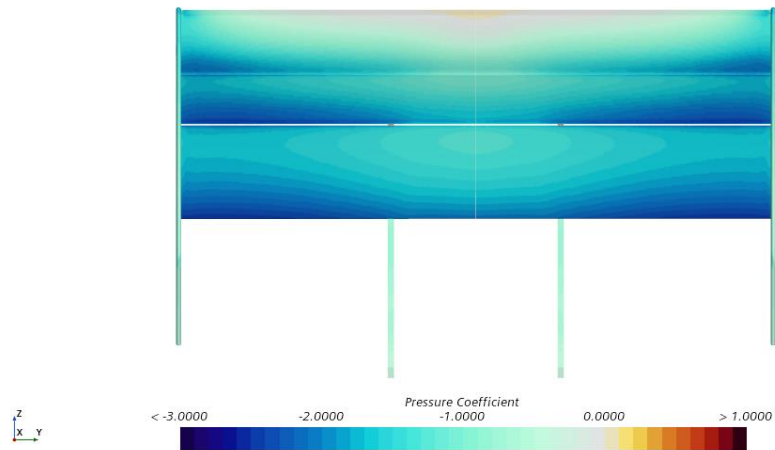
- Leading surfaces of the vehicle, such as the front face (nose area).
- Tires and nose wings, where the airflow stagnates and causes a buildup of pressure.

Low pressure zones can be identified near to the bottom surfaces of the vehicle, especially along the same regions of R13 simulation:

- The main profile of the front wing.
- Sidepods.
- Rear wing.

The main differences between these simulations are in the rear wing and diffuser regions, which show slight differences in pressure distribution. In R13 ANSA Mesh simulation these areas are characterized by lower depression (the blue color tends to be lighter). The radiator inlet area also displays a higher-pressure zone.

Simcenter STAR-CCM+



R13 ANSA Mesh Freestream: 16.6667 (m/s)

Figure 5.48 Rear wing rear view

Figure 5.48 represents the pressure coefficient distribution over the rear wing surface, in R13 ANSA Mesh simulation, with a rear view.

The  $C_p$  pattern and the high-low pressure regions are quite similar to R13 simulation. The main difference is that the depression zone in the main profile is a little bit wider in the central portion.

## R13 ANSA Mesh Conv2Poly Simulation

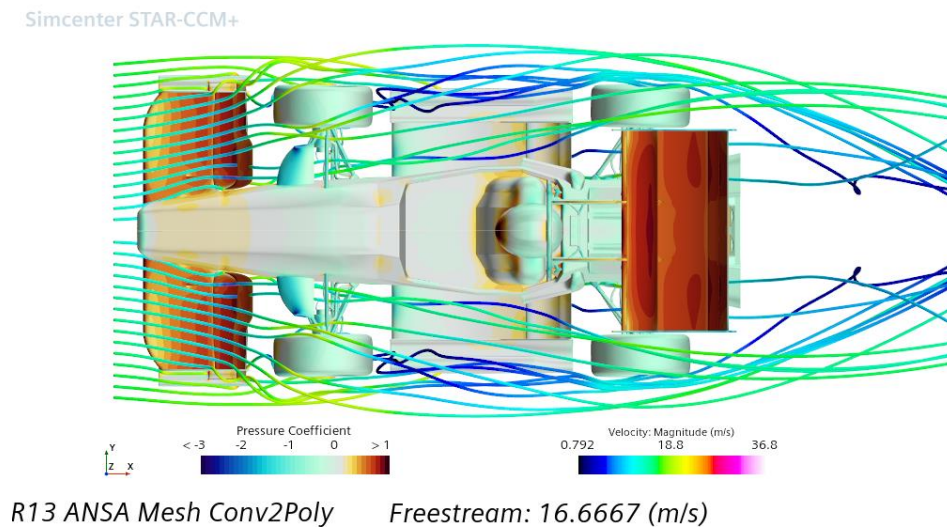


Figure 5.49 Full car streamlines top view

Figure 5.49 represents the pressure coefficient distribution over the car surface, in R13 ANSA Mesh Conv2Poly simulation, with a top view and the streamlines course around the vehicle.

High-pressure zones (orange/red areas) appear mainly on the front wing and rear wing. Another high-pressure area is the stagnation point in the front part of the helmet.

The streamlines represent the airflow around the car:

- Smooth airflow can be seen around the body of the car, with minimal disruption until the rear wing.
- High curvature of streamlines is present near the wheels and the rear wing, indicating strong aerodynamic interaction.
- The wake behind the car indicates a reduction in velocity and increased turbulence.

The comparison with figures 5.49 and 5.46 highlights the fact that they show similar flow paths around the car and there are slight changes in streamline density in the wake.

Figure 5.49 compared to figures 5.43-5.46 exhibits a slightly higher maximum velocity (36.8m/s vs 36.7m/s and 36.2m/s respectively).

Figures 5.49 and 5.46 with respect figure 5.43 may reflect improved meshing techniques, leading to more refined results (e.g., higher velocity magnitudes and altered wake patterns).



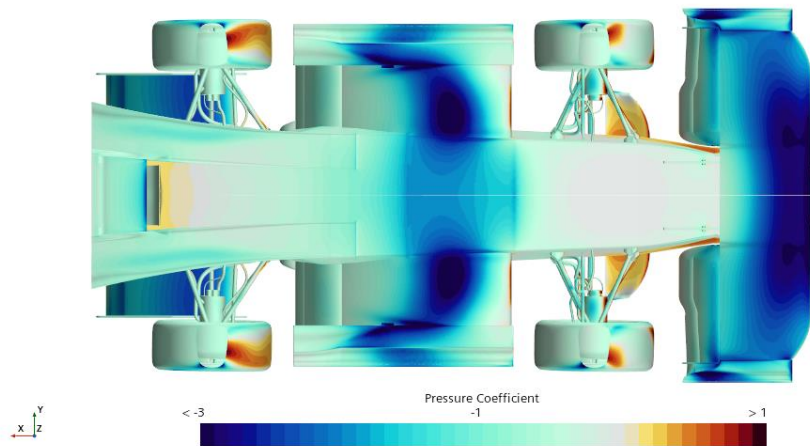


Figure 5.50 Full car bottom view

Figure 5.48 represents the pressure coefficient distribution over the surface of the car, in R13 ANSA Mesh simulation, with a bottom view.

High pressure zones can be identified near to the same regions of R13 simulation:

- Leading surfaces of the vehicle, such as the front face (nose area).
- Tires and nose wings, where the airflow stagnates and causes a buildup of pressure.

Low pressure zones can be identified near to the bottom surfaces of the vehicle, especially along the same regions of R13 simulation:

- The main profile of the front wing.
- Sidepods.
- Rear wing.

The main differences between these simulations are in the rear wing and diffuser regions, which show slight differences in pressure distribution. In R13 ANSA Mesh simulation these areas are characterized by lower depression (the blue color tends to be lighter). The radiator inlet area also displays a higher-pressure zone.

A consistent result that we can note that the pressure coefficient behavior on car bottom surfaces is the same as R13 ANSA Mesh simulation and this demonstrates the stability of ANSA Meshes in high-low-pressure detection.

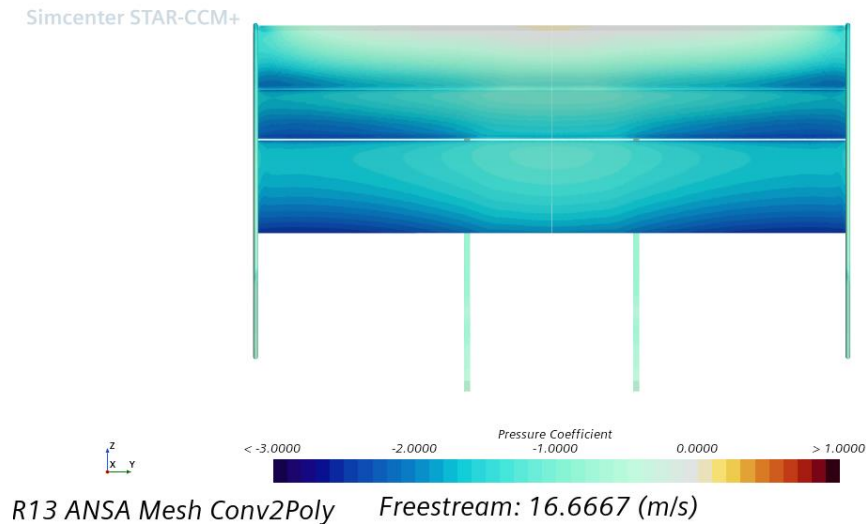


Figure 5.51 Rear wing rear view

Figure 5.51 represents the pressure coefficient distribution over the rear wing surface, in R13 ANSA Mesh Conv2Poly simulation, with a rear view.

The  $C_p$  pattern and the high-low pressure regions are really like to R13 ANSA Mesh simulation.

## Final considerations

### 1) Differences

In the simulations with ANSA meshes, in the third flap of the rear wing, the orange regions are bigger, and this indicates a more extensive high-pressure region.

Furthermore, the full car (bottom view) representations reveal that the diffuser area and the sidepod area create a lower suction compared to R13 simulation and this could explain the lower value of  $CL$  in ANSA mesh simulations

### 2) Similarities

Looking all the simulations, for example the rear wing (rear view) and full car (bottom view) representations,

it is known the overall  $C_p$  distribution is similar, with high-pressure and low-pressure regions located in the same areas.

### 3) Conclusions and recommendations

Thanks to pressure coefficient scenes we can say that the simulations with ANSA meshes have a very similar results. Looking into detail they have some differences in the dimensions of the low-pressure regions with the R13 simulation and, having a better quality then the STAR-CCM+ mesh we expect the results to be better than the R13 simulation, but this should be validated with wind tunnel tests.

# 6. Conclusions and Recommendations

## Conclusions:

This study successfully developed an alternative meshing methodology using ANSA software, achieving a high degree of customization, versatility, and compatibility with various CFD solvers. The ANSA mesh, generated with a combination of Tetra Rapid + Hexa Interior and polyhedral (Conv2Poly) algorithms, met rigorous quality criteria, producing stable, convergent simulations that performed comparably and, in some aspects, superiorly to the existing STAR-CCM+ mesh.

Regarding the time of execution of the mesh we have that the ANSA meshes about 40 minutes, of which: 13 minutes for surface mesh, 8 minutes for prism layers generation, 14 minutes for volume mesh and 3 minutes for fix quality. The STAR-CCM+ mesh instead takes about 15 minutes to generate.

Among the meshing approaches tested, the Conv2Poly method was particularly efficient, significantly reducing computational time (12 s/iteration compared to 14 s/iteration with STAR-CCM+), making it advantageous for iterative design processes that require numerous simulations.

In general, the time of meshing and simulation is influenced by available computational resources (in this case a computer with 48 cores and 376 GB of RAM was used) and any background operating software.

The ANSA mesh demonstrated enhanced ability to detect crucial aerodynamic features, particularly in areas where flow separation and pressure distribution play a pivotal role in aerodynamic performance, such as the rear wing and sidepods. Improved low-pressure region delineation contributed to better downforce prediction, offering an advantage in capturing the car's aerodynamic characteristics more accurately.

Having the ANSA meshes a better quality than STAR-CCM+ mesh, we think that they allowed to highlight better the dimensions of the low-pressure regions and separation regions of the car in the simulations. These factors most affect the downforce generation by aerodynamics components. This conclusion should be validated with wind tunnel tests.

From a numerical point of view, ANSA mesh simulations showed good stability and convergence, with low residuals in momentum and continuity variables, indicating numerical accuracy. Despite a minor oscillatory behavior in the Sdr residual, which did not critically impact overall results, the ANSA mesh proved capable of consistently capturing aerodynamic features with reliability.

The project also successfully highlighted the benefits of diversifying meshing software within Squadra Corse, reducing dependence on one tool and opening broader partnership opportunities with software sponsors like BETA CAE Systems and Siemens. This dual-software approach not only supports greater flexibility and adaptability in solver selection but also promotes economic sustainability by allowing Squadra Corse to work with various sponsor partners. By incorporating both meshing tools, the team is better positioned to enhance performance in Formula SAE competitions through a more adaptable and sponsor-aligned meshing strategy.

## **Recommendations:**

**Further Refinement of the Mesh for Turbulence Model Stability:** While the ANSA mesh demonstrated strong convergence and stability, the oscillatory behavior observed in the Sdr residual suggests that additional refinement around high-turbulence zones could improve accuracy further. Testing alternative settings within the turbulence model or refining mesh density in areas with high flow gradients may help stabilize these residuals and enhance solution reliability.

**Optimization of Flow Separation Detection:** The ANSA mesh displayed a good capability for capturing flow separation in critical areas, such as the rear wing's third flap and sidepods. However, additional mesh optimization in these areas could further improve the detection of separation zones, enhancing aerodynamic accuracy, particularly for simulations where precise downforce predictions are essential to the vehicle's performance.

**Parameter Optimization for Solver Settings:** Given the promising results with ANSA, experimenting with different solver parameters may yield further performance improvements. Adjusting parameters to suit the ANSA mesh structure, such as under-relaxation factors, could enhance both accuracy and stability.

**Exploration of Alternative CFD Solvers:** The compatibility of ANSA meshes with various solvers, including OpenFOAM, provides a valuable opportunity for Squadra Corse to expand their CFD tools. Conducting further studies to evaluate the performance of ANSA-generated meshes on alternative solvers could reveal additional computational or accuracy benefits, especially with open-source solvers that offer cost-effective simulation options.

In summary, this study demonstrates the feasibility and efficiency of ANSA mesh as an alternative to STAR-CCM+ mesh with benefits in both computational speed and solution accuracy.

By integrating a dual-meshing approach, Squadra Corse gains a more flexible, sponsor-aligned strategy that supports both current and future competitive needs in Formula SAE, enabling innovation in vehicle design and simulation accuracy.

So, the ANSA meshes are a good starting point that the team can use and modify in the future to further improve the car design process.



## List of figures

|             |   |    |
|-------------|---|----|
| Figure 1.1  | Formula Student Austria.....  | 7  |
| Figure 1.2  | Aerodynamics and CFD department and rollout event of SC24.....            | 9  |
| Figure 2.1  | Turbulence models in CFD.....   | 24 |
| Figure 2.2  | CFD modelling of a turbulent jet using different approaches.....          | 24 |
| Figure 2.3  | 2D element cells.....   | 25 |
| Figure 2.4  | 3D element cells.....   | 25 |
| Figure 2.5  | Structured and Unstructured Grids.....                                    | 26 |
| Figure 3.1  | Trimmed cell mesher used in meshing operations.....                       | 27 |
| Figure 3.2  | Parameters of the Trimmed Cell Mesher in STAR-CCM+ model.....             | 28 |
| Figure 3.3  | Polyhedral Mesher applied to Moving Reference Frame Regions.....          | 29 |
| Figure 3.4  | Parameters of the Polyhedral Mesher in the STAR-CCM+ model.....           | 29 |
| Figure 3.5  | Prism Layer Mesher used in meshing operations.....                        | 31 |
| Figure 3.6  | Example of prism layer built on the front wing mainplane.....             | 31 |
| Figure 3.7  | 3 layers and core mesh example.....                                       | 32 |
| Figure 3.8  | Total height of layers.....   | 32 |
| Figure 3.9  | Geometric progression stretching function of 10 layers.....               | 33 |
| Figure 3.10 | Prism layer settings in STAR-CCM+ Mesh model.....                         | 33 |
| Figure 3.11 | Full car side view.....   | 35 |
| Figure 3.12 | Full car and wake refinement.....   | 35 |
| Figure 3.13 | Computational domain.....   | 35 |
| Figure 4.1  | Batch Mesh Manager graphic interface.....                                 | 36 |
| Figure 4.2  | Scenarios and Sessions setted in the first version of Batch Mesh.....     | 38 |
| Figure 4.3  | Interruption of the Batch Mesh execution during Prism Layer scenario..... | 39 |
| Figure 4.4  | Fixing of peaks of local curvature.....                                   | 39 |
| Figure 4.5  | Movement of inlet/outlet interfaces.....                                  | 40 |
| Figure 4.6  | Movement of MRFs interfaces.....  | 41 |
| Figure 4.7  | Size Boxes panel.....   | 42 |
| Figure 4.8  | Controlled by Size Field option.....                                      | 42 |
| Figure 4.9  | Size Field rules.....   | 42 |
| Figure 4.10 | Size Field.....   | 43 |
| Figure 4.11 | Representation of refinement Size Boxes.....                              | 43 |
| Figure 4.12 | Automotive_y+1_StarCCM quality criteria enable in USFs of ANSA v24.....   | 44 |
| Figure 4.13 | Prism layers Scenario setted in the second version of Batch Mesh.....     | 45 |
| Figure 4.14 | Time taken by the “fix quality” visible in the log of mesh operation..... | 45 |
| Figure 4.15 | Computational domain.....   | 46 |
| Figure 4.16 | Off Inspector tool.....   | 46 |
| Figure 4.17 | Computational domain.....   | 47 |
| Figure 4.18 | Off Inspector tool.....   | 47 |

|             |   |    |
|-------------|---|----|
| Figure 5.1  | Skewness Angle representation.....  | 48 |
| Figure 5.2  | R13 STAR-CCM+ Mesh Skewness Angle histogram plot.....   | 49 |
| Figure 5.3  | R13 STAR-CCM+ Mesh number of cells off recommended skewness angle limit.....                  | 49 |
| Figure 5.4  | R13 STAR-CCM+ Mesh Skewness Angle critical areas.....   | 50 |
| Figure 5.5  | R13 ANSA Mesh Skewness Angle histogram plot.....  | 51 |
| Figure 5.6  | R13 ANSA Mesh Conv2Poly Skewness Angle histogram plot.....                                    | 52 |
| Figure 5.7  | R13 ANSA Mesh Conv2Poly number of cells off recommended skewness angle limit..                | 52 |
| Figure 5.8  | Face Validity representation.....   | 53 |
| Figure 5.9  | R13 STAR-CCM+ Mesh Face Validity histogram plot.....  | 53 |
| Figure 5.10 | R13 ANSA Mesh Face Validity histogram plot.....   | 54 |
| Figure 5.11 | R13 ANSA Mesh Conv2Poly Face Validity histogram plot.....                                     | 54 |
| Figure 5.12 | Cell Quality representation.....  | 55 |
| Figure 5.13 | R13 STAR-CCM+ Mesh Cell Quality metric histogram plot.....                                    | 55 |
| Figure 5.14 | R13 ANSA Mesh Cell Quality metric histogram plot.....   | 56 |
| Figure 5.15 | R13 ANSA Mesh Conv2Poly Cell Quality metric histogram plot.....                               | 56 |
| Figure 5.16 | Volume Change representation.....   | 57 |
| Figure 5.17 | R13 STAR-CCM+ Mesh Volume Change metric histogram plot.....                                   | 58 |
| Figure 5.18 | R13 STAR-CCM+ Mesh Volume Change areas of interest .....                                      | 58 |
| Figure 5.19 | R13 ANSA Mesh Volume Change metric histogram plot.....  | 59 |
| Figure 5.20 | R13 ANSA Mesh Conv2Poly Volume Change metric histogram plot.....                              | 60 |
| Figure 5.21 | Chevron Quality cell representation.....  | 61 |
| Figure 5.22 | R13 STAR-CCM+ Mesh Chevron Quality metric histogram plot.....                                 | 61 |
| Figure 5.23 | R13 ANSA Mesh Chevron Quality metric histogram plot.....                                      | 62 |
| Figure 5.24 | R13 ANSA Mesh Conv2Poly Chevron Quality metric histogram plot.....                            | 62 |
| Figure 5.25 | R13 Simulation Residuals .....  | 64 |
| Figure 5.26 | R13 Simulation Lift Coefficient monitor plot.....   | 65 |
| Figure 5.27 | R13 Simulation Drag Coefficient monitor plot.....   | 66 |
| Figure 5.28 | R13 ANSA Mesh Simulation Residuals.....   | 67 |
| Figure 5.29 | R13 ANSA Mesh Simulation Lift Coefficient monitor plot.....                                   | 68 |
| Figure 5.30 | R13 ANSA Mesh Simulation Drag Coefficient monitor plot.....                                   | 69 |
| Figure 5.31 | R13 ANSA Mesh Conv2Poly Simulation Residuals.....   | 70 |
| Figure 5.32 | R13 ANSA Mesh Conv2Poly Simulation Lift Coefficient monitor plot.....                         | 71 |
| Figure 5.33 | R13 ANSA Mesh Conv2Poly Simulation Drag Coefficient monitor plot.....                         | 72 |
| Figure 5.34 | R13 Simulation Skin Friction Coefficient Full car top rear view.....                          | 75 |
| Figure 5.35 | R13 Simulation Skin Friction Coefficient Full car bottom view.....                            | 75 |
| Figure 5.36 | R13 Simulation Skin Friction Coefficient Rear wing rear view.....                             | 76 |
| Figure 5.37 | R13 ANSA Mesh Simulation Skin Friction Coefficient Full car top rear view.....                | 77 |
| Figure 5.38 | R13 ANSA Mesh Simulation Skin Friction Coefficient Full Full car bottom view.....             | 78 |
| Figure 5.39 | R13 ANSA Mesh Simulation Skin Friction Coefficient Full Rear wing rear view.....              | 78 |
| Figure 5.40 | R13 ANSA Mesh Conv2Poly Simulation -<br>Skin Friction Coefficient Full car top rear view..... | 79 |
| Figure 5.41 | R13 ANSA Mesh Conv2Poly Simulation -<br>Skin Friction Coefficient Full car bottom view.....   | 80 |
| Figure 5.42 | R13 ANSA Mesh Conv2Poly Simulation -<br>Skin Friction Coefficient Rear wing rear view.....    | 80 |

|  |    |
|--|----|
| Figure 5.43 R13 Simulation Pressure Coefficient and Velocity Magnitude -<br>Full car streamlines top view.....                     | 83 |
| Figure 5.44 R13 Simulation Pressure Coefficient Full car bottom view.....  | 84 |
| Figure 5.45 R13 Simulation Pressure Coefficient Rear wing rear view.....   | 85 |
| Figure 5.46 R13 ANSA Mesh Simulation Pressure Coefficient and Velocity Magnitude -<br>Full car streamlines top view.....           | 85 |
| Figure 5.47 R13 ANSA Mesh Simulation Pressure Coefficient Full car bottom view.....  | 86 |
| Figure 5.48 R13 ANSA Mesh Simulation Pressure Coefficient Rear wing rear view.....   | 87 |
| Figure 5.49 R13 ANSA Mesh Conv2Poly Simulation Pressure Coefficient and -<br>Velocity Magnitude Full car streamlines top view..... | 88 |
| Figure 5.50 R13 ANSA Mesh Conv2Poly Simulation Pressure Coefficient Full car bottom view...  | 89 |
| Figure 5.51 R13 ANSA Mesh Conv2Poly Simulation Pressure Coefficient Rear wing rear view...   | 90 |



## Bibliography

- {1} Formula SAE, [https://it.wikipedia.org/wiki/Formula\\_SAE](https://it.wikipedia.org/wiki/Formula_SAE).
- {2} Mean free path, [https://en.wikipedia.org/wiki/Mean\\_free\\_path](https://en.wikipedia.org/wiki/Mean_free_path).
- {3} Knudsen number, <https://www.sciencedirect.com/topics/engineering/knudsen-number>.
- {4} Notes from CFD academic course, Professor D. D'Ambrosio.
- {5} Finite difference method, [https://en.wikipedia.org/wiki/Finite\\_difference\\_method](https://en.wikipedia.org/wiki/Finite_difference_method).
- {6} Turbulence models, <https://cfdflowengineering.com/turbulence-modeling-in-cfd-simulations/>
- {7} Types of mesh, [https://en.wikipedia.org/wiki/Types\\_of\\_mesh](https://en.wikipedia.org/wiki/Types_of_mesh).
- {8} STAR-CCM+ User Guide.
- {9} ANSA User Guide.